THE INFLUENCE OF MICROSTRUCTURE ON ELECTRICAL RESISTIVITY IN PALLADIUM ALLOYS

by

Candace Irene Lang

A thesis submitted to the Faculty of Engineering, University of Cape Town
in fulfilment of the degree of Doctor of Philosophy

Department of Materials Engineering
University of Cape Town
September 1993

ABSTRACT

The relationship between microstructure and electrical resistivity has been studied in palladium-tungsten and palladium-molybdenum alloys, which exhibit an anomalous increase in resistivity after annealing. The effect of dislocations and structural order on resistivity has been investigated in order to determine the mechanisms whereby changes in resistivity occur in these alloys.

The electrical resistivity of palladium-tungsten and palladium-molybdenum alloys has been determined as a function of annealing temperature, using a sensitive electronic apparatus purpose-designed for the present work. For alloys of low solute concentration a minimum in the electrical resistivity with respect to annealing temperature, which has not previously been reported, was observed. Specimens subjected to annealing experiments have been studied by means of transmission electron microscopy, in order to determine the effect of annealing on microstructure and structural order. The information obtained has been used to relate the measured changes in electrical resistance and microhardness to the structural evolution of the alloys.

It is concluded that the unusual resistance effects observed arise from competition between changing degrees of structural order and dislocation density. Which of these mechanisms predominates under given conditions varies as a function of solute concentration and annealing temperature. In alloys containing more than 6 at.% solute, recovery and recrystallisation processes are accompanied by an increase in resistivity and a decrease in microhardness; after recrystallisation is complete, further annealing has no significant effect on either property. In alloys containing less than 6 at.% solute, recovery and recrystallisation are accompanied by a decrease in both resistivity and microhardness; but further annealing results in an increase in resistivity. Consideration of this data leads to the conclusion that microhardness is more sensitive to changes in dislocation density than structural order, whereas electrical resistivity is more sensitive to structural order than dislocation density. On this basis it is shown that short-range order increases rapidly at low annealing temperatures in alloys containing more than 6 at.% solute, but slowly in alloys containing less than 6 at.% solute in which short-range order increases rapidly only at higher annealing temperatures.

ACKNOWLEDGEMENTS

I would like to express my appreciation for the assistance I have received in the course of this work, in particular from:

The late Professor MP Shaw, my supervisor, for guidance and encouragement; and Professor Allen for useful discussions;

Mr J Green and Mr J Tapson, of the Department of Electrical and Electronic Engineering, for contributions to the design and construction of the electronic apparatus;

The staff of the Electron Microscope Unit for technical support;

Dr PT Wedepohl, Director of the Physical Metallurgy Division, MINTEK (Council for Mineral Technology), for advice and the provision of materials;

Mr D van Heerden for useful discussions;

Mr N Dreze and Mr G Newins (workshop), Mr B Greeves and Mr J Petersen (photographic), Mr D Dean (electronic), Mrs M Hoosen and Mr S Coetzee (laboratory), for technical assistance;

Mrs JD Sharland and Mrs AC Ball for administrative support;

and the staff and students of the Department of Materials Engineering for support and encouragement.

The financial support of MINTEK and the FRD (Foundation for Research Development) is gratefully acknowledged.

Dedicated to my son Jonathan.

CONTENTS

ABBREVIATIONS

ρ	electrical resistivity
ρ_0	residual resistivity
$\rho(T)$	ideal or temperature-dependent resistivity
DSR	dislocation-specific resistivity (residual resistivity per unit dislocation density)
Λ	mean free path
APW	augmented plane wave
KKR	Korringa-Khon-Rostoker
RMTA	rigid muffin-tin approximation
LMTO	linear muffin-tin orbital
bcc	body-centred cubic
fcc	face-centred cubic
hcp	hexagonal close-packed
at.%	atomic per cent
S	Seebeck coefficient
EDS	energy dispersive spectroscopy
TEM	transmission electron microscope or transmission electron microscopy
AC	alternating current
DC	direct current
HV_{50g}	Vickers hardness number; 50g load
HV_{100g}	Vickers hardness number; 100g load
CN	co-ordination number

MINTEK	Council for Mineral Technology, Randburg, South Africa.

CHAPTER 1

INTRODUCTION

The electrical properties of palladium alloys are of interest owing to the wide use of these materials in electrical and electronic applications. Pure palladium exhibits desirable features such as stable electrical properties and oxidation resistance; its mechanical properties are however poor, a disadvantage which is commonly overcome by alloying. The addition of refractory metals to palladium improves mechanical properties at a small cost to oxidation resistance, although the effect of such additions on the electrical properties of palladium has not yet been extensively investigated. Palladium-rich alloys containing tungsten or molybdenum are reported to exhibit enhanced mechanical properties and high electrical resistance, and are of use in the manufacture of electrical instrumentation for which this combination of mechanical and electrical properties is desirable, such as in potentiometer windings. Since the stability of electrical properties is critical in electrical instrumentation materials, the appearance of an unusual resistance effect in these alloys is of particular importance: both palladium-tungsten and palladium-molybdenum are reported to exhibit a significant increase in electrical resistance after annealing. Such a phenomenon is of broader interest than its purely commercial implications, since normal metals and alloys exhibit a decrease in electrical resistivity - and hence in resistance - after annealing.

The residual resistivity of a pure metal arises from the presence of impurities and deviations from the idealised crystal structure due to features such as dislocations, grain boundaries and vacancies. Annealing results in a decrease in the concentration of one or more of these features and a corresponding decrease in residual resistivity is expected. In the case of a binary alloy there is an additional contribution to residual resistivity from the presence of solute atoms and, in a concentrated alloy (where the electronic structure of the host metal is altered by the presence of the solute), a possible

contribution from the presence of a non-random atomic configuration or a second phase. The residual resistivity of a binary alloy may nevertheless be expected to respond to annealing in a similar manner to the resistivity of a pure metal, owing to a decrease in the concentration of lattice defects, provided that a change in atomic configuration or crystal structure does not occur at elevated temperatures. Thus the annealing of a homogeneous binary solid solution, in a concentration and temperature range in which phase changes are not predicted, normally results in a decrease in resistivity corresponding to the reduction in the number of lattice defects.

A significant increase in electrical resistivity after annealing was first observed in apparently single-phase binary alloys of transition metals such as iron, nickel and chromium; this effect in transition metal alloys has been associated with short-range order. The development of short-range order during annealing of a binary alloy may result in either an increase or a decrease in residual resistivity; such changes may however be difficult to resolve if they are of the same sign and order of magnitude as changes in resistivity associated with changing defect concentrations. In the above alloys the change in residual resistivity due to short-range order is both opposite in sign and greater in magnitude than any changes due to a decrease in defect concentration. Reports of the effect of annealing on resistance in palladium-tungsten and palladium-molybdenum suggest that a similar mechanism occurs in these systems, but a systematic investigation of the stability of structure and properties under heat treatment has not previously been undertaken.

The calculation of the electrical resistivity of transition metals and alloys presents a greater degree of complexity than similar calculations for simple metals, since the details of electronic structure and scattering probabilities required for such calculations do not lend themselves to simplifying approximations. Advanced techniques for accurate determination of the effect of ordering on electronic structure generally require lengthy computation; the electrical resistivity of palladium alloys is thus not readily predictable in the absence of experimental data. The effect of structural order on residual resistivity in binary alloys of transition metals has been investigated experimentally; however, alloys of palladium with other transition metals have received little attention. Theoretical analyses are in general based on simple-metal models and are of uncertain value in calculating such effects in transition metal alloys. In palladium-tungsten and palladium-molybdenum alloys then, the contribution to resistivity of changing degrees of structural order presents an additional variable in a

complex structure-property relationship for which there is not yet a comprehensive experimental data base.

In the work presented here, the relationship between electrical resistivity and structure has been investigated in alloys of palladium with tungsten and molybdenum, with particular attention to the reported anomalous resistance effect. In Chapter 2, an overview of factors which give rise to electrical resistivity is followed by a more detailed literature survey regarding the contributions to residual resistivity of defects and structural order, and the electrical resistivity of transition metals and alloys. The published properties of palladium, palladium-tungsten and palladium-molybdenum are then reviewed in order to assess the effect of tungsten and molybdenum solute additions on the properties of palladium. It is noted that a systematic study of the affect of annealing on the electrical resistivity of palladium-molybdenum alloys has not been reported; nor has the atomic configuration of these alloys been previously investigated. The experimental approach, presented in Chapter 3, has been to produce specimens by means of annealing fully cold-worked material to a variety of stages of recovery and recrystallisation. Determination of the effect of heat treatments on electrical resistivity requires that resistance changes are measured to a degree of accuracy not easily obtainable from commercially available instruments: for this reason a low-noise precision electronic apparatus has been specifically designed and constructed for the experimental procedures and accuracy requirements of the present work, and is described in detail. The structural evolution associated with resistivity changes has been investigated by means of metallography, transmission electron microscopy and microhardness measurements. The experimental results are presented in Chapter 4, and are grouped by experimental procedure in order to facilitate discussion of the effect of solute concentration on structure and properties. The response of palladium-molybdenum alloys to annealing, and the variation in properties with solute concentration, is shown to be very similar to that of palladium-tungsten. In Chapter 5, the resistance changes measured after annealing are considered with reference to mechanisms whereby such changes may come about in binary alloys; it is concluded that a transition to a state of structural order, occurring at elevated temperatures, is the only mechanism which offers an explanation for the anomalous resistance effects observed. The effect of annealing temperature on electrical resistivity and microhardness is discussed with respect to microstructure and solute concentration, and is used to determine the effect of annealing temperature on the degree of structural order developed by each alloy. On this basis the unusual dependence of properties on

annealing temperature exhibited by alloys of low solute concentration, reported here for the first time, is rationalised.

CHAPTER 2

LITERATURE SURVEY

The effect of annealing on the structure and properties of the palladium-tungsten and palladium-molybdenum systems has not yet been comprehensively investigated. In particular, the anomalous electrical resistance effect manifested by the palladium-rich alloys of these systems has received little attention in the published literature, although the phenomenon is well established in other binary transition metal alloys. In order to place this resistance effect in perspective, some background to electrical resistivity is presented in section 2.1 of this chapter, followed by a review of the effect on resistivity of dislocations, alloying additions and structural order for both simple metals and transition metals. In section 2.2 a review of the structure and properties of pure palladium is presented, followed by a detailed survey of the palladium-tungsten and palladium-molybdenum systems in section 2.3. A concise overview of the issues central to the present work constitutes the final section of the chapter.

2.1 ELECTRICAL RESISTIVITY OF METALS AND ALLOYS

The electrical resistivity of metals is a consequence of departures from perfect periodicity in the crystal lattice. A perfectly periodic lattice at 0K has zero electrical resistivity in the presence of an electric field. Real metals have a finite resistivity which arises from the scattering of conduction electrons by lattice defects and (above 0K) as a result of the thermal vibration of atoms. Assuming the scattering from different types of deviations from periodicity to be additive, the total resistivity ρ may be expressed by Matthiessen's rule:

$$\rho = \rho_0 + \rho(T)$$

The residual resistivity ρ_0 due to the presence of lattice defects, including impurities, may be considered to be temperature-independent provided that the concentration of such defects remains constant. The temperature-dependent or ideal resistivity $\rho(T)$ arises from the thermal vibration of atoms; the magnitude of the temperature dependence is dependent on the electronic structure of the metal.

The presence of lattice defects such as vacancies, dislocations, grain boundaries and impurities alters the periodicity of the lattice and hence provides scattering centres for conduction electrons, even in the absence of the thermal vibration of atoms. Although the contribution of defects to resistivity is independent of temperature, the *concentration* of defects is almost certain to exhibit some temperature dependence. Changes in the number of vacancies, dislocations or grain boundaries occur - in temperature ranges characteristic of the metal in which they are present - by means of vacancy diffusion and annihilation, recovery and recrystallisation. The residual resistivity, and hence the total resistivity, will change under such circumstances even though the temperature dependence of resistivity remains unaffected. Figure 2.1 shows a schematic diagram of the effect of such an annealing experiment on the electrical resistivity.

An additional contribution to the residual resistivity of a metal arises from the presence of impurities or alloying additions, owing to localised deviations from periodicity at the site of impurity or solute atoms. Although the concentration of solute atoms in an alloy is clearly independent of temperature, the atomic *configuration* may exhibit a temperature dependence as a result of a decrease or increase in the degree of structural order in the lattice. A change in ρ_0 is to be expected as a consequence of deviations from the random atomic configuration in an alloy.

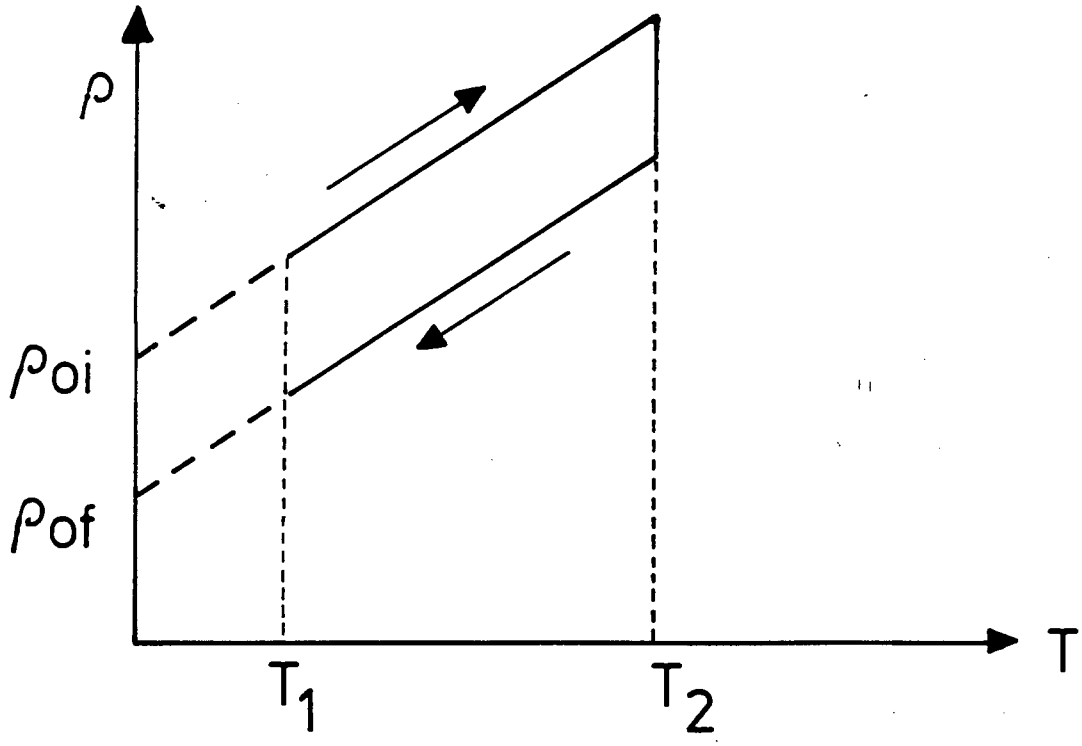

Figure 2.1: Idealised schematic diagram of the effect of annealing at T_2 on resistivity measured at temperature T_1, due to decrease in residual resistivity from ρ_{0i} to ρ_{0f}.

The addition of a small quantity of a second component to a pure metal, to form a dilute solid solution in which the electronic structure of the host metal remains unaltered, does not change the ideal resistivity of the host metal. At higher concentrations however, the electronic structure of the host metal undergoes changes; these changes are dependent on solute concentration, the electronic structure of the alloying addition and the atomic configuration of the alloy formed. The temperature dependence of resistivity of a concentrated alloy is therefore influenced by the presence of structural order in the lattice; since the degree of order may itself be significantly influenced by temperature, the temperature dependence of resistivity may show departures from linearity, as shown schematically in fig. 2.2.

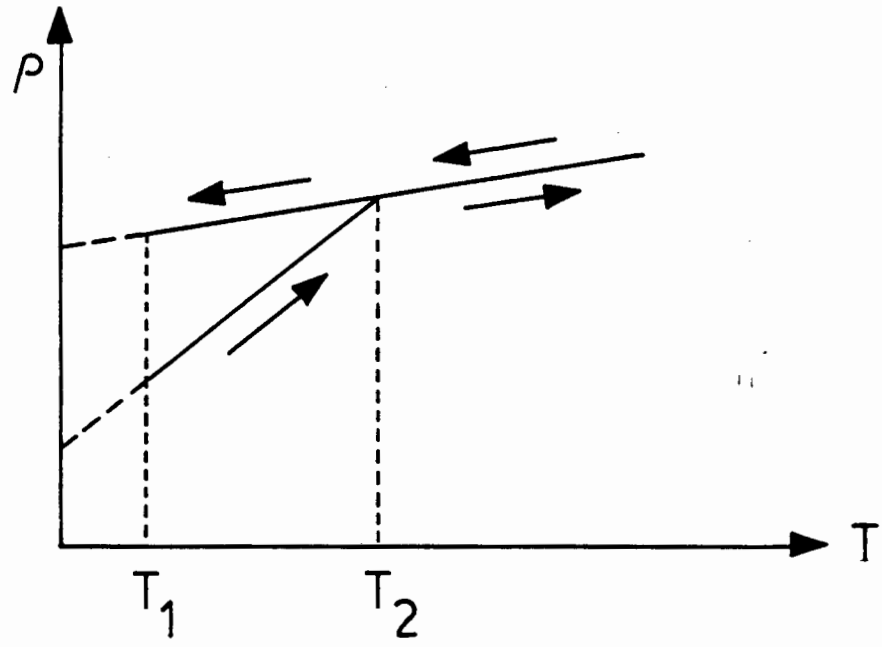

Figure 2.2: Idealised schematic diagram of the effect on resistivity measured at T_1, of a change in the temperature dependence of resistivity at T_2.

The electrical resistivity of metals is therefore dependent on electronic structure, microstructure and crystal structure. Microstructural imperfections and alloying additions give rise to the residual resistivity, which may be considered to be temperature-independent, whereas electronic structure determines the temperature dependence of resistivity. In concentrated alloys, both the residual and ideal resistivity may be affected by the development of structural order in the lattice. The present work concerns the effect on electrical resistivity of changes in microstructure and structural order in transition metal alloys. Published calculations of the electrical resistivity due to features such as lattice defects and ordering, however, are commonly based on the electronic structure of simple metals (with only s-like electrons at the Fermi surface) and their alloys. This allows the utilisation of simplifying assumptions such as s-s electron scattering, free or nearly free electrons and the Born approximation. Although in general these assumptions are inappropriate for transition metals and alloys, the simple-metal models allow a qualitative understanding of the processes which determine the electrical resistivity.

2.1.1 DISLOCATION-SPECIFIC RESISTIVITY

The electrical resistivity of metals is observed to increase after the introduction of dislocations by cold deformation. In 1949 Koehler[1] published a pioneering analysis of the electrical resistivity of polycrystalline copper due to the scattering of electrons by dislocations. The value obtained was, however, far too low to account for the measured increase in resistance with cold work. The published literature in this field since Koehler's work has been characterised by considerable debate, and to date accord has not been reached regarding a theoretical approach although calculated and experimental values are in improved agreement.

Early treatments of dislocation-specific resistivity (DSR, the residual resistivity per unit dislocation density) were hampered experimentally by difficulties such as the determination of dislocation densities, which were generally estimated from stored energy measurements or sample dilation, and the relative contribution to resistivity of point defects such as vacancies and impurities, which may be of the same order as DSR[2,3]. Theoretically, the major difficulty lay in the choice of a scattering mechanism on which to base calculations of DSR. Koehler considered electron scattering from long-range atomic displacements brought about by the presence of parallel edge dislocations. More rigorous calculations on the basis of strain fields by workers such as Mackenzie and Sondheimer[4], Landauer[5] and Dexter[6,7] failed to produce an improved agreement between theory and data. Hunter and Nabarro[8] considered both dilation of the lattice due to dislocations and the associated shear strains by using a perturbing potential proportional to elastic strain, concluding that large-angle scattering from the core of the dislocation, and not the long-range strain field, was predominant. Harrison[9] subsequently examined the spatial variation of strains in the lattice due to dislocations and concluded that shear strains made a negligible contribution to the scattering of conduction electrons, confirming that scattering from the core region of the dislocation, where Hunter and Nabarro's approximation was inappropriate, was predominant. Harrison's DSR analysis[10], later refined by Bhatia and Gupta[11], represented the dislocation core by a hollow cylinder, of atomic radius, with an associated square-well potential. Calculated resistivities were in better agreement with experimental data but too low to account for measured DSR.

Both Harrison's and Bhatia and Gupta's value for the volume of the hollow dislocation core - one atomic volume per atomic length - was however unrealistically high, and a more accurate volume removes the theoretical value still further from measured DSR. Broom[12] and Howie[13] suggested that the discrepancy between theory and experiment might be due to the resistance of the stacking faults associated with partial dislocations. Clareborough et al[14], however, found that metals of widely differing stacking fault energies showed similar dislocation-specific resistivity, and hence concluded that stacking faults did not make a significant contribution to DSR. Basinski et al[15] based a calculation of the relationship between DSR and ideal resistivity on a comparison of the deformation of the lattice due to a dislocation and the deformation due to thermal vibrations, assuming that the resistivity in both cases was proportional to the mean square displacement of atoms. Improved agreement with experimental data for DSR was obtained; comparison with calculations based on lattice dilation, stacking faults and the hollow dislocation core suggested the dominance of scattering from atomic displacements near the dislocation core.

The theoretical treatments of dislocation-specific resistivity which followed Koehler's work thus varied widely. An improvement in the experimental data base in more recent times - in particular more accurate determination of dislocation density, orientation and configuration by means of transmission electron microscopy - allowed comparison of theory with more realistic values for DSR. Early analyses commonly assumed or calculated an anisotropy in resistivity relative to dislocation orientation; experimental measurements of resistivity such as those performed on deformed single crystals of aluminium by Sosin and Koehler[16], and on single crystals of copper by Basinski et al[17,18], however, revealed no significant anisotropy in DSR. Conversely another common assumption, of the independence of dislocations as scattering centres, was experimentally firmly established[e.g.19,20,21]. The measured isotropy of DSR and the linear relationship between resistivity and dislocation density suggested that long-range strain fields were relatively unimportant and hence lent weight to theories based on scattering close to, but not necessarily confined to, the disocation core. Recently Watts[22] calculated the resistivity produced by the long-range strain field of a dislocation, finding it to be negligible in a region greater than a few Burger's vector lengths from the dislocation.

The de Haas-van Alphen effect is a useful tool for investigation of the scattering of conduction electrons, since it is sensitive to both small- and large-angle scattering of electrons; there has however been some debate regarding the sensitivity of electrical resistivity to scattering angle. An argument has been made for the predominance of small-angle scattering of electrons by dislocations by Rowlands and Woods[23] on the basis of low-temperature experimental data which suggests anisotropic scattering of electrons at the Fermi surface. Kaveh and Wiser[24,25,26], who assume small-angle scattering and a marked anisotropy of scattering, have concluded that the relationship between dislocation density and resistivity is non-linear at low dislocation densities. The dominance of large-angle scattering in DSR was however extablished by Chang and Higgins[27] and Basinski et al[28] on the basis of de Haas-van Alphen effect studies of dislocated copper; additional experimental evidence published by Trattner et al[29] also indicates that large angle scattering is dominant in DSR. Watts[30] has published an analysis of the scattering from atomic displacements at a dislocation, showing that large angle scattering can account for the measured values of DSR.

Brown[e.g.31,32] has suggested the presence of scattering resonances at or near the Fermi energy in scattering from the hollow dislocation core. The solution of the transport equation for electrons in a deformed lattice on this basis allows for complex Fermi surfaces but assumes negligible interband scattering, although a qualitative discussion of this effect is given[33]. The resulting expression for the dislocation-specific resistivity of metal gives values in reasonable agreement with experiment for simple metals, but as might be expected differs considerably with experiment for transition metals. An investigation of the effects of scattering resonances on the de Haas-van Alphen effect[34] met with limited success.

A calculation of DSR which takes into account the underlying crystal structure of the metal in which the dislocation occurs has been published by Watts[35]. By considering the structure factor of a metal containing dislocations, it is shown that anisotropic arrays of dislocations can give rise to fairly isotropic resistivity, which is in agreement with experimental observations. This approach also gives results which account for the different DSR values measured in different

metals[30]. In a detailed monograph, Watts[36] considers the complementary information provided by the electrical resistivity and the de Haas-van Alphen effect (in which scattering from the long-range strain field is predominant) of dislocated metals to assess the likely origins of dislocation-specific resistivity; the conclusion reached is that any successful model must take account of atomic displacements near the core of a dislocation.

Analyses of the electrical resistivity of dislocations have been extended to compute the resistivity of grain boundaries for which a dislocation model is appropriate. Brown[37] has calculated the resistivity per unit grain boundary area by assuming that scattering from the dislocations which constitute the grain boundary is predominant. The values for grain boundary resistivity calculated on this basis are in reasonable agreement with experimental data for several metals[37,38].

2.1.2 RESISTIVITY DUE TO STRUCTURAL ORDER

An analysis of the residual resistivity of alloys was first published by Nordheim[39] in 1931. Considering only random binary alloys of elements of similar atomic number, he proposed that an alloy be treated as a periodic structure, with a potential equal to the mean potential of the constituent atoms. Under these conditions, at a given lattice site conduction electrons would undergo scattering due to the difference between the mean potential and the actual potential of an atom at that site. The total probability of scattering is obtained by summing the probabilities of scattering from each type of atom; the residual resistivity ρ_0 hence shows a parabolic dependence on concentration. Nordheim's calculation did not take into account the effect on the residual resistivity of deviations from a random atomic configuration such as the presence of long- or short-range order (in which the number of unlike nearest neighbours exceeds the random probability) or the clustering of like atoms. The effect of structural order on residual resistivity may be considerable, as illustrated in fig. 2.3 which shows local minima in the resistivity of copper-gold alloys at compositions corresponding to the long-range ordered structures Cu_3Au and CuAu.

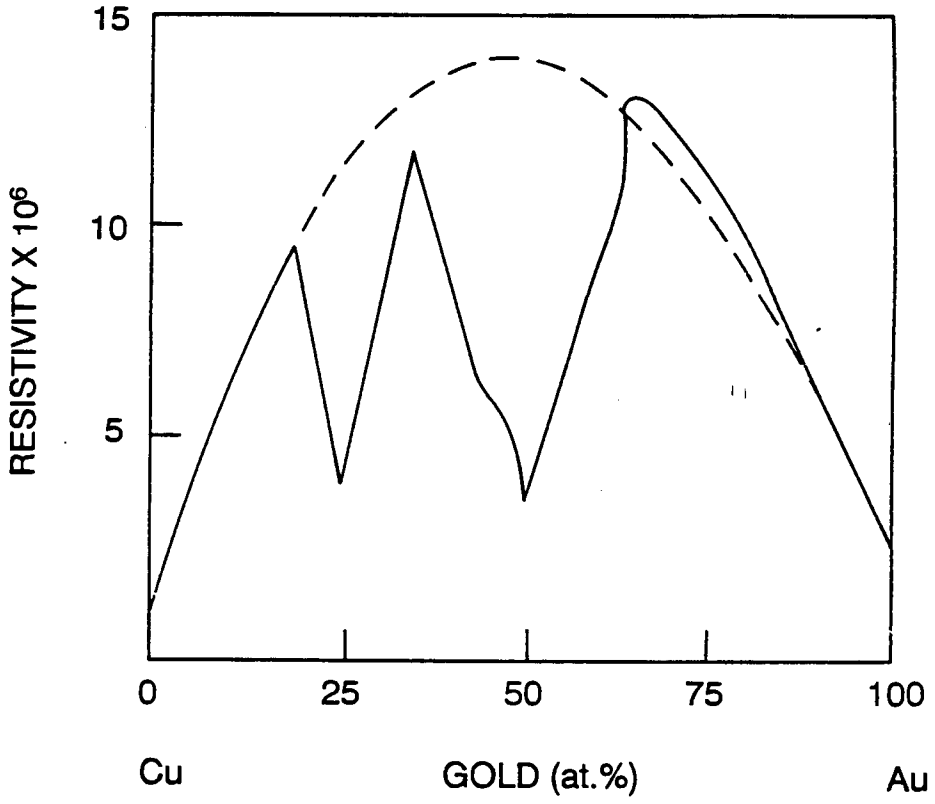

Figure 2.3: Graph of resistivity vs. composition for random (dashed curve) and ordered (full curve) copper-gold alloys (after Barret[40]; resistivity units not given).

The degree to which the number of unlike atomic nearest neighbours exceeds the random probability in a binary alloy may be expressed by an order parameter. Bragg and Williams[41] introduced a long-range order parameter *S*, which ranges in value between unity (perfect long-range order, with only A atoms on A sites and B atoms on B sites) and zero (random site occupation). Cowley[42] later defined short-range order parameters

$$\alpha_i = 1 - (p^i_{AB}/c_B)$$

where p^i_{AB} = probability of finding a B atom in the ith coordination shell
c_B = concentration of B atoms

to express the interaction between an (A) atom and the shells of atoms surrounding it, so that $\alpha_i = 0$ for complete randomness and $\alpha_i < 0$ for an excess of unlike neighbours, or short-range order. Cowley's short-range order parameter was used by Flinn[43] in an analysis of the energy of a binary solid solution, leading to an electronic theory of local order which predicted short-

range order for alloys with electron/atom ratios of about one, and clustering for electron/atom rations of between two and three. Hall[44] also published an extension of Nordheim's work, taking into account order of any range, using Flinn's notation[43] for the Cowley order parameter.

Gibson[45] published an analysis of the effect of short-range order on residual resistivity in a binary alloy, based on Nordheim's work[39] and using Cowley's notation[42]. Considering the effect of ordering on the structure of Brillouin zones in alloys, he concluded that changes in ρ_0 would arise from the resulting alterations to the Fermi surface and current carrier velocities, and hence that ρ_0 depended on the relative positions of the Brillouin zone boundaries and the Fermi surface. The development of short-range order would accordingly be accompanied by either a decrease in ρ_0 (when the Fermi surface and Brillouin zone boundaries are in close proximity in the random lattice) or an increase in ρ_0 (when the Fermi surface and Brillioun zone boundaries are in close proximity in the ordered lattice).

Asch and Hall[46] calculated the residual resistivity due to short-range order in a binary alloy on a quantum-mechanical basis, taking into account the effect of short-range ordering on the volume enclosed by the Fermi surface owing to changes in lattice parameter and the number of conduction electrons. The calculated residual resistivity depended on the degree of short range order, composition and the valency difference between the constituent atoms. Katsnel'son and Shevchuk[47] used Asch and Hall's formalism to perform numerical calculations, concluding that an increase in resistivity as a result of annealing is to be expected in transition metal alloys, containing 0.4 - 0.6 conduction electrons/atom.

Wang and Amar[48] developed a pseudopotential theory of the residual resistivity of binary alloys as a function of short-range order and showed that the resistivity could be expressed as a linear combination of the Cowley parameters. Rossiter and Wells[49] calculated the residual resistivity of binary alloys in terms of the degree of short range order, composition and the number of conduction electrons. The results showed the sign of the change in resistivity due to an increase in ordering to be dependent on the number of conduction electrons per atom.

Both the above analyses utilised the pseudopotential method, which replaces the exact electron wavefunction with planewave electron states and the lattice potential V(**r**) with a weak nonlocal pseudopotential W(**r**). W(**r**) may be expressed in terms of Fourier components W(**q**), which in turn may be expressed by:

$$W(\mathbf{q}) = w(\mathbf{q})S(\mathbf{q})$$

where	$\mathbf{q}$	=	$\mathbf{k} - \mathbf{k}'$	is the scattering vector,
	$w(\mathbf{q})$	=	$\langle \mathbf{k}+\mathbf{q} \vert w(\mathbf{r}) \vert \mathbf{k} \rangle$	is the form factor,
and	$S(\mathbf{q})$			is the structure factor.

The form factor w(**q**) depends on the internal structure of the atoms present and the structure factor S(**q**) depends on the configuration of the atoms. In a random binary alloy the structure factor has a parabolic dependence on solute concentration, leading to the parabolic dependence of resistivity on concentration predicted by Nordheim[39]. In alloys which deviate from a random atomic configuration, the deviation lattice structure factor may be expressed in terms of the Cowley[42] parameters (referred to hereafter as the Warren-Cowley parameters) α_i:

$$|S^d(\mathbf{q})|^2 = (1/N)\,\Sigma_i c_i \alpha_i \sin(qr_i)/(qr_i)$$

The pseudopotential analyses resulted in expressions for ρ_{SRO} of the same general form as the formulation of Rossiter[50]:

$$\rho_{SRO} = C c_A c_B \Sigma\, c_i \alpha_i Y_i$$

where	C	=	constant
	c_A	=	atomic fraction A
	c_B	=	atomic fraction B
	c_i	=	no. of atoms in i_{th} shell at distance r_i from origin
	α_i	=	Warren-Cowley parameter

and $\quad Y_i = \int_0^{2k_F} |\langle \mathbf{k}+\mathbf{q} | w^d(\mathbf{r}) | \mathbf{k} \rangle|^2 q^3 [(\sin qr_i)/qr_i]\, dq$

Thus if the α_i and Y_i are of the same sign, ρ_{SRO} is positive; if they are opposite in sign, ρ_{SRO} is negative. Since α_1 is negative for short-range order, a positive contribution to resistivity (from the first co-ordination shell) will result if Y_1 is negative. Figure 2.4 shows Y_i as a function of $2k_Fr_i$ (where k_F is the magnitude of **k** at the Fermi surface) using a screened Coulomb scattering potential with screening parameter $Q = 2.5k_F$, where the integral has been normalised to unity at R = 0[49].

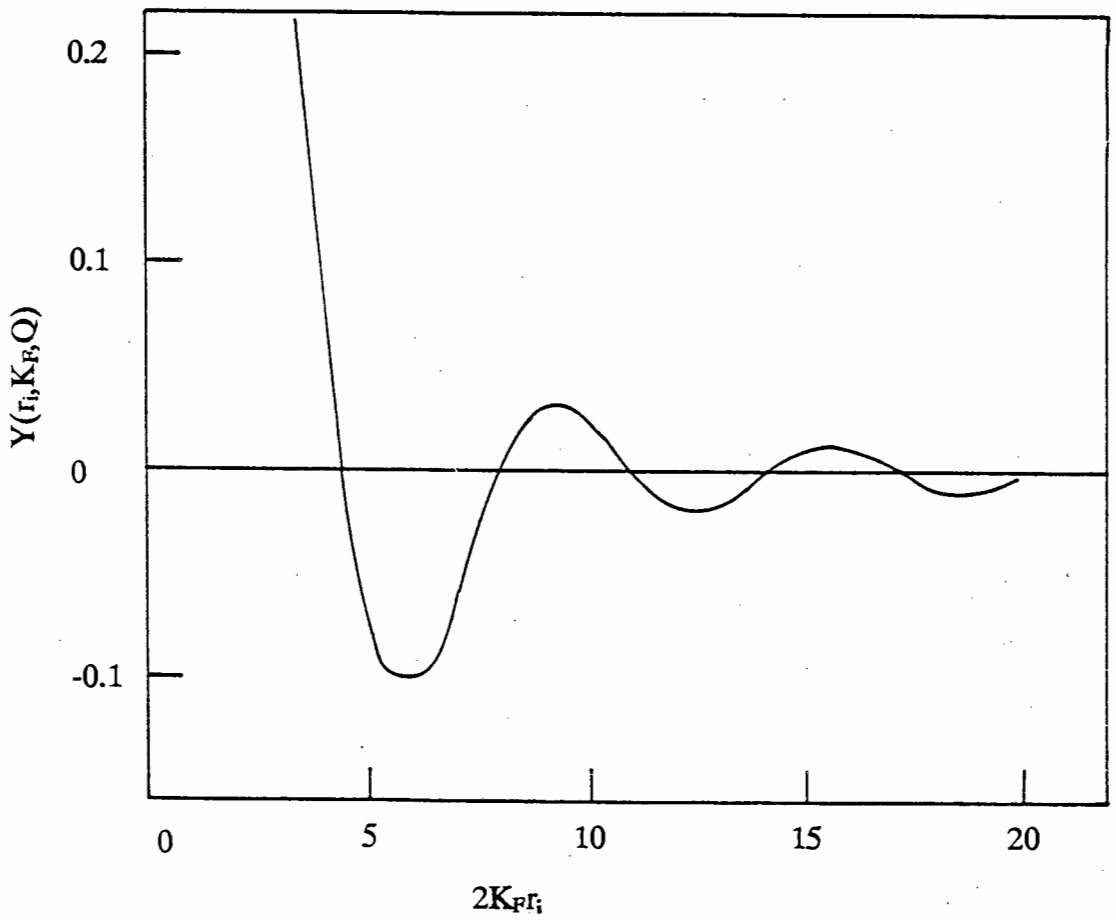

Figure 2.4: The integral Y_i as a function of $2k_Fr_i$ (after Rossiter and Wells[49]).

It may be seen that Y_i changes sign at certain critical values of $2k_Fr_i$, which is in turn related to the number of conduction electrons per atom, n, by the relationship:

$$n = a_0^3 k_F^3 / 12\pi^2$$

and by the dependence of r_i on a_0 (e.g. $r_1 = a_0/\text{root2}$ for fcc crystals).

Rossiter and Wells' analysis[49] predicted an increase in resistivity with increased short-range order for alloys with about one conduction electron per atom. This conclusion was later supported by a computer simulation of conduction electron scattering, by the same authors[51]. The theoretical analysis[49] showed good agreement with experimental results using a screened Coulomb potential; although this choice of potential gave rise to some criticism[e.g.52,53], substitution of alternative potentials showed the calculation not to be sensitively dependent on the form of the scattering potential[e.g.49]. Vigier and Pelletier's[52] calculation of the influence of short-range order on resistivity and thermo-electric power predicted a proportionality between variations in resisitivity and thermo-electric power; theoretical calculations of ρ_{SRO} however showed a strong dependence on the scattering potential used, only a point ion potential giving good agreement with experimental results.

Experimental evidence has shown the theoretical formalism of Rossiter and Wells[49] to be in good agreement with experimental results where both the short-range order parameters and resistivity have been measured[e.g.54,55,56,57]. There is general agreement that ρ_{SRO} (the resistivity due to short-range order) is linearly dependent on the short-range order parameters, and hence on the degree of short-range order. A factor which must however be taken into account is that the atomic configuration of an alloy may not show short-range order in the statistical (Cowley) sense. Rossiter[50] distinguishes three different types of short-range order, where atomic correlations are defined to be "short-range" if they are smaller in extent than the conduction electron mean free path Λ: homogeneous (statistical) short-range order, heterogeneous short-range order (microdomain model) and heterogeneous short-range order (antiphase domain model). The size of the ordered regions is a critical factor for resistivity due to heterogeneous short-range order: for alloys exhibiting an increase in resistivity as a result of the development of ordered regions, a maximum in the resistivity is observed, followed by a decrease in resistivity with increasing order. Rossiter and Wells[51,58] showed that this maximum occurred when the size of the ordered regions became comparable with Λ, at which point the lattice potential within the ordered regions and at the boundaries must be

taken into account in calculating resistivity. The decrease in resistivity with increasing size is then due to the decrease in total boundary area. Hillel et al[53] argued that this resistivity decrease was related to the increasing anisotropy in Bragg scattering and consequently in the relaxation time. This controversy continued[e.g.59,60] until Hillel and Rossiter[61] showed both mechanisms to be important, the mean free path effect dominating for spherical zones and the anisotropy effect dominating for platelets.

The foregoing analyses are based on the electronic structure of simple metals and alloys: in transition metal alloys the effect of short-range order on residual resistivity is complicated by the dependence of electronic structure on local atomic configuration. Furthermore, the effect of short-range order on the temperature coefficient of resistivity, which is small and commonly neglected in simple metal alloys[62], may be significant in transition metal alloys. The standard theoretical formalisms are therefore not appropriate to palladium-rich alloys, as noted by Rossiter and Wells[49]. The resistivity of transition metals and alloys in general must therefore be covered before ordering effects in paladium alloys are considered.

2.1.3 RESISTIVITY OF TRANSITION METALS

The transition metals are characterised by partially filled d-bands in their electronic structure: the energy range of the conduction s-band overlaps that of the d-band, leading to the presence of both s and d electrons at the Fermi level. As a consequence, the approximations used to derive an expression for the electrical resistivity of simple metals - such as a spherical Fermi surface, free electron behaviour and weak scattering - are no longer valid. In simple metals, with only s electrons at the Fermi level, a spherical approximation to the Fermi surface may reasonably be employed; in transition metals, the additional presence of d electrons at the Fermi level results in a Fermi surface which has both s and d characteristics and may be too irregular to be approximated in this way. The scattering rate of an electron in the presence of an applied field is determined by the scattering potential V(r) of the lattice and by the availability of states into which it may be scattered: in simple metals, a constant potential (free electron theory) or smoothly varying potential (nearly-free electron

theory) may be used for solution of the Boltzman equation; and only s-s scattering is considered. In transition metals, account must be taken of the d band electrons, which may no longer simply be incorporated into a smoothly varying lattice potential. The energy states of the electron must take into account both the localised atomic states and the influence of the crystal lattice. This may be accomplished by using the "muffin tin" model which approximates the periodic field of the lattice as constant and free-electron like between spheres around the nuclei; within these spheres the potential is a spherically symmetric atomic potential. This model is consistent with the behaviour of many transition metals; however, it presents difficulties in the construction of an electron wavefunction which is valid both inside and in between the "muffins". Calculations of the electronic structure of transition metals commonly make use of the augmented plane-wave (APW) or Korringa-Kohn-Rostoker (KKR) methods with the muffin tin potential[63]. The APW method matches atomic core wavefunctions to plane-wave wavefunctions at the surface of the muffins; these APWs are then summed to make a Bloch wave. The KKR method uses Green's functions to measure and sum the attenuation of waves scattered by the potential, in order to construct the wavefunctions in a self-consistent manner. Although computationally arduous, these methods have been successful in calculating the band structures of a number of transition metals.

The s-band in transition metals is broad with a low density of states, having a maximum of two electrons (of opposite spin) per atom. The narrow d-band, with a capacity of ten electrons per atom, has a high density of states. The scattering probability $P_{kk'}$ may be expressed by:

$$P_{kk'} = 2\pi/h \left| \langle \psi_{k'} | V(r) | \phi_k \rangle \right|^2 N(E_F)$$

where $\langle \psi_{k'} | V(r) | \phi_k \rangle$ is the scattering amplitude for transitions between an initial state ϕ_k and a final state $\psi_{k'}$, and $N(E_F)$ is the density of states at the Fermi energy into which electrons may be scattered[50]. Since $N_d(E_F) > N_s(E_F)$, there is a higher probability that electrons will be scattered into a d-state than an s-state. The strong scattering in transition metals means that the weak pseudopotential picture, which simplifies calculations involving simple metals, is no longer applicable.

It may be seen from the above that calculations of the resistivity of transition metals, requiring determination of the electronic structure, lattice potential and scattering probabilities, present a higher level of complexity than the same calculations for simple metals. Mott[64] suggested that conduction in transition metals might be regarded as due to the fast s-electrons, the d electrons having a reduced mobility owing to their greater effective mass. The s-electrons may be scattered into vacant s or d states; but s-d scattering, rather than s-s scattering, predominates. Since electrons scattered into the d-band make little further contribution to conduction, this type of interband scattering offers an explanation for the high resistivities of transition metals. However, the distinction between s and d electrons is not sharp in many transition metals, for which the above may be an oversimplification. Voloshinskiy and Savitskaya[65] analysed the effect of phonon-induced interband transitions on the electrical resistivity of transition metals; using a two-band model, they found that the resistivity was dependent on the occupation of the d-band. Allen et al[66] have published a survey of electron-phonon effects in transition metals; calculations of the electrical resistivity were performed by solving the integral form of the Boltzmann equation, using KKR computations and the rigid muffin-tin approximation (RMTA), which relies on an assumption that when an atom in a crystal is displaced its muffin-tin potential displaces rigidly with it. Calculated results are in excellent agreement with experimental data not only for resistivity but also for other transport coefficients.

White and Woods[67] reviewed the results of electrical resistance measurements of a number of transition metals, deducing values for the ideal resistivity between 10K and 295K; they found that in general the ideal resistivity could be understood on the basis of the relaxation time approximation except at very low temperatures.

2.1.4 RESISTIVITY OF TRANSITION METAL ALLOYS

Nordheim's model[39] for the resistivity of alloys assumed that the temperature coefficient of resistivity was independent of alloy composition. However, a subsequent investigation by Grum-Grzhimailo[68] found a generally linear

relationship between the reciprocal of the temperature coefficient of resistivity and composition, the influence of composition being marked in transition metal alloys. A further shortcoming of the Nordheim model is that it does not take into account the electronic structure of the constituent atoms, other than in formulating the mean lattice potential. In a transition metal alloy the presence of unfilled d-bands and differences in electronic structure between constituent atoms may lead to composition-dependent variations in both the number of current carriers and the availability of states into which they may be scattered, and hence to a more complex dependence of resistivity on concentration. In particular, the construction of an average lattice potential from the potentials of the constituent atoms will, for transition metal alloys, predict a single d-band, whereas in fact two separate d-bands are common (one associated with each constituent).

The latter shortcomings are to some extent taken into account by Mott's[64] rigid-band model, which allows for a change in occupation of states with a change in concentration, but assumes that the shape of the electron energy bands of the host metal is not changed by alloying. As atoms of the second component are added to the host metal, its Fermi level changes to accommodate the additional electrons. This may result in an increase or decrease in the density of states, depending on the shape of the energy bands of the host metal. However, the density of states curve for many concentrated transition metal alloys varies with concentration, necessitating the use of more specialized techniques such as the coherent-potential approximation.

The coherent-potential approximation (CPA) approximates the lattice surrounding a single atom by an effective medium in which the Wigner-Seitz sphere is imbedded; the potential of this medium is then determined self-consistently by a method such as the KKR method. Velicky[69] used the CPA to develop an expression for the electrical conductivity of disordered binary alloys using the Kubo formalism, which lends itself more readily to Green's functions methods than the Boltzmann equation, obtaining reasonable results. Lengthy computations are however in many instances required in order to obtain the details of electronic structure required for calculation of resistivity. Butler and Stocks[70] used a KKR CPA method to calculate the electronic structures of gold-palladium alloys in order to calculate the electrical resistivity and

thermopower, obtaining good agreement with experimental results. Johnson et al[71] have developed a fast computational method for calculating the self-consistent electronic structure of random solid-solution alloys, using a KKR CPA. Results of calculations performed for the copper-palladium system are in good agreement with experimental results.

2.1.5 STRUCTURAL ORDER IN TRANSITION METAL ALLOYS

Thomas[72] first reported that alloy systems containing at least one transition metal exhibit an anomalous increase in resistance after annealing. A decrease in slope of the resistance vs. temperature curve of binary alloys of metals such as iron, nickel and chromium was observed during heating; since this decrease was not completely reversed during cooling, a hysteresis in the curve developed which resulted in a higher room-temperature resistance than prior to heat treatment. This phenomenon was attributed by Thomas to an ordering phenomenon, the development of a "k-state" at elevated temperatures. The "k-state" was subsequently identified with the presence of short-range order[e.g.73,74,75]; on this basis Gibson's theory[45] provided a qualitative explanation for the observed resistivity anomaly. The theoretical formalism of Rossiter and Wells[49], although based on the usual simple-metal approximations, has been used to calculate the resistivity due to short-range order in alloys of transition metals such as nickel with some success[e.g.54,57]. Accurate determination of the effect of short-range order on the resistivity of transition metal alloys, however, may require the use of more complex techniques.

The nature of the CPA, in which a single site is decoupled from the remainder of the lattice, presents difficulties in the determination of short-range order effects, necessitating an extension of the theory to take atomic configuration into account. Plischke and Mattis[76,77] demonstrated the usefulness of the CPA in non-random alloys by using a modified CPA to investigate the stability of structural order in binary alloys, and showed the short-range order free energy to be lower than the long-range order free energy. Brouers et al[78] extended this model to establish the relation between the Bragg-Williams theory and the CPA to describe the order-disorder transition in alloys. Calculations to take account of short-range order using a single-site CPA Green's function also showed short-range order to be energetically stable. Moraga and Ramirez[79]

recently calculated two-particle Green's functions for electrons in alloys with short-range order using the CPA.

Although theoretical anaysis of the effect of ordering on transition metal alloys requires complex techniques, the detection by means of resistance measurements of short-range ordering may present less difficulty than in simple metals. In alloys exhibiting "k-state" behaviour the increase in resistivity due to short-range ordering is frequently sufficiently large to result in a nett increase in resistivity after annealing, even though the dislocation-specific resistivity decreases.

2.2 STRUCTURE AND PROPERTIES OF PALLADIUM

2.2.1 STRUCTURE

Palladium has a face-centred cubic (fcc) crystal structure with a lattice parameter of 3.89Å. It is a group VIIIC transition metal, with ten outer electrons. The atomic electron structure of palladium is $4d^{10}$; however, in the metal the broad s band overlaps the energy range of the d band; the Fermi level lies below the top of the d-band, and there are both s and d electrons at the Fermi surface. Early experiments with palladium-silver alloys led Mott[64] to conclude, on the basis of the rigid-band model, that the d band in palladium contained approximately 0.6 holes per atom and that the Fermi level accordingly lay near the top of the d-band, just above a peak in the density of states. Measurement of the low-temperature electronic specific heat[80] and the magnetic susceptibility[81], properties which are proportional to the density of states at the Fermi level, confirmed that palladium has an extremely high density of states at the Fermi level. Since the d-band is nearly full in palladium, Friedel[82] suggested that the high density of states would lead to a low Fermi energy for the fcc crystal structure. It is clear from the density of states curve, illustrated in fig. 2.5, that there is a high density of states at the Fermi level into which conduction electrons may be scattered.

The principal tool for experimental determination of the shape of the Fermi surface is the de Haas-van Alphen effect, which allows measurement of extremal cross-sections of the Fermi surface. Vuillemin[83] performed a detailed study of the de Haas-van Alphen effect in palladium, which showed the Fermi surface to consist of three parts: an approximately spherical electron surface due to the s band, a set of ellipsoidal hole surfaces and a further hole surface of intersecting cylinders (the jungle gym), due to the d bands. The volume of the electron surface was shown to be 0.36 electrons/atom, a much smaller value than Mott's[64]. Since palladium is a compensated metal (the ten outer electrons being shared between the s and d bands) the total number of holes is also 0.36/atom, practically all of which are contained in the jungle gym. A section of the Fermi surface of palladium is shown in fig. 2.6. The response of the Fermi surface to strain in the lattice has been investigated both theoretically (by the linear muffin tin orbital (LMTO) method) and experimentally (by the

de Haas-van Alphen effect) by Skriver et al[84] and Cavalloni et al[85]. The theoretical calculations were in reasonable agreement with experimental results, suggesting that the band-structure formalism used is adequate in spite of the complexity of the calculations. Calculations by Das et al[86] have shown that a 2% change in the lattice spacing may change the density of states at the Fermi level by approximately 10%. The band structure of palladium has been theoretically calculated by Anderson[87,88] using the relativistic augmented-plane-wave (APW) technique; by Gay et al[89] using a self-constistent local orbital method; and by Mueller et al[90] using the APW technique. Comparison with experimental results, including the measurements of Asonen et al[91], shows good agreement.

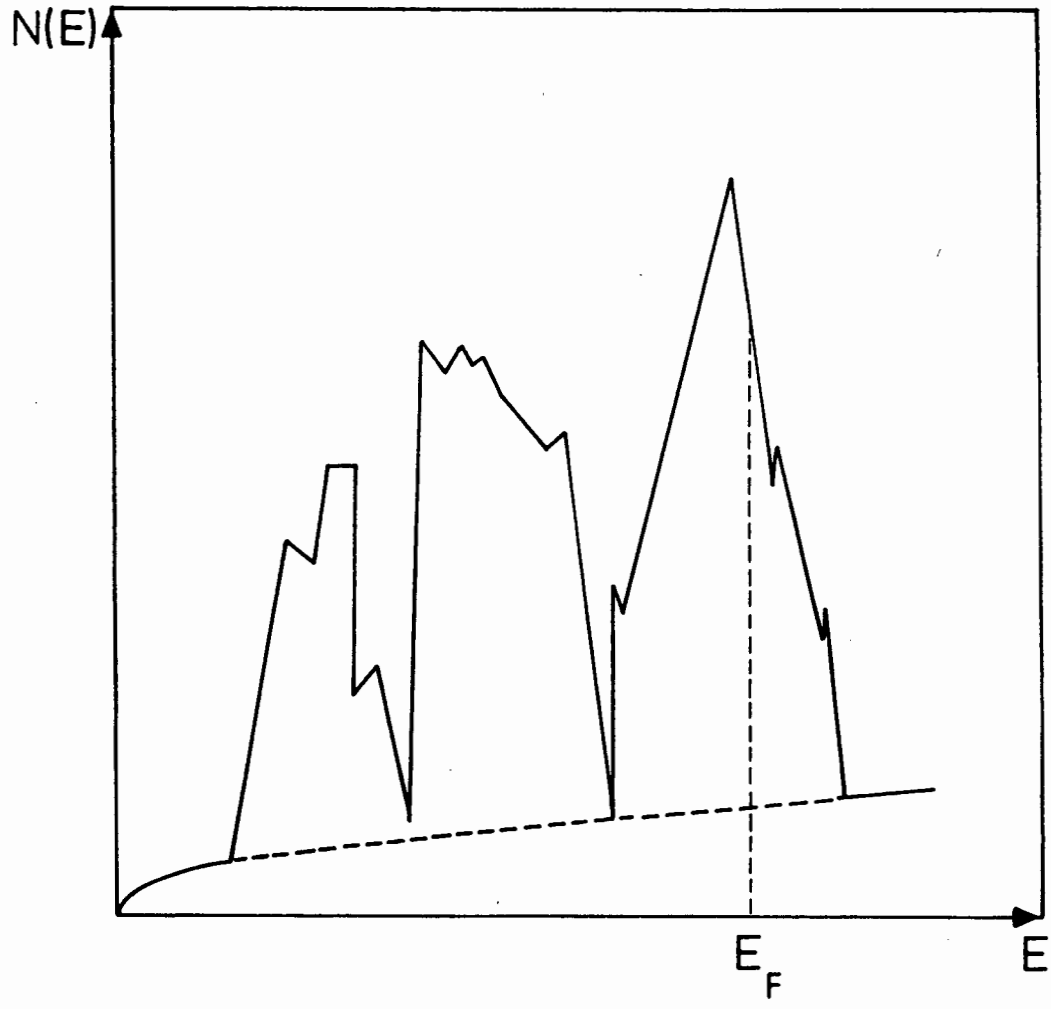

Figure 2.5: Idealised schematic diagram of density of states of palladium (after Dugdale[92]).

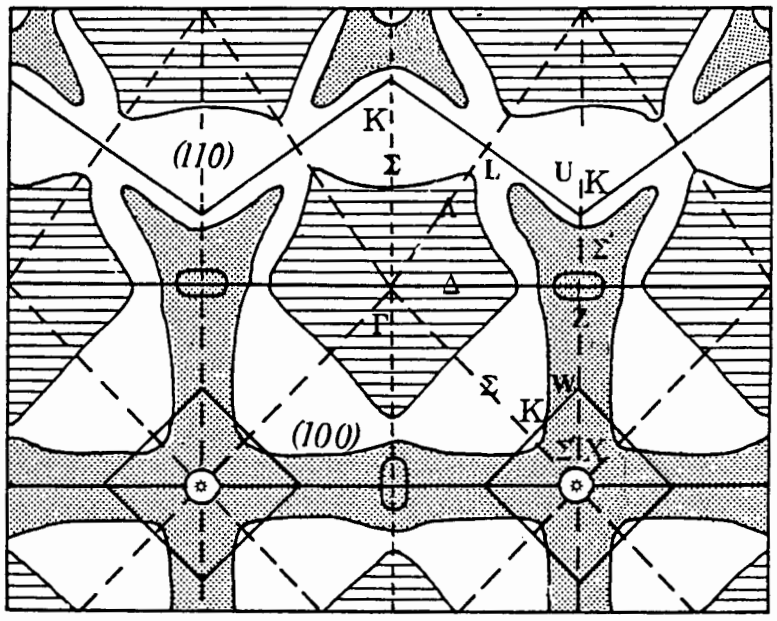

Figure 2.6: Cross section in the central (100) and (110) planes of the Fermi surface of palladium (after Anderson[88]).

2.2.2 PROPERTIES

Palladium has a large paramagnetic susceptibility even at room temperature, and a strong Stoner enhancement factor[90,93]. Highly paramagnetic, or "nearly ferromagnetic" materials exhibit behaviour similar to ferromagnets above the Curie point: such materials have been likened to ferromagnets with Curie points suppressed to just below absolute zero. Above the Curie temperature spin disorder scattering occurs due to spin fluctuations or paramagnons. At very low temperatures, the resistivity due to spin disorder scattering in a nearly ferromagnetic material such as palladium increases with temperature to a maximum before decaying asymptotically towards the spin disorder limit.

Superconductivity has not been experimentally observed in palladium, in spite of a high density of states at the Fermi surface and a phonon spectrum which suggests strong electron-phonon coupling[88] and hence a relatively high superconducting transition temperature. Calculations of the electron-phonon mass enhancement factor by Evans et al[94] give a lower value for the electron-

phonon mass enhancement factor than those obtained by Anderson[88]. The absence of superconductivity in palladium has been attributed to spin fluctuations due to a strong Stoner enhancement factor. Measurements by Strizker[95,96] have shown that palladium, when disordered by low-temperature irradiation, superconducts at T_c = 3K due to a reduction in magnetic susceptibility - and hence in spin fluctuations - relative to the annealed metal.

A general decrease in resistivity is observed in transition metals from left to right across the periodic table, owing to the progressive increase in occupation of the d-band and consequent decrease in vacant d-states into which s-electrons may be scattered. Palladium, however, has a higher resistivity than its neighbours. Pinski et al[97,98] have computed the electrical resistivity of palladium using a rigid muffin-tin approximation (RMTA) to the potential; they found good agreement with experimental data, demonstrating the applicability of such an approach. Interestingly, their results agreed qualitatively with Mott's s-d model: the fast electrons are on the electron surface, which has a low density of states while carrying almost all of the current; the slow electrons are on the jungle gym. Scattering is thus predominantly from the electron surface to the jungle gym.

Rowlands and Woods[99] and Zwart and Schroeder[100] have published measurements of the residual resistivity of palladium for varying degrees of plastic deformation. The values of ρ_0 vary between 1 and 25 nΩ-cm, but although details of deformation procedures are provided no dislocation densities, and hence no values for DSR, are quoted. The electrical resistivity of palladium has been measured at low temperatures by Schriempf[101] and Uher and Schroeder[102], and over the temperature range 100-500K by Powell et al[103]; the measured resistivity of palladium at 300K was 10.9μΩ-cm.

The thermoelectric power or Seebeck coefficient (S) of palladium has a large negative value at room temperature[93]. This is related to the strong energy dependence of the density of states at the Fermi level, and hence to the scattering probability. The linear or diffusion component of S may be approximately expressed in terms of the energy dependence of conductivity; since this decreases rapidly with increasing energy and electrons are carriers, S is negative.

2.3 PALLADIUM ALLOYS

2.3.1 STRUCTURE

Palladium is compatible (forming a solid solution with alloying additions of more than 1%) with a wide range of metals. The lattice parameters of several palladium alloys have been investigated by Kudielka-Artner and Argent[104], who noted a tendency for alloys to have lattice parameters closer to the lattice parameter of palladium than expected from Vegard's law. Fuggle et al[105] have investigated the electronic structure of a large number of palladium alloys by X-ray photoelectron spectra. Their results showed that electropositive alloying additions result in a decrease in the density of palladium d-states at the Fermi level and a narrowing of the palladium d-band. The CPA has been used to calculate the electronic structure of palladium alloys, showing good agreement with experiment[e.g.70,71].

The palladium-silver system has been extensively studied. A decrease in the density of states at the Fermi level with the addition of silver to palladium is consistent with Mott's rigid-band model[64], providing a quaitative expanation for electronic specific heat data. However, the form of the density of states curve shows a sensitive dependence on concentration. Norris and Myers[106] suggested, on the basis of a photoemission study of palladium-silver alloys, that the decrease in the density of palladium d-states with the addition of silver is the result both of electron transfer and structural disorder. Stocks et al[107] calculated the density of states for various compositions using the CPA, taking into account the sensitive dependence of the lattice parameter on composition, and obtained results consistent with experimental results.

Palladium forms ordered phases with a variety of alloying additions, including transition and rare earth elements[e.g108,109,110]. The presence of short-range order in palladium-noble metal alloys has been extensively investigated[e.g.111,112,113]. Short-range order parameters for palladium with transition metal additions platinum and cobalt were measured by Katsnel'son et al[114,115]. Deformed equiatomic palladium-platinum alloys were shown to develop short-range order after annealing at 500°C and 600°C, the degree of short-range order decreasing after annealing at higher temperatures[114]. Palladium 25 at.% cobalt

alloys were also found to develop short-range order after annealing, the short-range order parameters suggesting that small highly short-range ordered regions were present in a less ordered matrix[115].

2.3.2 PROPERTIES

The magnetic susceptibility of palladium is reported to fall rapidly with the addition of non-ferromagnetic alloying elements[104,116,117,118]. The residual resistivity of palladium is observed to increase particularly rapidly with the addition of transition metals such as vanadium and molybdenum[104,117,119]. A detailed study of electrical resistivity in nickel-palladium alloys by Schindler et al[120] showed s-d scattering to increase with palladium concentration, leading to an asymmetry in the resistivity vs. solute concentration curve. Coles and Taylor[121] investigated alloys of the palladium-silver system, calculating the electrical resistivity on the basis of the electronic structure derived from specific heat measurements. Their analysis, on the basis of Mott's[64] ideas, was in good agreement with experimental results.

The effect of alloying on the thermoelectric power of palladium has been investigated for a number of binary systems[117,119,122,123]. The addition of vanadium, molybdenum and ruthenium results in a large decrease in the (negative) thermo-emf of palladium; a (positive) sharp maximum is reported to occur in palladium-vanadium at a concentration of 8 at.% solute concentration[123].

The effect of short-range order on resistivity has been studied in several palladium alloys. An investigation of gold-palladium and copper-palladium alloys, which show an anomalous decrease in resistivity upon cold-working, was carried out by Kim and Flanagan[111,124,125]. A comparison between calculated and experimental values for the residual resistivity of annealed gold-palladium showed the presence of short-range order to influence s-d scattering at compositions below 55 at.% gold[111]. The anomalous decrease in resistivity due to plastic deformation in both the abovementioned systems was shown to occur as a result of a reduction in short-range order normally present in the alloys[125]. Resistivity was found to increase due to annealing, in spite of decreasing defect

concentrations due to recovery processes, as a consequence of the development of short range order[124]. Chen and Sivertson[126] investigated the effect of ageing on copper-palladium alloys and observed a decrease in resistivity which they attributed to short-range order. A calculation using Gibson's[45] method which predicted an increase in resistivity due to short-range order in the same system was assumed to be valid only for s-s scattering, and hence incomplete for transition metals. Haas et al[112,127] found short-range order to increase the resistivity of gold-palladium alloys, noting that Mathiessen's rule was approximately fulfilled. Westerlund and Nicholson[113] investigated the effect of plastic deformation on silver-palladium alloys, which also show a decrease in resistivity due to cold work. Measurement of the Hall constant indicated a significant increase in the effective number of conduction electrons as a result of cold work, suggesting that cold work disorders the short-range order present in these alloys after annealing.

The development of short-range order in alloys of palladium with platinum and with cobalt results in an increase in resistivity[114,115]. Katsnel'son et al[115] used the formalism of Asch and Hall[46] to calculate the change in resistivity due to short-range order, achieving only limited agreement with experimental results, and concluded that for palladium-cobalt alloys, the increase in resistivity is brought about by electron scattering from the boundary of small short-range ordered regions.

Note: several articles cited in this and the following sections (particularly those published in the *Russian Journal of Inorganic Chemistry* and *Fiz. Metal. Metalloved/Physics of Metals and Metallography*) are extremely brief, primarily consisting of reported results with little or no discussion.

2.3.3 THE PALLADIUM-TUNGSTEN SYSTEM: PHASE EQUILIBRIA AND STRUCTURE

The equilibrium phase diagram of the palladium-tungsten system was first published in complete form by Tylkina et al[128] and subsequently investigated by Goetz and Brophy[129]. The equilibrium diagram is of the peritectic type with two terminal solid solutions; no compounds are formed. At 1000°C tungsten is soluble in palladium up to 15.3 at.%; at the same temperature palladium shows a much smaller solubility in tungsten of 1.5 at.%. The face-centred cubic α-solid solution (tungsten in palladium) is separated from the body-centred cubic β-solid solution (palladium in tungsten) by a broad two-phase region. The addition of tungsten to palladium increases the melting point from 1552°C to 2100°C at the solubility limit. Figure 2.7 shows the equilibrium phase diagram of the palladium-tungsten system above 1100°C proposed by Tylkina et al.

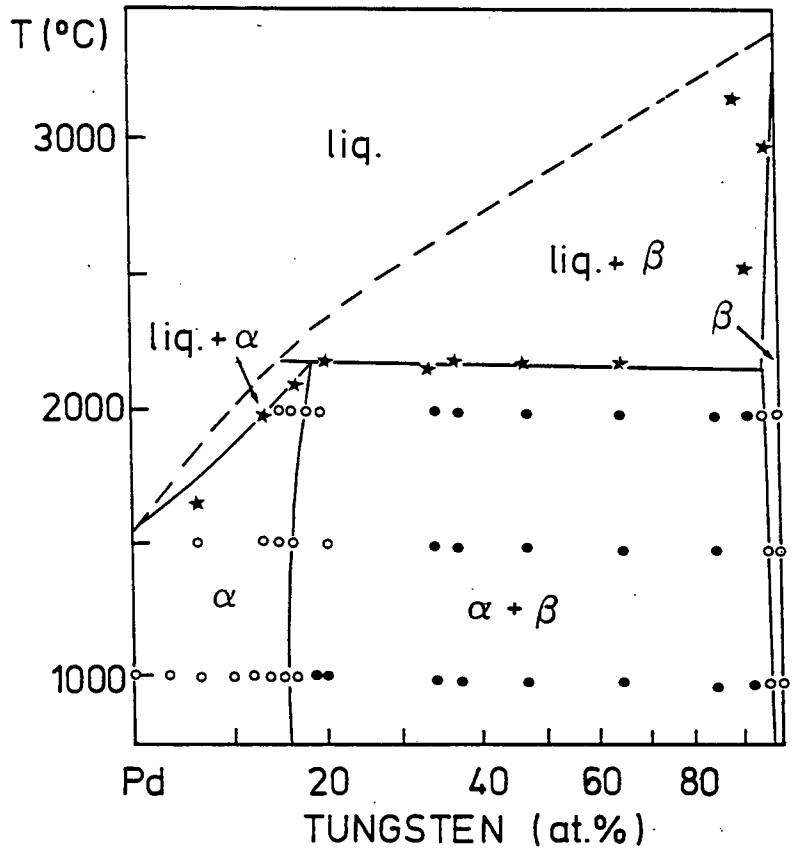

Figure 2.7: Equilibrium phase diagram of the palladium-tungsten system (after Tylkina et al[128]).

Khan and Raub[130] investigated the palladium-tungsten system below 1100°C and reported a much reduced solubility of 5 at.% tungsten in palladium at room temperature in alloys prepared by reduction with hydrogen at 500°C. The solubility however increased to 15 at.% tungsten after annealing at 700°C for 1000h; such alloys were found to consist of face-centred cubic α-solid solution only. On the basis of X-ray diffraction data the possibility of an intermediate phase between 20 at.% and 70 at.% tungsten was suggested[130]. Weaver and Ardell[131] reported the formation of the tetragonal ordered phase Pd_8W (D^{17}_{4h}) after proton irradiation of alloys containing 10 at.% and 18 at.% tungsten. Cheng and Ardell[132] found Pd_8W to be stable in irraditated palladium 10 at.% tungsten even after lengthy post-irradiation annealing at temperatures up to 735°C; however, similar heat treatment of this alloy in the unirradiated condition failed to result in the formation of Pd_8W. The authors accordingly suggested that Pd_8W may be an equilibrium phase which does not appear in the equilibrium phase diagram owing to its extremely slow rate of formation, which is accelerated under irradiation by the thermally activated migration of large concentrations of excess point defects such as vacancies. This enhances the rate of atomic diffusion and hence the rate of ordering[132].

The lattice parameter of palladium-tungsten alloys, shown in fig. 2.8, has been measured by several workers[129,130,133]. In the palladium-based solid solution range the lattice parameter decreases on the addition of tungsten, reaches a minimum at 10 at.% tungsten, then increases up to 15 at.% tungsten. The lattice parameter appears to vary little in the two-phase region above 15 at.% tungsten[130]. Luo[134] reported that the phase boundary of face-centred cubic palladium-tungsten may be extended by rapid solidification to a concentration of more than 40 at.% tungsten. Lattice parameter measurements of such alloys exhibit the above-mentioned minimum at around 10 at.%, followed by a monotonic increase up to 40 at%.

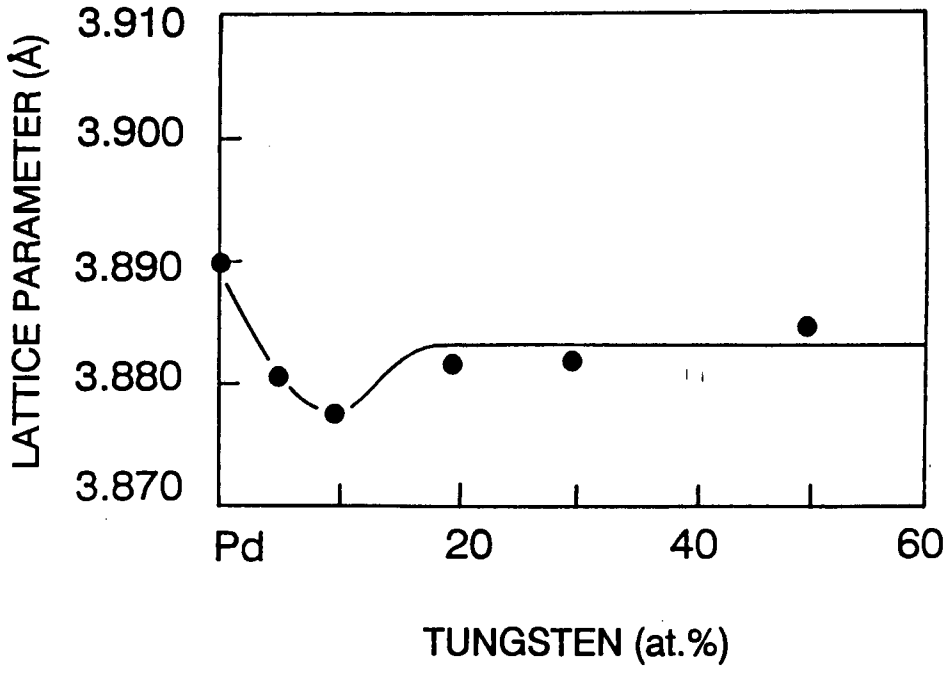

Figure 2.8: Graph of lattice parameter vs. concentration for palladium-tungsten (after Khan and Raub[130]).

Pure tungsten has a body-centred cubic (bcc) crystal structure and its atomic radius is slightly smaller than that of face-centred cubic (fcc) palladium. At concentrations below 15 at.% tungsten, however, the palladium-based solid solution is expected to be fcc and comparison of the Goldschmidt radii (CN12), rather than the atomic radii, of palladium and tungsten is appropriate in this composition range. On this basis the tungsten solute atoms are slightly larger than those of palladium[135], and it should be noted that under such conditions a disordered solid solution is expected to exhibit an increasing lattice parameter with increasing solute concentration. The lattice parameter of palladium-tungsten, however, decreases to a minimum at 10 at.% tungsten, increasing only with higher solute concentration. At all compositions below 15 at.% tungsten, the lattice parameter of palladium-tungsten is smaller than that of palladium[129,130,133]. The unexpected behaviour of the lattice parameter of palladium-tungsten led Babanova et al[136] to investigate the possibility of short-range order, for alloys in the concentration range 2 at.% - 12.7 at.% tungsten. An earlier work by Alimov and Katsnel'son[137] had identified short-range order in palladium 11.3 at.% tungsten on the basis of an increase in the intensity of a

diffuse X-ray scattering peak after annealing. Table 2.1 shows the short-range order parameters, assigned by Babanova[136] on the basis of X-ray diffraction data, of palladium-tungsten alloys after annealing for one hour at 900°C (note: see Appendix). The parameters α_i are negative in the first co-ordination sphere, indicating the presence of short-range order.

Table 2.1: Values of short-range order parameters α_i determined from the diffuse X-ray scattering intensity of alloys $Pd_{1-x}W_x$ (after Babanova et al[136])

Parameters α_i	x				
	0.026	0.062	0.077	0.093	0.127
α_0	0.01	0.02	0.01	0.008	0.08
α_1	-0.02	-0.07	-0.07	-0.122	-0.17
α_2	0	-0.07	-0.06	-0.09	-0.15
α_3	0	0.01	0.02	0.02	0.08
α_{1max}	0.03	0.066	0.083	0.101	0.145

2.3.4 THE PALLADIUM-TUNGSTEN SYSTEM: PROPERTIES

The addition of tungsten to palladium results in a significant decrease in magnetic susceptibility with solute concentration[116,138]. Khan and Raub[139] measured the magnetic susceptibility of palladium-tungsten over a wide concentration range, reporting a minimum in magnetic susceptibility at 12 at.% tungsten, as shown in fig. 2.9. The subsequent increase appears to decrease in slope at approximately 15 at.% tungsten, the boundary of the single-phase region. Klyuyeva et al[133] reported a slight decrease in the magnetic susceptibility of cold-worked palladium-tungsten after heat treatment at 900°C.

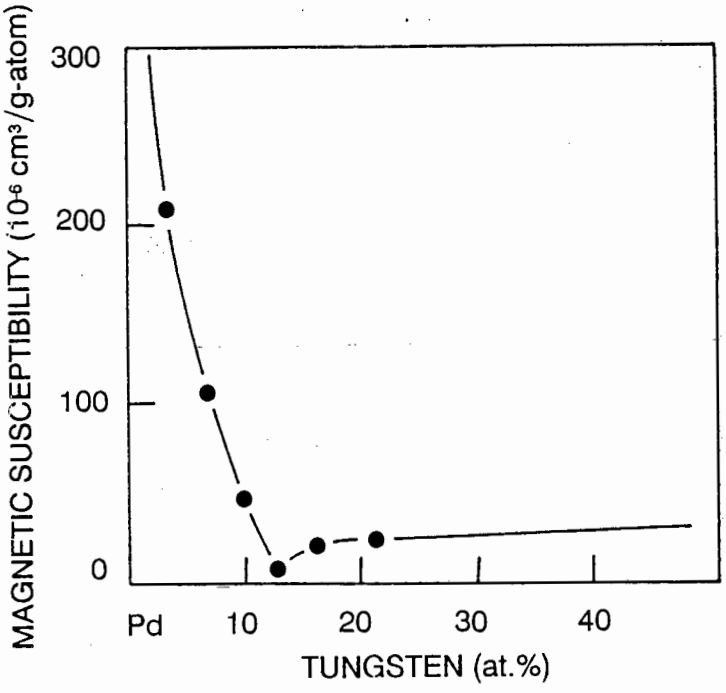

Figure 2.9: Graph of magnetic susceptibility vs. concentration for palladium-tungsten: filled circles denote cold-worked specimens (after Khan and Raub[139]).

The electrical resistivity of palladium-tungsten increases by an order of magnitude in the concentration range 0 at.% - 12 at.% tungsten[93,133]; the temperature coefficient of resistivity shows a decrease with increasing concentration in this range[133]. In terms of the rigid-band formalism tungsten, of valence six, might be expected to contribute sufficient electrons to fill the d-band of palladium at a concentration of about 6 at.% tungsten. However, the published resistance data are insufficient to determine any change in the dependence of resistivity on solute concentration in this composition range. Mes'kin et al[140] investigated the effect of annealing on palladium-tungsten alloys and reported the formation of a "k-state": after annealing at 700°C for one hour, alloys in the 8 at.% - 12 at.% tungsten concentration range showed an increase in resistance and a decrease in temperature coefficient of resistivity. (Khan and Raub[130] also noted a change in the slope of resistivity vs. temperature at about 700°C in palladium 15 at.% tungsten, but no data was presented). Mes'kin et al[140] concluded that the "k-state" resulted from the development of short-range order and the effect of this changed atomic configuration on the electronic structure of the atoms. Fig. 2.10 shows the effect of annealing at 700°C on the resistivity and temperature coefficient of

resistivity of palladium-tungsten alloys, as a function of composition. The change in these electrical properties is observed to reach a maximum at around 10 at.% tungsten.

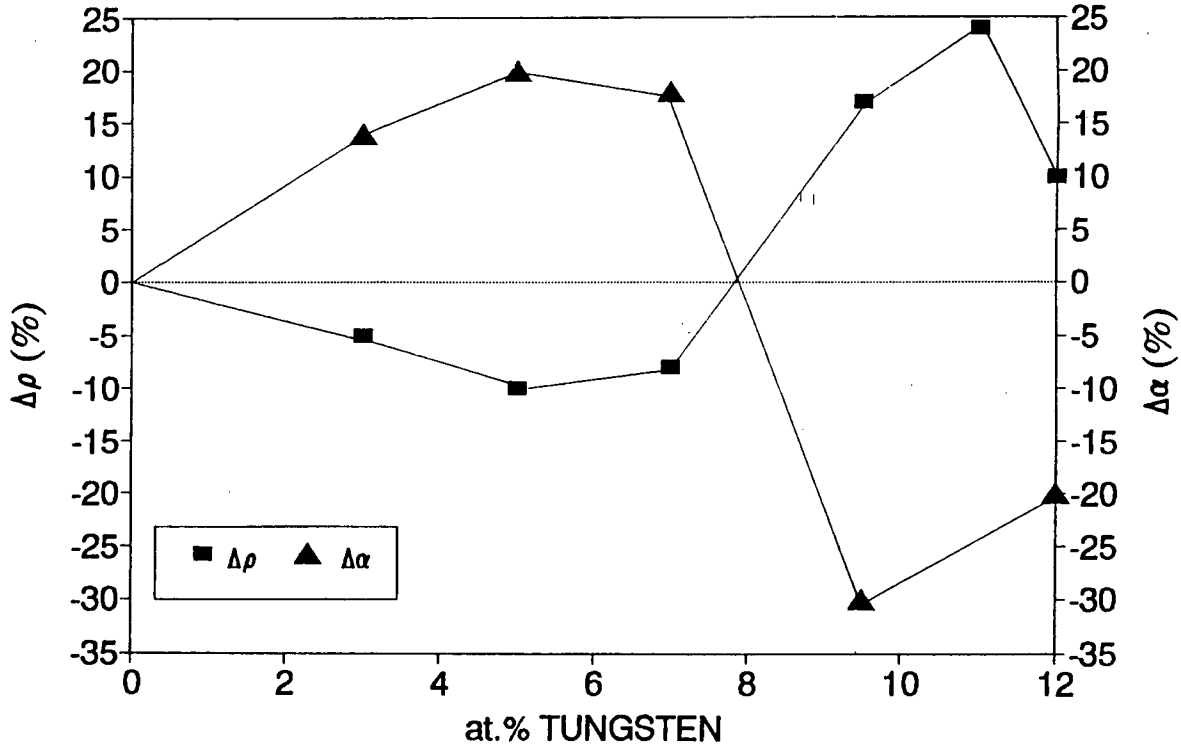

Fig. 2.10: Graph of change in resistivity and temperature coefficient of resistivity due to annealing at 700°C, vs. tungsten concentration (after Mes'kin et al[140]).

Klyuyeva et al[133] measured the resistance of palladium-tungsten alloys during continuous heating followed by cooling at 5°C/min, as shown in fig. 2.11. The decrease in the temperature coefficient of resistivity which occurs during heating results, after cooling, in an increased room-temperature resistivity. A decrease in the slope of the resistance vs. temperature curve occurs between 700°C and 800°C in alloys containing 9.3 at.% and 12.7 at.% tungsten; a further change in slope to a negative value may be observed above 800°C in the 12.7 at.% tungsten alloy. The authors noted that the increase in resistivity after annealing increased with increasing tungsten content[133]; and suggested that the presence of short-range order with a heterogeneous structure was responsible for the high resistivity of palladium-tungsten alloys.

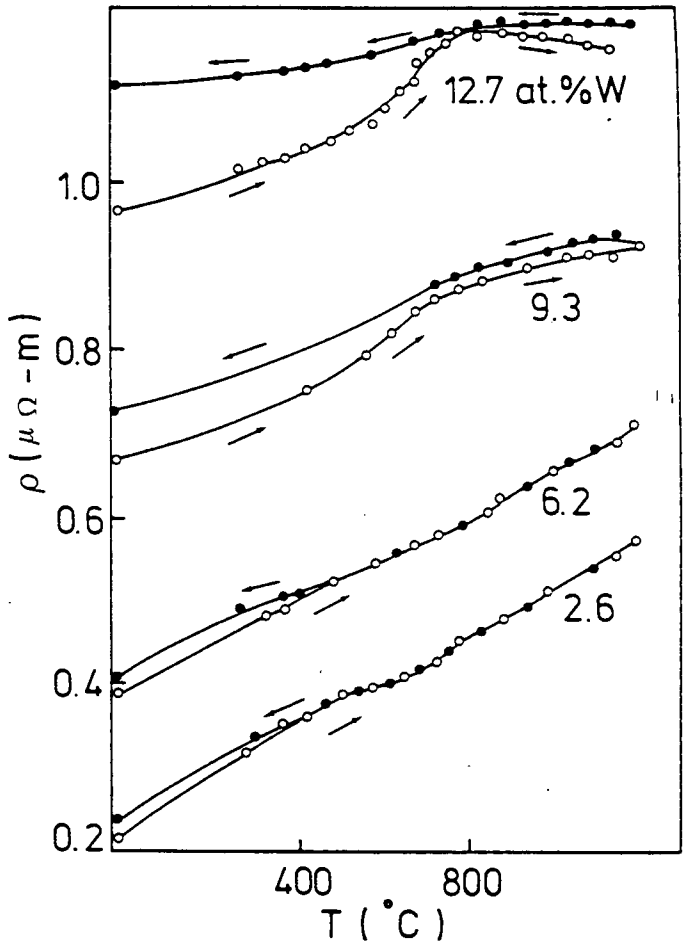

Figure 2.11: Resistance vs. temperature curves for palladium-tungsten alloys (after Klyuyeva et al[133]).

The absolute thermoelectric power (thermo-emf) of palladium-tungsten alloys, shown in fig. 2.12, has been measured by Tylkina et al[128] and by Mes'kin et al[140]. The negative thermo-emf of palladium is decreased by the addition of tungsten, reaching zero at a concentration of approximately 4 at.% tungsten. At higher solute concentrations an increase in positive thermo-emf is seen to reach a maximum at about 9 at.% tungsten, subsequently decreasing slowly to a small positive value at 20 at.% tungsten. Mes'kin et al[140] report that the thermo-emf of palladium-tungsten, in the range 8 at.% - 12 at.% tungsten, increases after annealing at 700°C; and note that this is roughly the concentration range in which an increase in resistivity is observed after annealing.

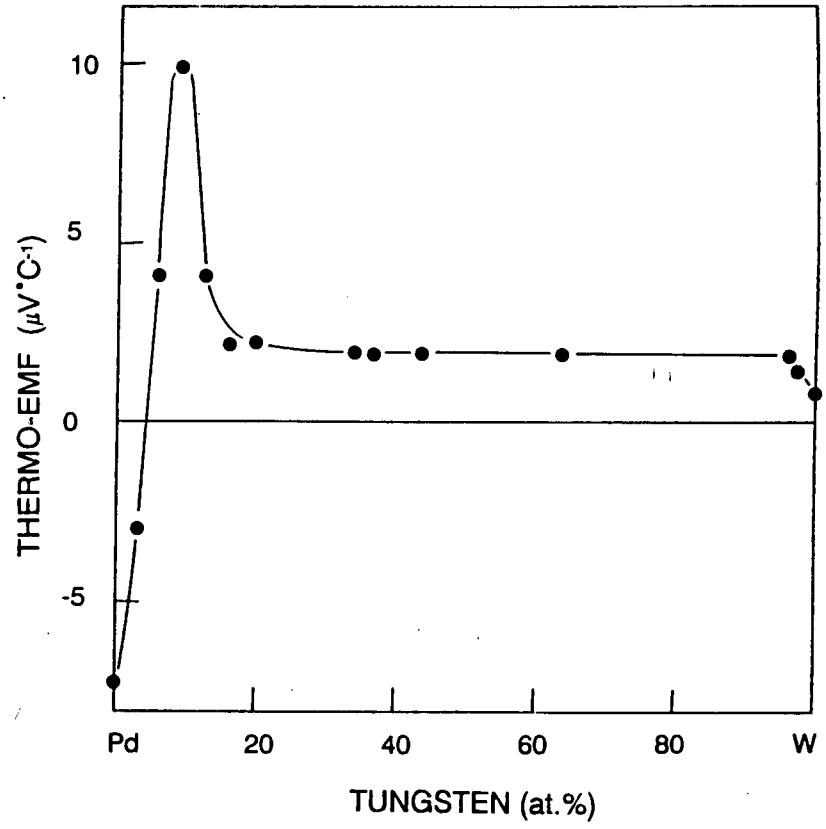

Figure 2.12: Graph of thermo-emf vs. concentration for palladium-tungsten (after Tylkina et al [128]).

The hardness and strength of palladium are reported to be greatly enhanced by the addition of tungsten[93,128,129]. The hardness of palladium-tungsten up to 20 at.% tungsten, measured by Goetz and Brophy[129] and shown in fig. 2.13, increases with increasing solute concentration up to 5 at.% tungsten, little further increase occurring up to the limit of the α-solid solution at 15 at.%. A steep linear increase in microhardness with tungsten concentration in the solid solution range has been measured by Tylkina et al[128]. Savitskii et al[93] report an increase in strength with tungsten concentration, with cold drawing and rolling properties remaining unaffected up to 15 at.% tungsten. Meskin et al[140] investigated the effect of annealing on the microhardness of palladium 12 at.% tungsten; the results show a small increase in hardness to occur after annealing in the range 600°C - 700°C.

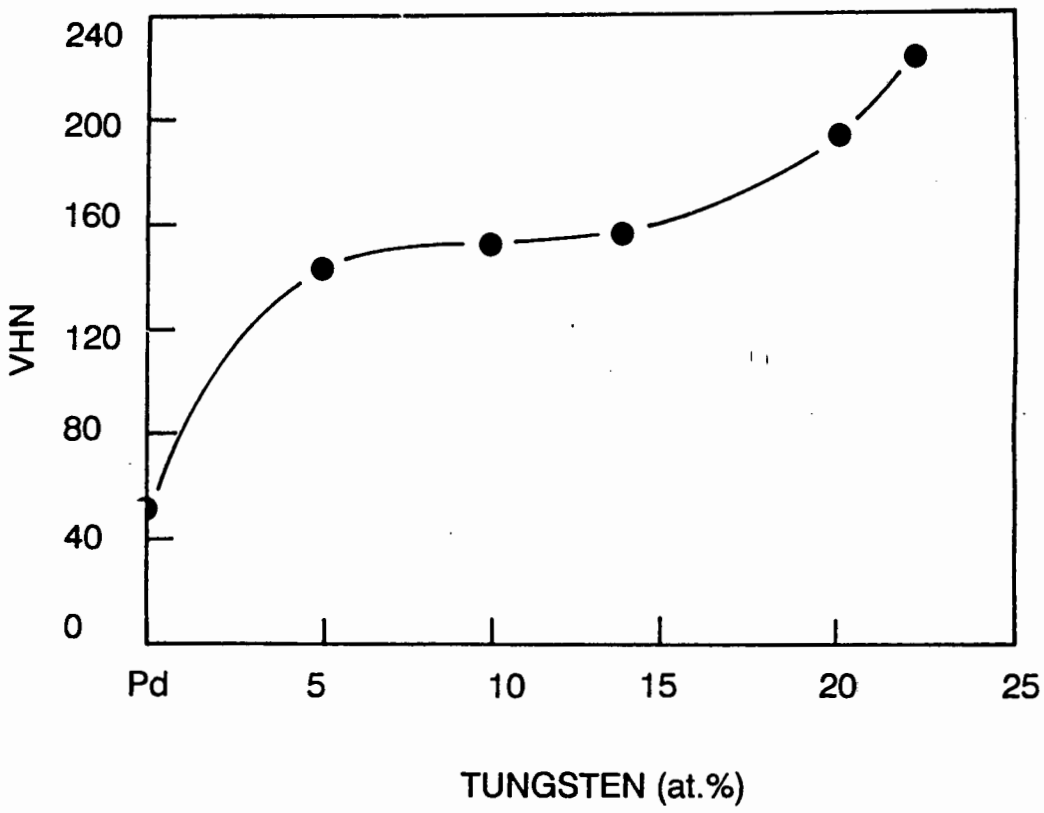

Figure 2.13: Graph of hardness vs. concentration for palladium-tungsten (after Goetz and Brophy[129]).

2.3.5 THE PALLADIUM-MOLYBDENUM SYSTEM: PHASE EQUILIBRIA AND STRUCTURE

The equilibrium phase diagram of the palladium-molybdenum system, published in complete form by Savitskii et al[141] and shown in fig. 2.14, is of the peritectic type with two terminal solid solutions and a single intermetallic compound[141,142,143]. The solubility limit of molybdenum in palladium lies above 30 at.% molybdenum at 1000°C, decreasing slightly as temperature is reduced. The solubility limit of palladium in molybdenum at 1000°C is far smaller, lying at 4 at.% palladium. A hexagonal close-packed (hcp) ϵ-phase, stable above 1400°C, appears in the concentration range 40 at.% - 60 at.% molybdenum.

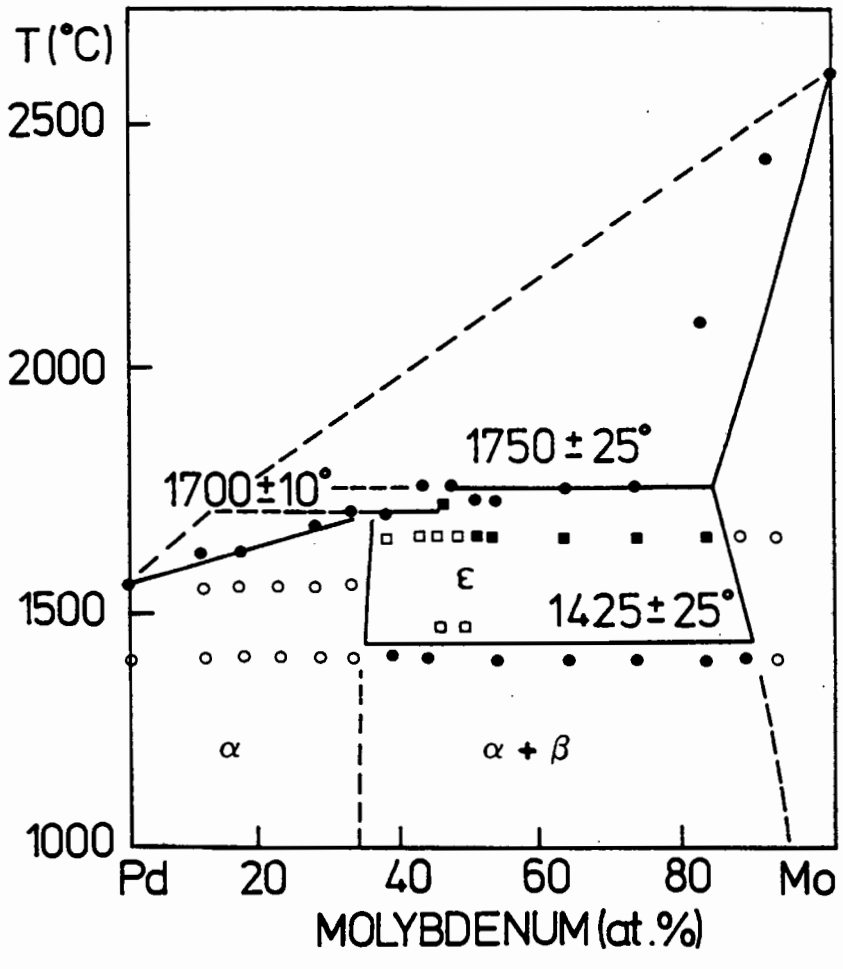

Figure 2.14: Equilibrium phase diagram of palladium-molybdenum (after Savitskii et al[141]).

Mostafa and Ardell[144] reported the formation under proton irradiation of the tetragonal ordered phase Pd_8Mo, crystallographically identical to Pd_8W (D^{17}_{4h}), at compositions of 10 at.% molybdenum and 18 at.% molybdenum. Cheng et al[145] reported this phase to be stable below 430°C in the 10 at.% alloy and below 600°C in the 18 at.% alloy, and suggested that this thermodynamic stability indicates that Pd_8Mo may be an equilibrium phase whose formation is accelerated by irradiation, although lengthy heat treatments have failed to produce it in unirradiated specimens.

The lattice parameter of palladium-molybdenum alloys, shown in fig. 2.15, shows a similar dependence on concentration to that of palladium-tungsten, exhibiting a minimum at 10 at.% molybdenum[104,142,146]. A comparison of the Goldschmidt radii (CN12) of palladium and molybdenum shows molybdenum to be an oversized solute in the face-centred cubic palladium-based solid solution[135]; an increase in lattice parameter with the addition of molybdenum to palladium is accordingly expected. An increase in lattice parameter with increasing concentration is however only observed at concentrations above 10 at.% molybdenum.

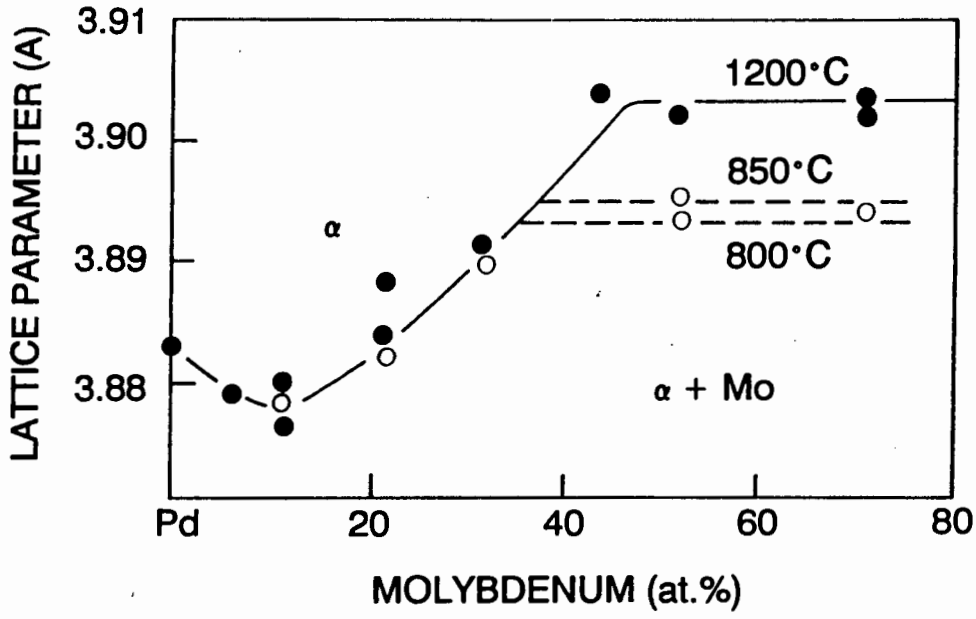

Figure 2.15: Graph of lattice parameter vs. concentration for palladium-molybdenum (after Raub[146]).

2.3.6 THE PALLADIUM-MOLYBDENUM SYSTEM: PROPERTIES

The magnetic susceptibility of palladium-molybdenum decreases significantly with increasing molybdenum concentration[116,138,147]. Kudielka-Artner and Argent[104] and Koster and Hagmann[117] report a minimum at 10 at.% molybdenum followed by a very small increase in susceptibility, as shown in fig. 2.16, suggesting a trend in concentration dependence similar to that exhibited by palladium-tungsten.

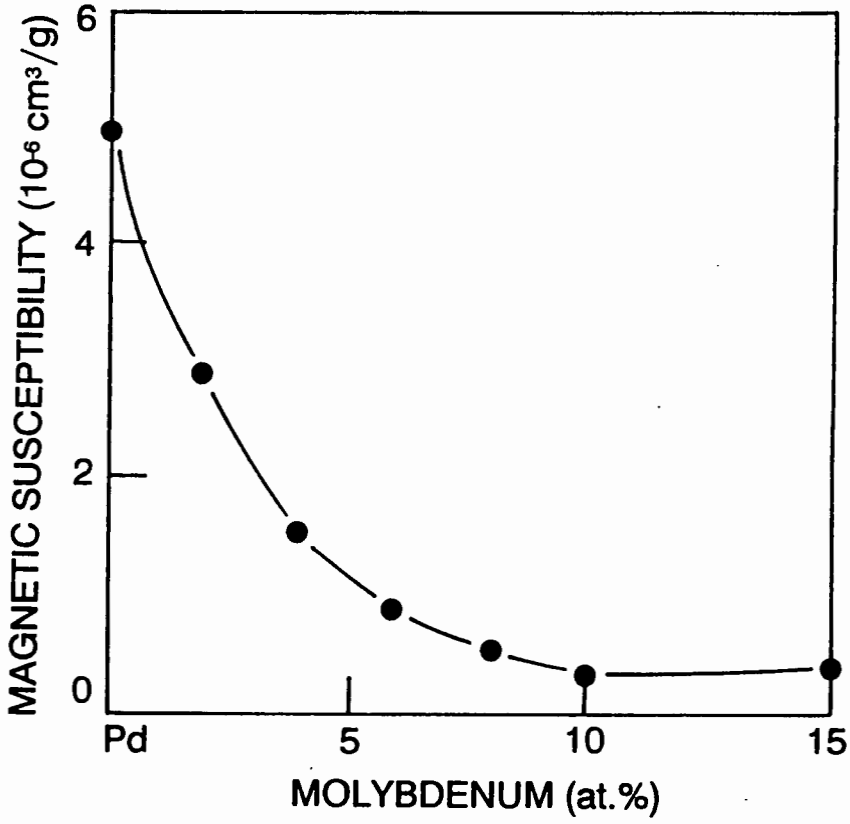

Figure 2.16: Graph of magnetic susceptibility vs. concentration for palladium-molybdenum (after Koster and Hagmann [117]).

The addition of molybdenum to palladium results in a steep increase in electrical resistivity[104,117,119,141]. Resistivity measurements in the concentration range 1 at.% - 10 at.% molybdenum, made by Kudielka-Artner and Argent[104] and shown in fig. 2.17, show a steep linear increase in resistivity with increasing molybdenum concentration. These results show no evidence of a significant

deviation from linearity in the dependence of resistivity on solute concentration in this concentration range; Kudielka-Artner and Argent suggest that this indicates that the d-band is still incomplete. The temperature coefficient of resistivity of palladium-molybdenum decreases with the addition of molybdenum[104,119], to a very small value at about 10 at.% molybdenum[141]. Kudielka-Artner and Argent[104] measured a large decrease in $d\rho/dT$ between 6 at.% and 10 at.% molybdenum as shown in fig. 2.17, suggesting that this reflects a decrease in the density of states in the d-band with increasing solute concentration, as occupation of the d-band increases.

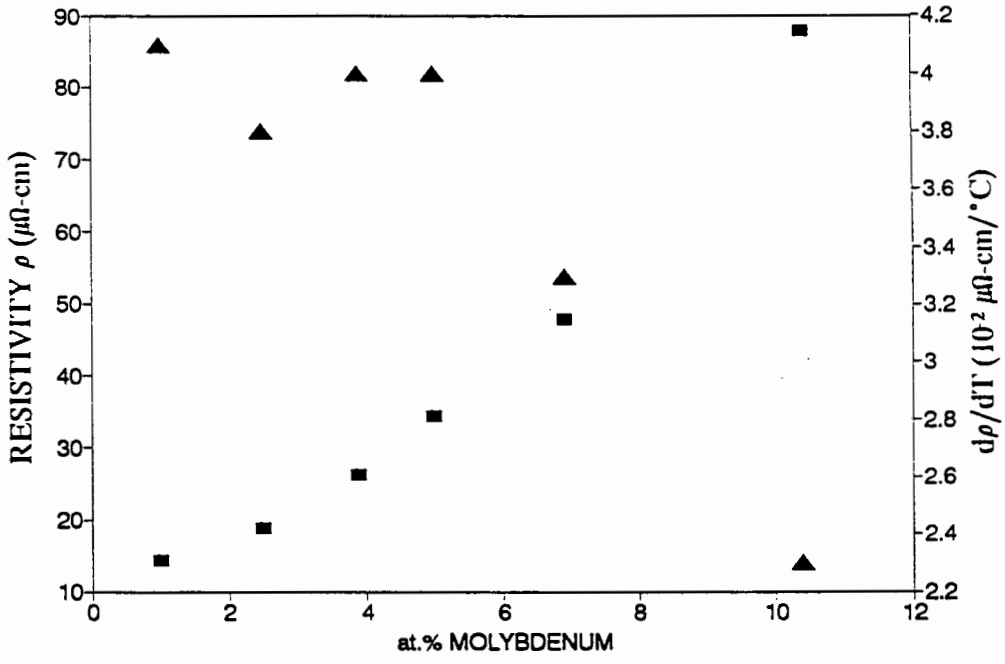

Fig. 2.17: Graph showing dependence of resistivity ■ and temperature coefficient of resistivity ▲ on molybdenum concentration (after Kudielka-Artner and Argent[104]).

Mes'kin et al[140] reported that the resistivity of palladium-molybdenum increases, and the temperature coefficient of resistivity decreases, after annealing at 700°C for concentrations between 6 at.% molybdenum and 12 at.% molybdenum, as shown in fig. 2.18. The development of a "k-state" is suggested as a probable cause[140], as for palladium-tungsten (section 2.3.4); as observed in palladium tungsten, a maximum change is shown at around 10 at.% molybdenum.

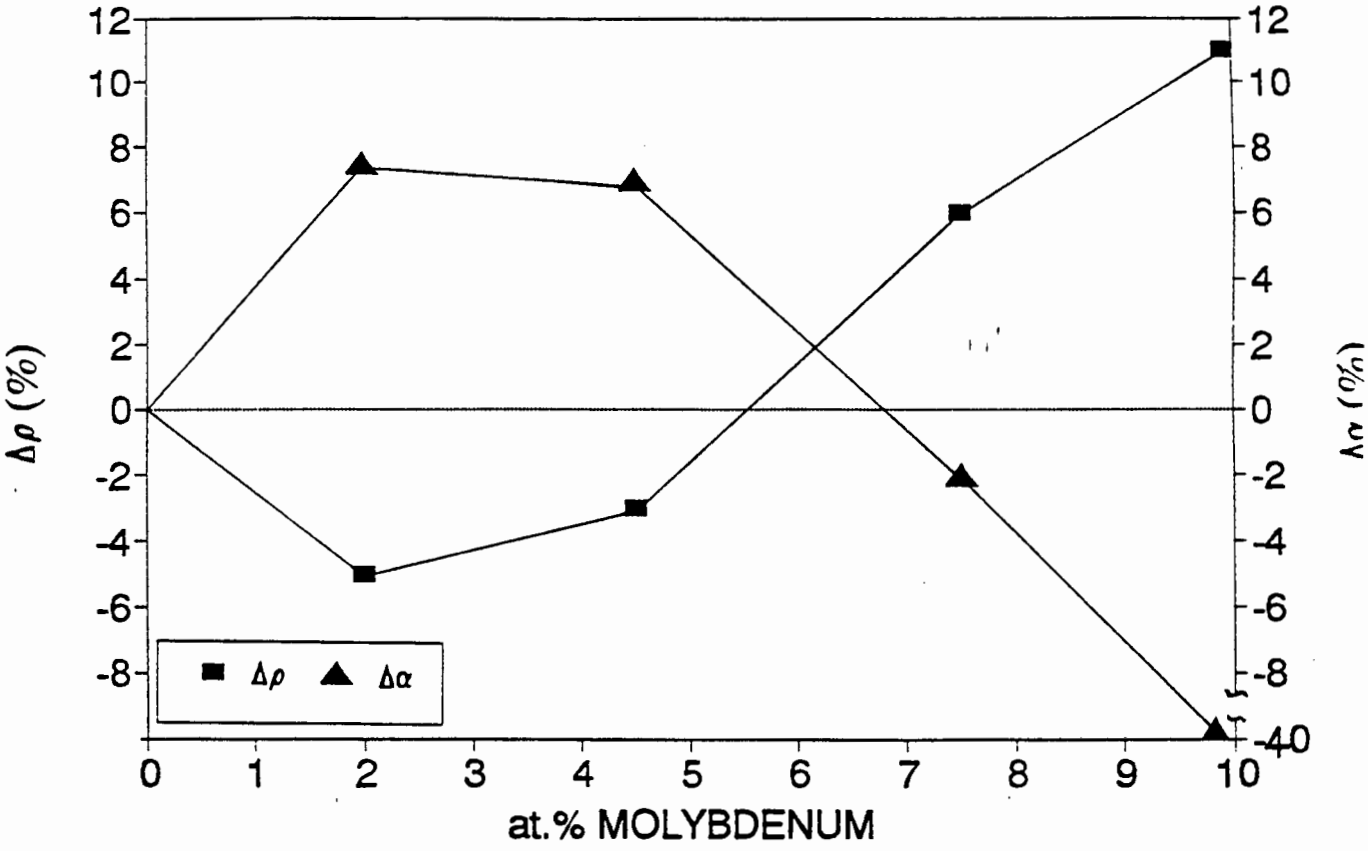

Fig. 2.18: Graph of change in resistivity and temperature coefficient of resistivity, due to annealing at 700°C, as a function of composition (after Mes'kin et al[140]).

The negative thermo-emf of palladium decreases with the addition of molybdenum, reaching zero at a concentration of 5 at.% molybdenum[117,119]; the subsequent increase reaches a maximum at about 8 at.% molybdenum[140,141]. This dramatic variation in thermo-emf is shown in fig. 2.19 to be limited to the palladium-based solid solution, smaller variations occurring above 35 at.% molybdenum. Mes'kin et al[140] reported an increase in the thermo-emf of cold-worked palladium-molybdenum, in the concentration range 5 at.% - 12 at. % molybdenum after annealing at 700°C. As noted for palladium-tungsten alloys, this is roughly the concentration range in which an increase in resistivity is observed after annealing.

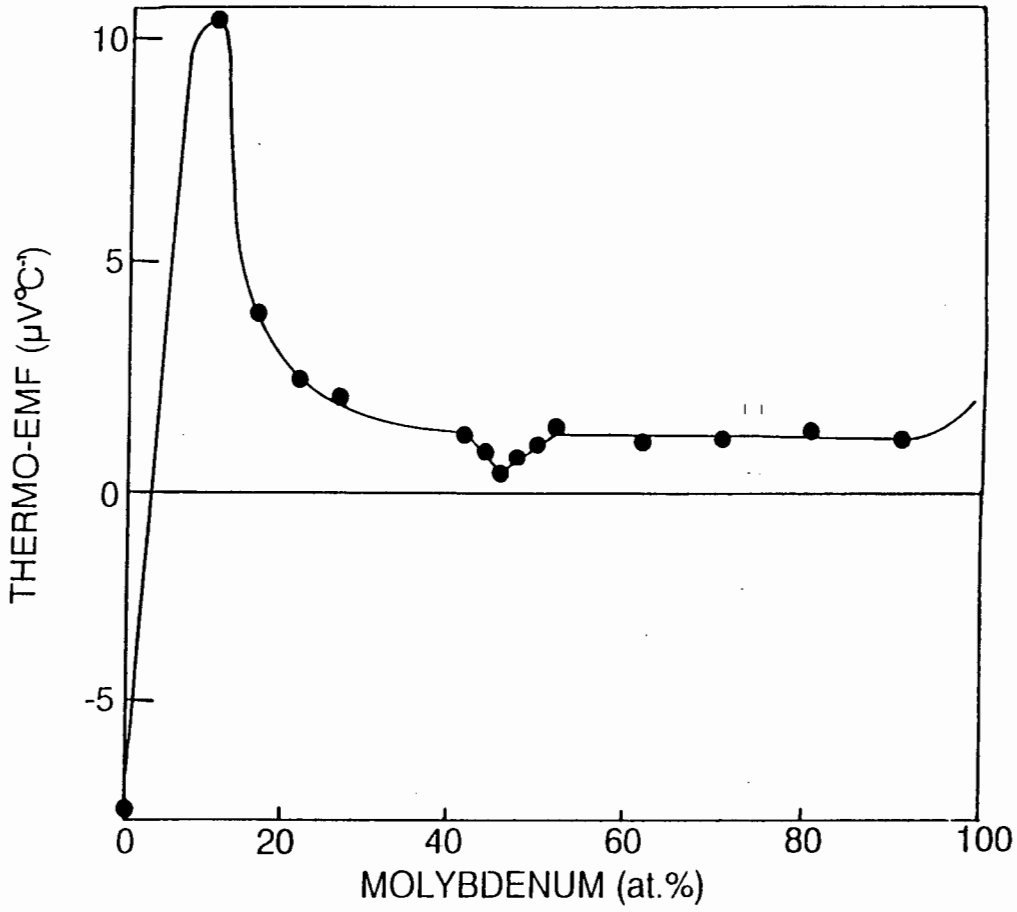

Figure 2.19: Graph of thermo-emf vs. concentration for palladium-molybdenum (after Savitskii et al[141]).

The mechanical properties of palladium-molybdenum alloys have been measured by Savitskii et al[141], by Raub[146] and by Zwingmann[119]. The tensile strength and microhardness of palladium are reported to be greatly enhanced by the addition of molybdenum up to 22 at.% molybdenum, with a reduction in elongation. Figure 2.20 shows the microhardness of as-cast palladium-molybdenum[141].

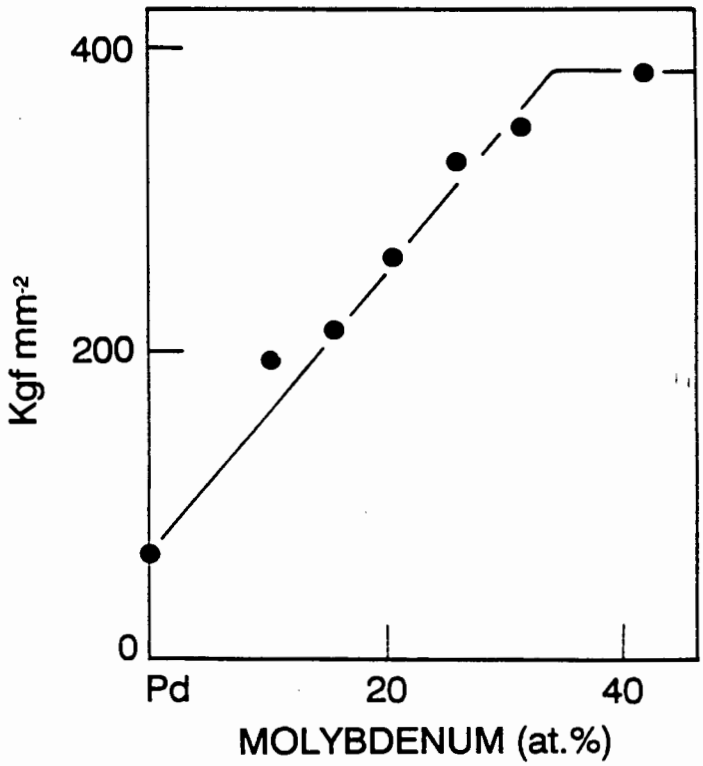

Figure 2.20: Graph of microhardness vs. concentration for as-cast palladium-molybdenum (after Savitskii et al[141]).

2.4 OVERVIEW

The electronic structure and electrical resistivity of pure palladium are well understood; a number of theoretical analyses, made using the more complex formalisms required for transition metals, are consistent with experimental results. The effect of alloying additions on the structure and properties of palladium, including electrical resistivity, may be theoretically calculated at a cost of lengthy computation; however, the contribution to the residual resistivity of additional factors such as lattice defects and ordering presents some difficulty. The effect of cold work on resistivity in pure metals has been extensively investigated and some successful theories presented; however, little attention has been paid to this effect in alloys. Similarly, analyses of the effect of structural order on resistivity in alloys of simple metals are not necessarily appropriate to alloys of transition metals, which may require more sophisticated techniques. Experimentally, the resistivity of a large number of palladium alloys has been determined but far less data is available concerning the effect on resistivity of either cold work or ordering, although many palladium alloys form ordered phases.

The properties of the palladium-tungsten and palladium-molybdenum systems exhibit a number of unusual features. Of primary interest is the increase in resistivity of these alloys after annealing, which may be due to the development of short-range order at elevated temperatures; for an annealing temperature of 700°C, this effect is reported to reach a maximum at around 10 at.% solute concentration. Other properties of these two systems show singularities in their dependence on solute concentration at around 10 at.% solute concentration: lattice parameter shows an unexpected minimum, while thermo-emf exhibits a maximum. In this respect the appearance, after irradiation, of the stable long-range ordered forms Pd_8W and Pd_8Mo is of interest since the stoichiometric concentration for this structure lies at 11.1 at.% solute. The properties of palladium-tungsten and palladium-molybdenum are thus sensitive to solute concentration in the composition range of interest; and are also sensitively dependent on heat treatment condition.

CHAPTER 3

EXPERIMENTAL PROCEDURES

The purpose of the experimental programme was to investigate the relationship between electrical resistivity and structure in selected palladium alloys. The initial aim was therefore to prepare specimens, suitable for resistivity determination and microstructural investigation, which exhibited a wide range of microstructures. The preparation of severely cold-worked specimens is described in section 3.2. A range of microstructures was achieved by systematic annealing of these specimens, as described in section 3.3.

In order to determine the change in resistivity associated with microstructural changes brought about by cold work and annealing, a sensitive resistance measurement apparatus was designed and constructed, the details of which are presented in section 3.4. Microhardness was assessed (section 3.5) and microstructures examined using optical and electron microscopy, described in section 3.6.

The experimental sequence for each material commenced with the measurement of electrical resistance and assessment of microstructure of specimens in the cold-worked condition. Specimens were then annealed at successively higher temperatures, resistance being measured after each heat treatment. Specimens representative of each annealing condition were used to assess changes in microhardness, microstructure and crystal structure.

3.1 MATERIAL SELECTION

In addition to pure palladium, alloys of palladium with tungsten and molybdenum were selected for investigation. The solubility limit of tungsten in palladium is 15 at.%; that of molybdenum in palladium is 30 at.%. In order to facilitate comparison of the two alloy systems, it was necessary to select solute concentrations in a similar range for both alloys. The survey of published data regarding these systems shows a number of properties to exhibit maxima or minima at concentrations of around 10 at.% solute concentration in both systems; the long-range ordered forms Pd_8W and Pd_8Mo are also reported to be stable at 10 at.% solute. Accordingly, three compositions in each alloy system, in a range containing 10 at.% solute concentration, were selected. Alloy preparation was not without difficulty, since the melting points of both tungsten and molybdenum are above the vaporisation temperature of palladium. The concentrations investigated, determined by electron microprobe analysis and shown in Table 3.1, are hence not identical for the two alloy systems, although they fall within the same range.

TABLE 3.1: Composition of materials selected.

PALLADIUM at.%	TUNGSTEN at.%	MOLYBDENUM at.%
99.5	-	-
95.9	4.1	-
89.7	10.3	-
88.4	11.6	-
94.7	-	5.3
90.3	-	9.7
84.0	-	16.0

3.2 SPECIMEN PREPARATION

Samples were received from MINTEK in the form of arc-melted buttons of approximately 5mm thickness and 8mm diameter. The as-cast buttons were cold-rolled into sheet in a Dinkel laboratory rolling mill, prior to final specimen preparation. The following rolling methods were assessed in order to optimise specimen preparation.

(i) Vacuum inter-anneal: specimens were reduced in steps of 100 μm or less, and were passed through the rollers several times at each roller displacement. After a total reduction of 20%, specimens were annealed under vacuum at 1000°C for times varying between one and eight hours. This process was repeated until a specimen thickness of 300 μm or less was achieved. Although time-consuming, this method was satisfactory for palladium and the alloys of lowest solute concentration; but buckling of the specimen in the final stages of rolling was not uncommon. The alloys of higher concentrations, however, tended to fail by cracking at an early stage of the rolling process. Energy-dispersive spectroscopy (EDS) of failed specimens showed some to contain undissolved solute inclusions.

(ii) Flame inter-anneal: specimens were reduced in steps of up to 250 μm, and passed through the rollers twice for each roller displacement. After a cumulative reduction of 50%, specimens were annealed in the flame of an oxy-acetylene torch until red-hot and quenched in water. The process was repeated until the desired thickness was reached. This method gave improved results for all materials. In particular, undissolved solute inclusions became visible due to oxidation during the flame anneal: this allowed the sections surrounding inclusions to be cut away and discarded.

(iii) Cold rolling without inter-anneal: specimens were reduced in large steps of up to 500 μm at the outset, decreasing with specimen thickness. No annealing was performed. This method was, somewhat surprisingly, successful for all but the most inhomogeneous of alloy samples, which were discarded. Where small inhomogeneous regions existed, the large reductions caused either local blistering of the surface or exposure to the atmosphere of the

inclusion, which then oxidised rapidly. In both cases inhomogeneous parts of the material were identified and discarded as in method (ii). Minor cracking tended to occur at the edges of the alloys of high concentrations; where this occurred, the specimen edge was ground on 100 grit paper to beneath the crack tip. Careful inspection after each pass through the rollers allowed the early identification of cracking, and material loss due to grinding was hence minimal.

Method (iii) was selected for initial preparation of all specimens, since the absence of annealing provided the maximum degree of cold deformation.

3.2.1 RESISTANCE SPECIMENS

The determination of the electrical resistivity of a material requires measurement of both the dimensions and the electrical resistance of a specimen. Where a value for resistivity was required, specimen dimensions were measured in several locations and an average taken. Where comparitive resistance measurements are to be made using the same specimen however, the precise specimen dimensions are unimportant since the relationship between resistivity and resistance is linear:

$\rho = RA/L$ where

ρ = resistivity
R = resistance
A = cross-sectional area of specimen
L = length of specimen or distance between potentiometric contacts

It is clear that determination of resistivity may be optimised by selection of a suitable specimen geometry. A large ratio of length to cross-sectional area will thus serve to produce a magnified resistance change in the specimen relative to the resistivity change in the specimen material. Taking into account the constraints imposed by the expense of the materials used, and hence their availability, small specimen dimensions of 90mm length and 3mm width were selected and standardised. Thickness was determined by the maximum reduction possible for each material, but was in all cases less than 300 μm.

In order to avoid the local distortion and poor finish produced by cutting the

rolled sheet to the required dimensions, resistance specimens were produced by clamping the sheet and machining the material to the required dimensions.

3.2.2 METALLOGRAPHY AND MICROHARDNESS SPECIMENS

Small offcuts of rolled material were subjected to the same annealing experiments as the resistance specimens. These small specimens were mounted in resin and polished for microhardness measurements and optical microscopy. Since the material thickness was less than 300 μm, specimens were mounted at an oblique angle in Araldite resin in order to prevent them from breaking free of the mounting during polishing. The procedure, shown in fig. 3.1, is as follows: a specimen is placed on an angled base in a mould, which is partially filled with resin (a); after hardening of the resin the mounted specimen is inverted and replaced in the mould, which is filled with resin (b); the specimen is thus contained within the resin at an oblique angle, and the resin may be removed from one side by successive turning and grinding until a tapered section of the specimen is exposed (c).

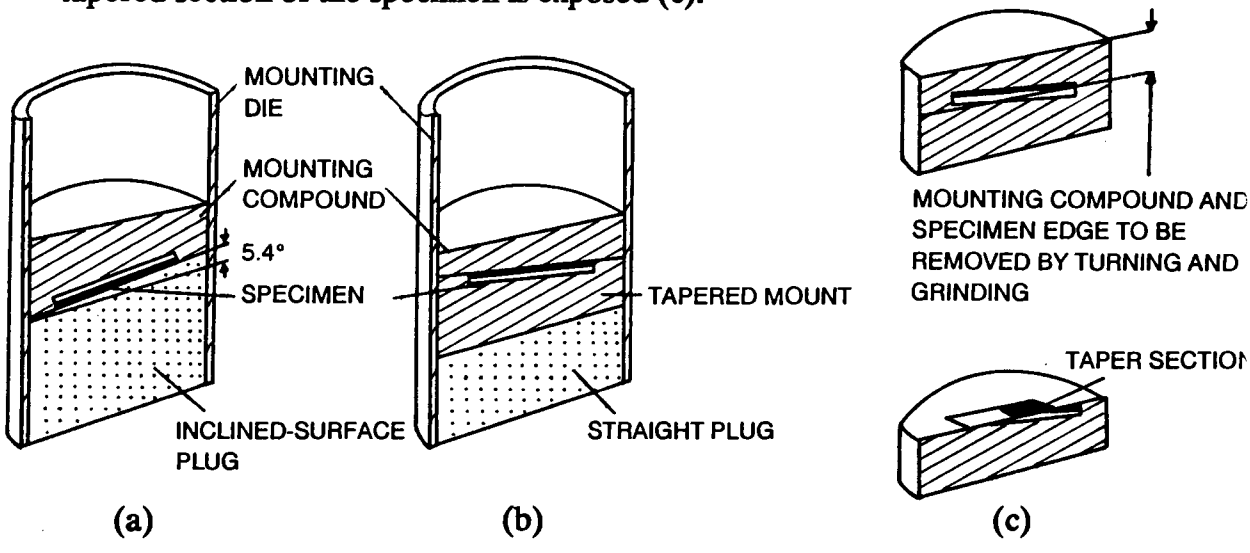

Figure 3.1: Procedure for oblique mounting of thin specimens.

Palladium and its alloys are relatively soft materials, and mechanical grinding on 1000 grit paper proved adequate to remove surface scratches. Mechanical polishing then commenced with 3 μm diamond paste, progressing to a 0.25 μm finish.

3.2.3 TRANSMISSION ELECTRON MICROSCOPE FOILS

Three millimeter disks for transmission electron microscopy (TEM) were spark-eroded using a Materials Science spark-erosion apparatus. A low voltage was used, but difficulty was experienced in obtaining even erosion of material around the circumference of the disk. This resulted in part of the circumference perforating while the remainder was relatively uneroded; at this point the disks showed a tendency to bend upward, undergoing accelerated erosion and becoming lozenge-shaped. This problem was resolved by attaching the material to a thick backing sheet of aluminium by means of a contact adhesive, thus maintaining a flat surface and preventing lifting of the disk during erosion. The disks, once the full circumference had perforated, were removed from the backing by immersion in acetone, which dissolved the contact adhesive. The length of time for spark-erosion of disks 150 μm - 300 μm in thickness was 30-60 minutes. Disks were then mechanically ground to a thickness of 100 μm.

Palladium and palladium-rich alloys do not lend themselves easily to electrochemical polishing since they are relatively chemically inert under ordinary conditions. A Struers Tenupol twin-jet polishing apparatus was used, at a potential of 42V, current of 30mA and a low flow rate; the polishing solution consisted of 4% perchloric acid, 70% acetic acid, 18% glycerol and 8% 2-butoxyethanol, maintained at a temperature of 6°C[148]. Perforation of the foils occurred after approximately 20 - 30 minutes, initially near the rim of the specimen but growing rapidly towards the centre. For this reason the photoelectric cell in the polishing apparatus, which cuts off current when a central perforation is detected, was dispensed with. The specimen was instead kept under visual observation and the specimen holder removed from the apparatus and immersed in methanol immediately after perforation. Lowering the voltage to 20-30V, while maintaining other polishing conditions, resulted in a more central perforation and an increased polishing time of 40 - 60 minutes; however, the quality of the polish was erratic. Specimens were immersed in acetone for 15 minutes prior to final rinsing in methanol.

3.3 ANNEALING EXPERIMENTS

The conditions under which specimens were annealed were selected on the basis of reported results in the open literature and on preliminary testing. It was necessary to select a single material for these preliminary tests in view of the limited availability of material. The information in the published literature concerning the electrical resistance of the alloys under investigation suggests that palladium-tungsten alloys in the solute concentration range 8 at.% - 13 at.% tungsten exhibits the greatest variation in resistance due to annealing[133,140]. Significant increases in the resistance of alloys in this composition range have been reported after annealing at 700°C[140] and 1200°C[133]. Palladium 10.3 at.% tungsten was accordingly selected for preliminary annealing experiments.

The results of the first preliminary test are presented in fig. 3.2, which shows the cumulative effect on electrical resistance of successively annealing palladium 10.3 at.% tungsten at temperatures from 200°C - 1000°C. The time at each temperature was one hour; specimens were cooled to room temperature and the resistance measured after each heat treatment. Successive annealing experiments in the range 200°C - 400°C were observed to result in a change in resistance of less than one per cent. Annealing the the temperature range 500°C - 800°C resulted in an increase in resistance after each heat treatment; annealing at temperatures above 800°C, however, resulted in very little further variation in resistance. Since annealing at 200°C - 400°C produced a very small increase in resistance, a temperature range of 500°C - 1000°C was selected for annealing experiments on palladium alloys.

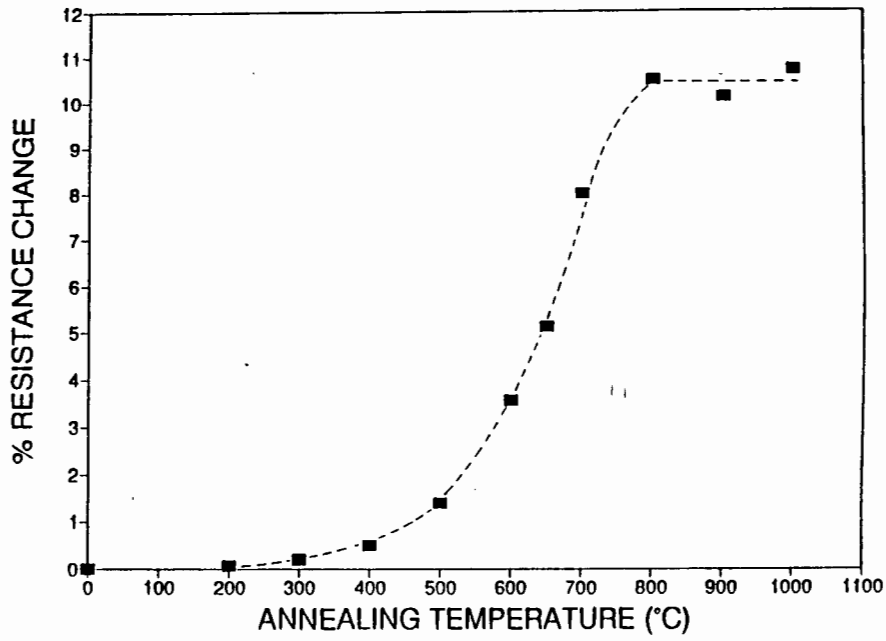

Figure 3.2: Graph of percentage change in resistance of palladium 10.3 at.% tungsten vs. annealing temperature.

A further series of preliminary annealing experiments was performed at 500°C, 600°C and 700°C for annealing times varying from one to twenty-four hours, as shown in fig. 3.3. The results show a general increase in resistance with increasing time at temperature. At each of the annealing temperatures evaluated, there is a steep increase in resistance after the first hour, followed by a smaller increase after six hours. For annealing times greater than six hours, the response of resistance to annealing time shows a wide variation between annealing temperatures; it should be emphasised however that fig. 3.3 shows the results of a single series of preliminary tests, limited by availability of material, and that each data point represents a single heat treatment. Nevertheless, an annealing time of one hour consistently produces a significant increase in resistance, reported as development of the "k-state" in this and other transition metal alloy systems. A standard annealing time of one hour was accordingly selected for all annealing experiments.

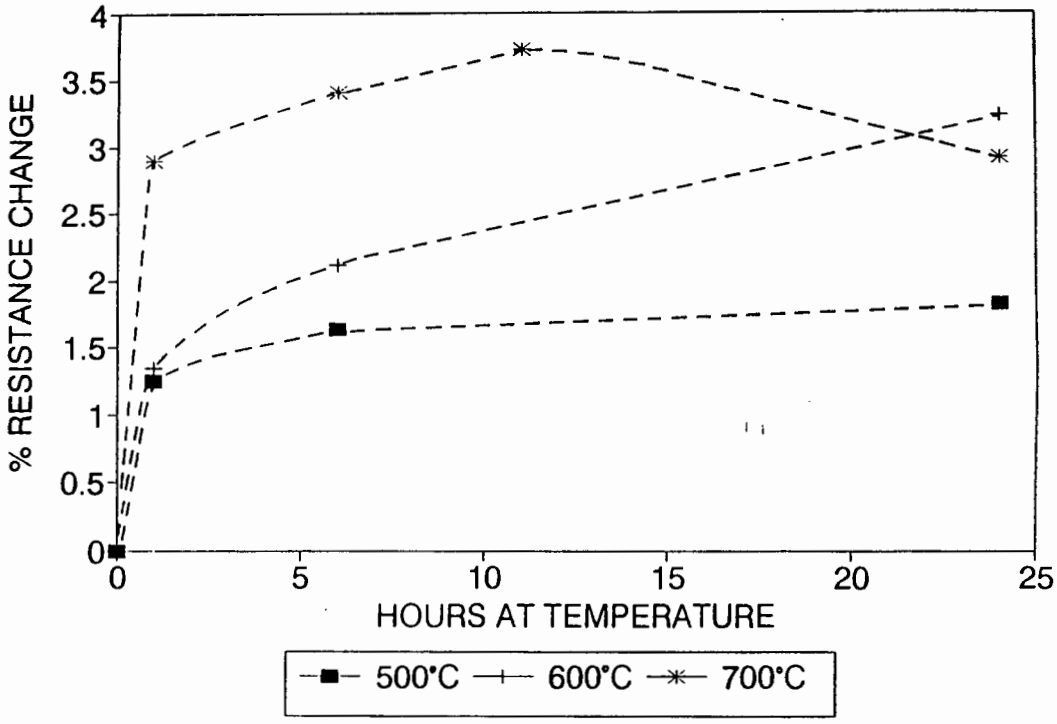

Figure 3.3: Graph of percentage change in resistance of palladium 10.3 at.% tungsten vs. time at temperature.

All annealing experiments were carried out in a vertically supported platinum-rhodium winding furnace equipped with a vacuum pumping system. Specimens were heated in a vacuum of 10^{-3} Pa after flushing the furnace tube with argon. Heat treatments were standardised at a duration of one hour at temperature. Specimens were cooled by switching off the furnace, which resulted in an average cooling rate of 10°C/minute.

As far as possible resistance specimens were annealed simultaneously with microhardness and metallography specimens and TEM disks, in order that the microstructures examined in the latter be as representative as possible of the condition of the resistance specimens. TEM disks were annealed subsequent to spark erosion and mechanical thinning.

3.4 RESISTANCE MEASUREMENTS

Resistance was measured at room temperature after each annealing experiment. Resistance measurements were carried out using the experimental apparatus shown in fig. 3.4, specifically constructed for the experimental procedure and specimen geometry selected. The current-carrying contacts consisted of brass disks clamping the specimen ends, whereas the potentiometric inner contacts were brass point contactors, spring-loaded to ensure consistent contact pressure throughout each test series. Extensive initial testing showed the effect on resistance of careful removal and replacement of the specimen to be negligible.

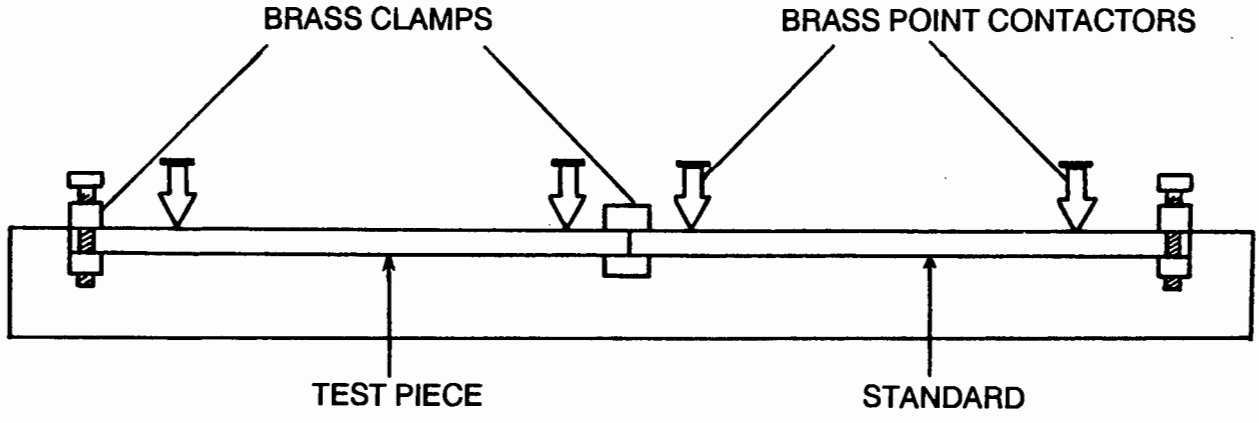

Figure 3.4: Schematic diagram of experimental apparatus.

Resistance measurements were performed using the purpose-designed circuit shown in fig. 3.5 and fig. 3.6. In order accurately to determine changes in resistance it is necessary to measure the resistance of a test specimen with respect to the resistance of a standard. For all tests, the standard used was of the same material and dimensions as the test specimen.

For electrical connection of standard and test specimens a series configuration was selected, which has the advantage of cancelling out variations in potential drive since the current is the same through both standard and test piece. An alternating current is used; hence the resistive voltage drop is an AC signal which is easily distinguished from drift and thermal contact potentials. A

frequency of 230 Hz for the AC signal was selected in order to avoid mains interference; at the same time this frequency is sufficiently low to avoid skin effect artefacts. A modified four-terminal technique, with separate contacts to the specimens for current supply and to measure the potential drop, ensures that potential drop due to contact resistance at the (current-carryng) outer contacts does not contribute to the potential measured by the inner pairs of contacts. The inner contacts are connected to circuitry of sufficiently high impedance that contact resistance is negligible. At the point of contact between the specimens the circuit is grounded; hence the signal in each specimen, relative to the centre, is opposite in sign to the other. Differences may thus be detected with a summing amplifier.

The difference in potential between the two specimens is thus an AC signal, which may be extremely small. In amplifying such a signal, it is important to minimise the effect of noise. The method used for the minimisation of the effect of noise is synchronous detection, whereby the amplified signal is inverted synchronously with the driving signal. This method is analogous to lock-in amplification. The resultant product is then low-pass filtered, so that the component caused by the potential drive results in a DC signal, while other unwanted components result in an AC signal which is attenuated by the filter.

In building the above circuitry, 1% accuracy components were used, and in some cases (for example the differential measurement) were matched by direct measurement. The intention was to measure changes in the resistance *difference* to an accuracy of 0.1% at room temperature, and this was satisfactorily achieved for palladium alloys. The only component which was susceptible to drift over time and temperature was the diode D1 (fig. 3.5 (b)) in the automatic gain control circuit and this drift was nullified by resetting the current in the automatic gain control circuit manually at suitable intervals. The current was monitored continuously during measurement, so that drift could not occur unnoticed. The apparatus as a whole was sited in an internal, ground-floor room offering an airconditioned and thermostatically controlled environment. Room temperature was 22°C +/- 0.5°C and was monitored throughout the test period.

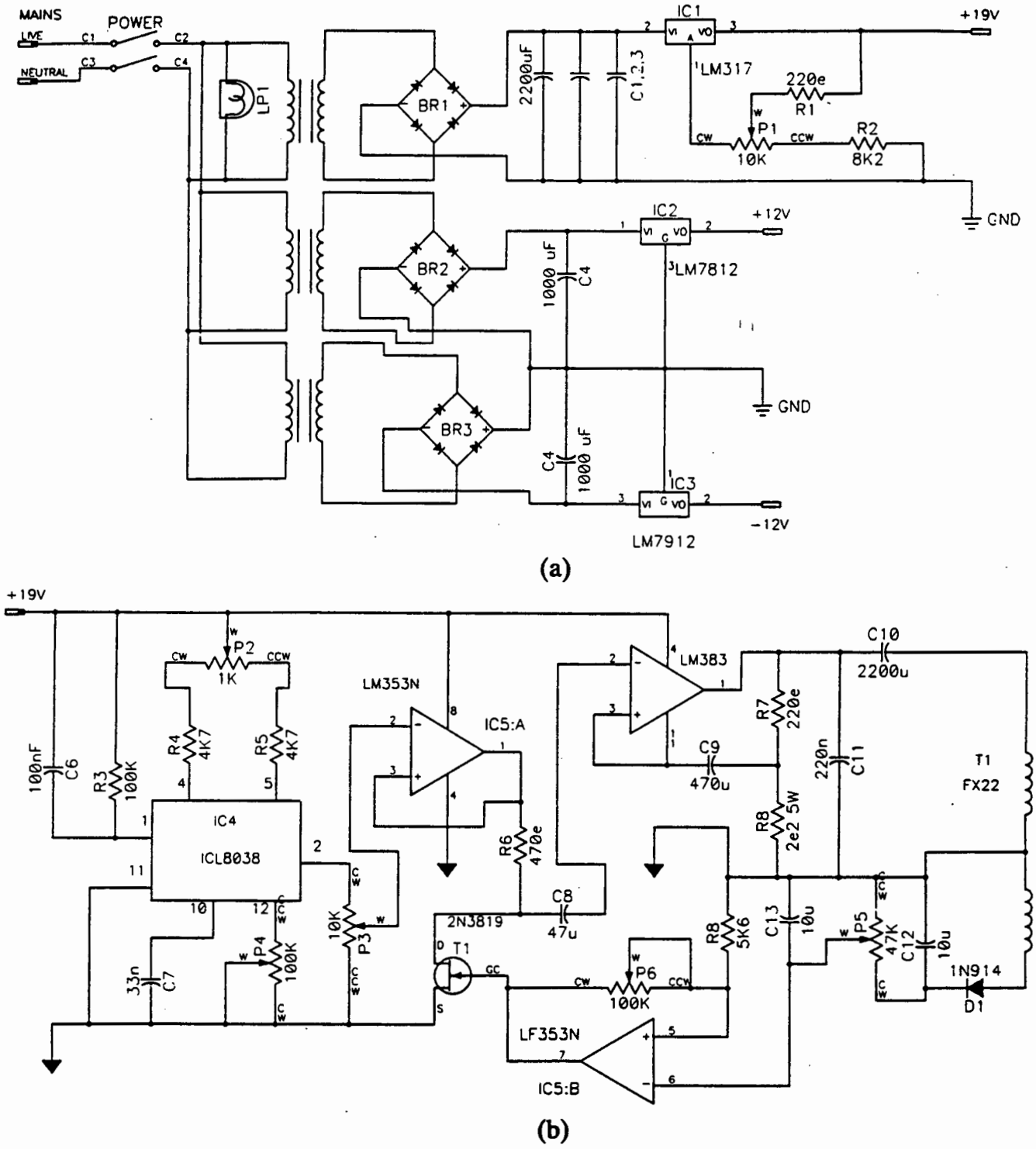

Figure 3.5: Circuit diagram showing the power supplies of conventional design (a) and sine-wave generator and power amplifier (b). The power amplifier drives a transformer T1 through which an AC wave is applied to the specimens (see fig. 3.6); the automatic gain control circuitry is also shown.

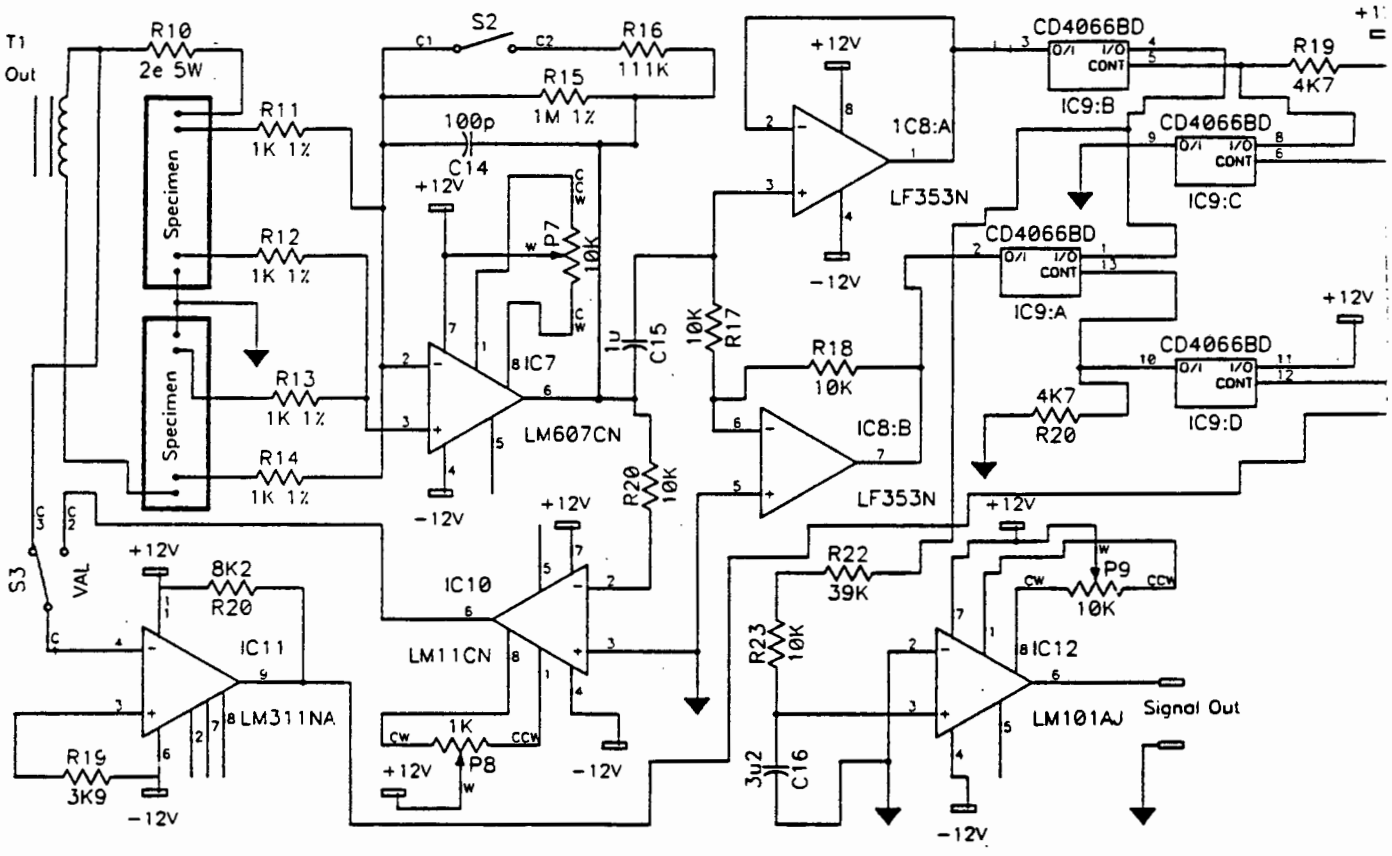

Figure 3.6: Circuit diagram showing the transformer (T1) drive to the specimens, precision differential amplifier, and synchronous detection to provide a DC level output (V_{out} = 100ΔR or 1000ΔR for S1 closed or open). S3 offers two options for recovering the original synchronous signal: the switch position shown is most often used.

The amplified DC difference in potential between specimen and standard was measured using a Fluke four and a half digit multimeter. Current was measured to the nearest milliamp using an Escort three and a half digit multimeter. In addition to DC readings of the difference in voltage across standard and test piece, measurements were made of absolute AC potential drop across each specimen, using the Fluke multimeter, in order to determine specimen resistance and to confirm the sign of resistance changes.

For each test series, a cold-worked test specimen was clamped to the apparatus in contact with the standard. After allowing for warming up and stabilisation of the measuring circuitry, twenty readings of potential and current were taken over a period of an hour. Measurements taken regularly over a period of several days showed no evidence of long-term fluctuations. The test specimen was then removed, annealed and replaced in the apparatus for further measurements, this cycle being repeated until the series of annealing experiments was complete.

3.5 MICROHARDNESS TESTING

Microhardness tests were carried out in order to assess changes in mechanical properties brought about by annealing experiments. A Shimadzu microhardness tester was used, with a Vickers diamond pyramid. In the cold-worked condition, a 100gf load was used for both palladium and palladium alloys; however, after annealing the indentation size for this load became rather large in pure palladium, and a 50gf load was used.

3.6 MICROSCOPY

3.6.1 OPTICAL METALLOGRAPHY

Polished specimens were chemically etched in order to determine the evolution of grain structure with successive annealing. The etchants used are shown in Table 3.2. Etched specimens were examined and photographed in a Reichert MeF2 metallograph in bright-field mode.

TABLE 3.2: Chemical etchants for optical metallography specimens.

MATERIAL	COMPOSITION	CONDITIONS
Palladium	60 ml HCl 40 ml HNO_3	10°C one minute
Pd alloys	HNO_3	10°C 5-10 seconds

3.6.2 SCANNING ELECTRON MICROSCOPY

Scanning electron microscopy was carried out on a Cambridge S200 SEM equipped with a TRACOR TN5400 energy dispersive analytical facility (EDS), in order to assess the chemical homogeneity of the palladium alloys.

3.6.3 TRANSMISSION ELECTRON MICROSCOPY

Transmission electron microscopy was carried out on a JEOL 200CX at an accelerating voltage of 200 KeV, using a double-tilt specimen holder. A variety of diffraction contrast techniques was used for assessment of dislocation density, grain size and the presence of twins and stacking faults.

Selected area diffraction, with a fully spread beam to provide parallel illumination, was used to detect the presence of scattering in the background of electron diffraction patterns since the presence, and location relative to zone axis lattice reflections, of scattering may provide information regarding the presence of structural order. By means of controlled tilting of the specimens, the high symmetry [001], [110], [111] and [112] zone axis diffraction patterns were examined. Diffuse scattering is however not necessary clearly visible either in the microscope or in normally exposed diffraction patterns. Accordingly, zone axis diffraction patterns, using a fully spread beam, were photographed at exposure times of up to 30 minutes.

CHAPTER 4

RESULTS

The initial aim of the experimental programme was to establish the conditions under which changes in electrical resistance occur in palladium-tungsten and palladium-molybdenum alloys, and the magnitude of these changes. Experimental data regarding electrical resistance are accordingly presented first, in section 4.1 of this chapter: in section 4.1.1 the results of experiments to determine the effect of annealing on electrical resistance are presented, followed in section 4.1.2 by an evaluation of the dependence of resistance on solute concentration for alloys in both the cold-worked and annealed condition. An investigation of the effect of annealing on crystal structure by means of selected area electron diffraction is presented in section 4.2; transmission electron micrographs showing the evolution of microstructure due to annealing follow in section 4.3. Measurements to determine the effect of annealing and solute concentration on microhardness are presented in section 4.4.1 and 4.4.2. A summary of the effect of annealing on the structure and properties of each material is presented in section 4.5.

The changes in resistance and microhardness due to annealing are presented in graphical form. It should be emphasised that annealing experiments were carried out at successively higher temperatures in 100°C intervals for each specimen, in the range 500°C - 1000°C for palladium alloys. Pure palladium specimens were annealed successively in lower temperature range of 300°C - 800°C. Accordingly, properties measured "after annealing at" a particular temperature pertain to the state of the specimen after successive heat treatments in the temperature range selected for the material, up to the stated temperature. It should also be noted that constraints imposed by the availability of material placed a limit on the number of resistance specimens

prepared from each alloy. In the graphs which follow, the resistance data points represent an average of the data from at least three specimens; the bars show the range of resistance measurements. Graphs of microhardness show the average microhardness, with bars showing the standard deviation.

4.1 ELECTRICAL RESISTANCE

The magnitude of a change in electrical resistance is dependent on both the resistivity change and on specimen geometry. Although the length and width of specimens was standardised, there was an unavoidable variation in the thickness of specimens. The resistance changes measured were therefore evaluated, and are presented, as a percentage of initial (cold-worked) resistance to facilitate comparison of materials. Since in this way specimen geometry effects are excluded, the percentage resistance change is equivalent to the percentage resistivity change.

4.1.1 ELECTRICAL RESISTANCE CHANGES DUE TO ANNEALING

Palladium

The electrical resistivity of the cold-worked palladium specimens was 12.9 μΩ-cm at 22°C. This is somewhat higher than the published value of 10.9 μΩ-cm[103], probably as a result of the presence of impurities (see Table 3.1). The measured variation in electrical resistance due to annealing in the temperature range 300°C - 800°C is shown in fig. 4.1. The resistance does not show a monotonic relationship with annealing temperature; however, the resistance changes measured are at the limit of the accuracy of the measuring apparatus. No definite trend can therefore be identified, beyond placing an upper limit on changes in the resistance of pure palladium brought about by annealing in the temperature range shown.

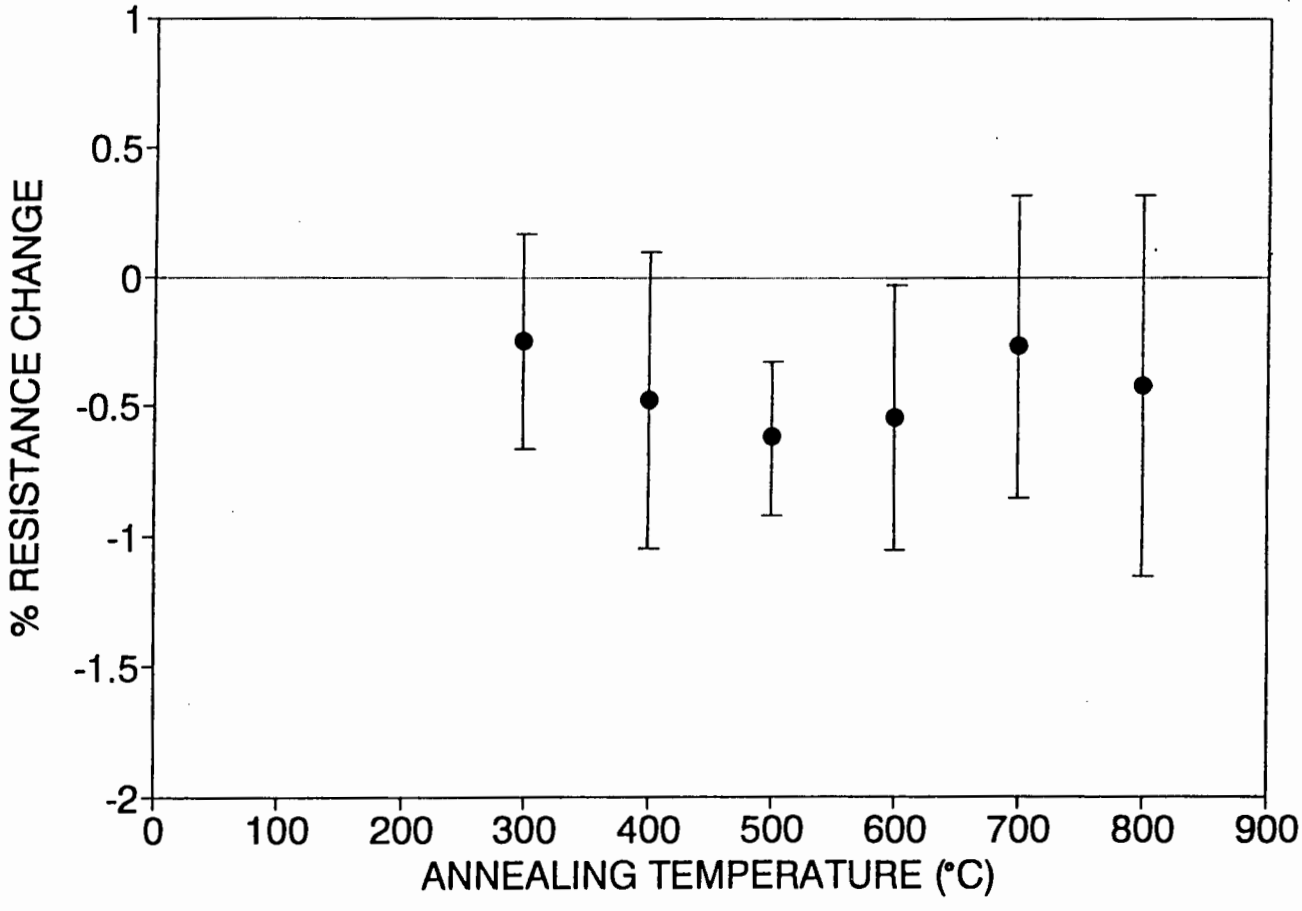

Figure 4.1: Graph of percentage change in resistance of pure palladium vs. annealing temperature.

Palladium-tungsten

The electrical resistivity of cold-worked palladium 4.1 at.% tungsten was 36 μΩ-cm at 22°C, which is consistent with the measurements of Klyuyeva et al[133]. The effect of annealing on electrical resistance is shown in fig. 4.2. In the range 500°C - 800°C the resistance is observed to decrease after successive annealing. The largest decrease, to a value more than 8 per cent lower than the cold-worked resistance, occurs after annealing at 700°C. Mes'kin et al[140] reported a similar decrease after annealing at this temperature (fig.2.10). After annealing at 900°C, however, an increase in resistance occurs which is not significantly affected by subsequent annealing at 1000°C.

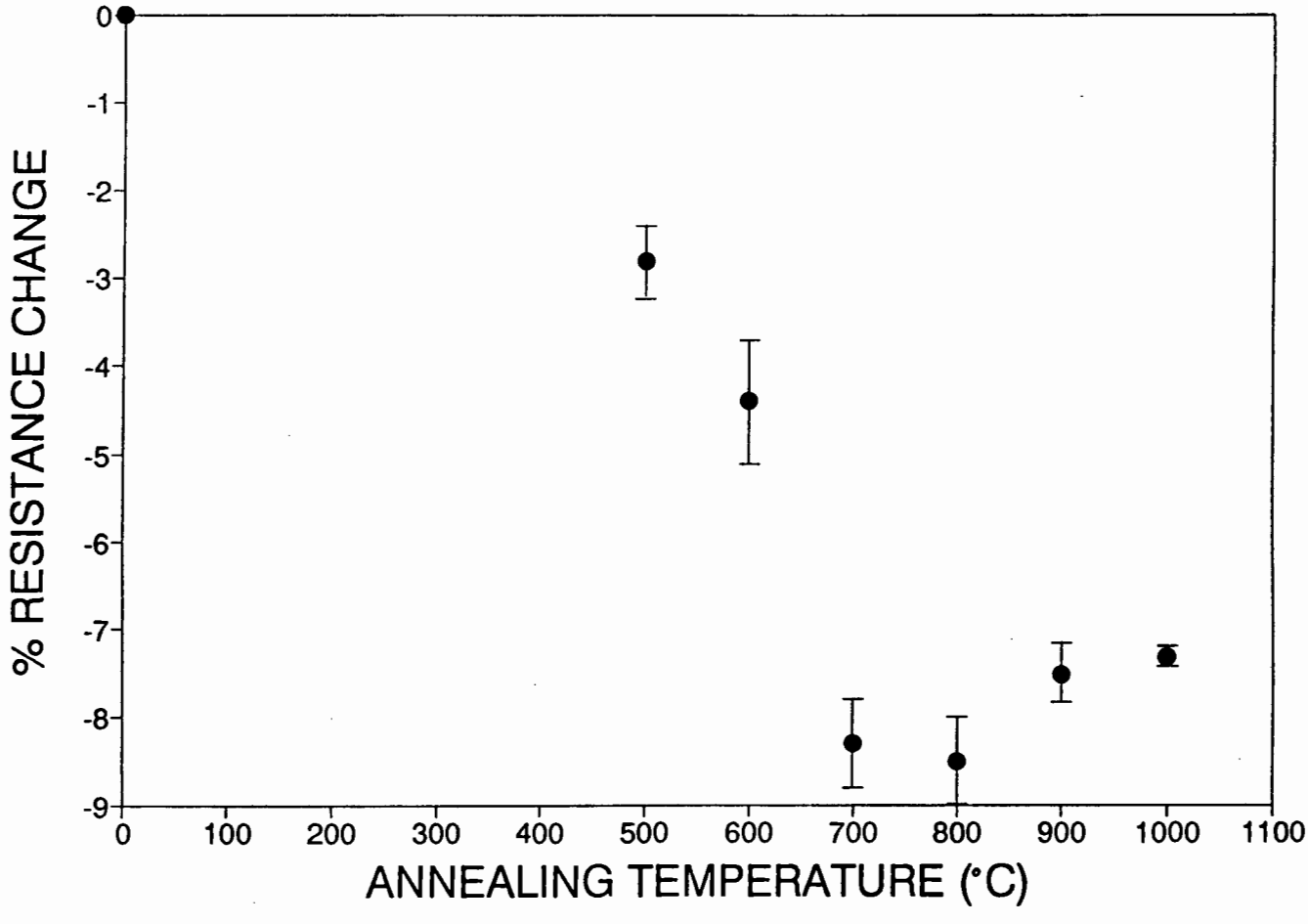

Figure 4.2: Graph of percentage change in resistance of palladium 4.1 at.% tungsten vs. annealing temperature.

The electrical resistivity of cold-worked palladium 10.3 at.% tungsten was 104 μΩ-cm at 22°C; this value is slightly higher than Klyuyeva et al's[133] figure of less than 100 μΩ-cm for palladium 12.7 at.% tungsten. The effect of annealing on resistance is shown in fig. 4.3. Annealing at temperatures up to 600°C results in a cumulative increase in resistance of three per cent; a much larger increase in resistance is observed after annealing at 700°C. The maximum change in resistance, approximately eight per cent, is reached after annealing at 800°C; this is considerably lower than Meskin et al's[140] figure of more than eighteen per cent (fig. 2.10). Higher temperature heat treatments have little effect on this value; a decrease in resistance was however observed in one specimen after annealing at 1000°C.

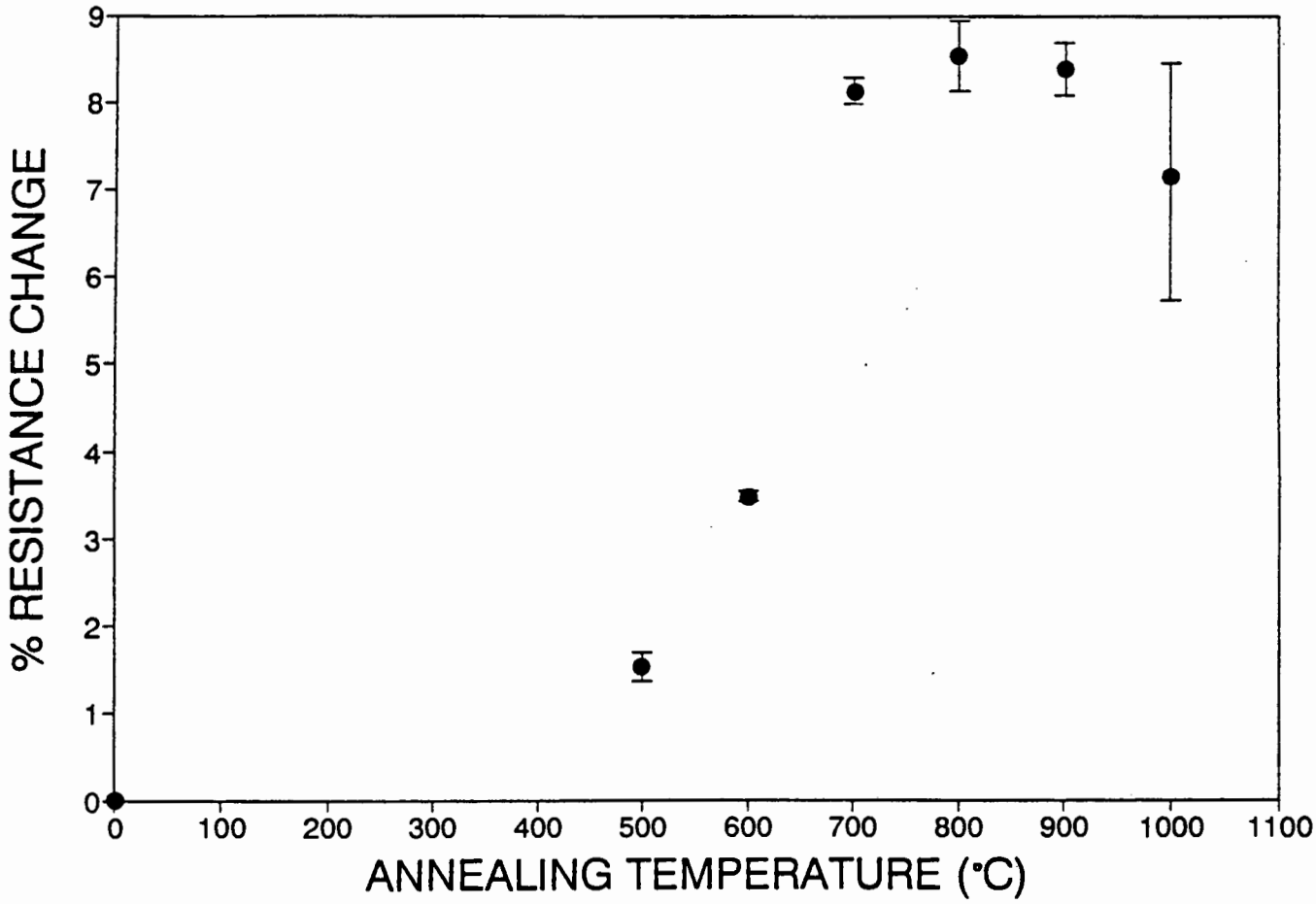

Figure 4.3: Graph of percentage change in resistance of palladium 10.3 at.% tungsten vs. annealing temperature.

The electrical resistivity of cold-worked palladium 11.6 at.% tungsten was 127 μΩ-cm at 22°C. The change in resistance due to annealing is shown in fig. 4.4. An increase in resistance of approximately four per cent is observed after annealing successively at 500°C and 600°C. Annealing at 700°C and 800°C produces large increases in resistance, followed after annealing at 900°C and 1000°C by smaller increases to a maximum resistance fourteen per cent greater than the resistance of the cold-worked specimen.

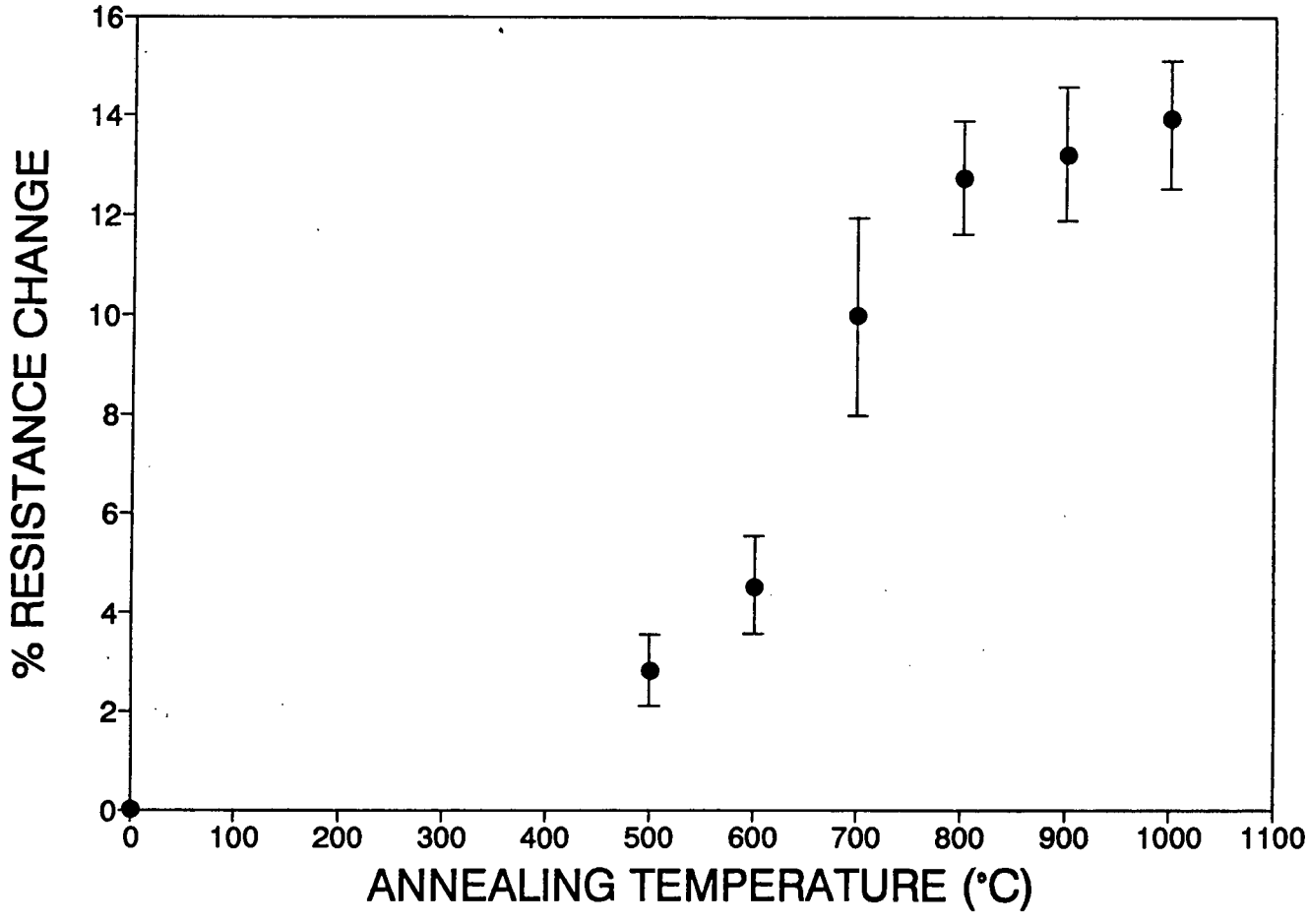

Figure 4.4: Graph of percentage change in resistance of palladium 11.6 at.% tungsten vs. annealing temperature.

Palladium-molybdenum

The electrical resistivity of cold-worked palladium 5.3 at.% molybdenum at 22°C was 33 μΩ-cm; this figure compares well with Kudielka-Artner and Argent's[104] measurement of 34.4 μΩ-cm for palladium 5 at.% molybdenum. Figure 4.5 shows the effect of annealing on electrical resistance. Successive annealing at temperatures up to 700°C is observed to result in a steady decrease in resistance, to a maximum resistance change of approximately four per cent; this is consistent with Mes'kin et al's[140] measured decrease of about three per cent (fig. 2.10). Annealing at temperatures above 700°C, however, increases the resistance to a final value, after annealing at 1000°C, approaching the resistance of the cold-worked specimen.

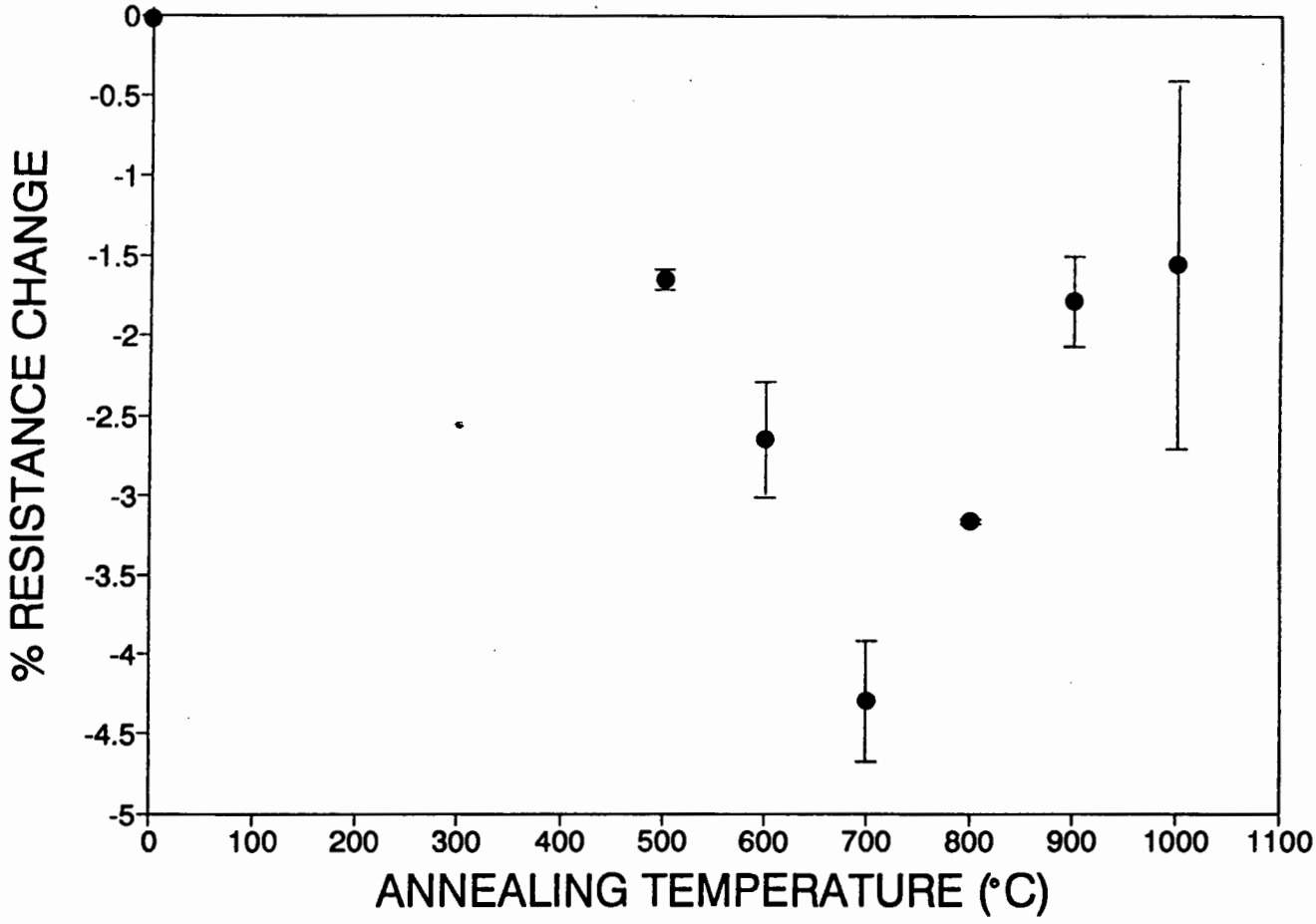

Figure 4.5: Graph of percentage change in resistance of palladium 5.3 at.% molybdenum vs. annealing temperature.

The electrical resistivity of cold-worked palladium 9.7 at.% molybdenum was 85 μΩ-cm at 22°C, which is consistent with Kudielka-Artner and Argent's figure of 87.9 μΩ-cm for palladium 10.4 at.% molybdenum[104]. The change in resistance due to annealing is shown in fig. 4.6. The resistance is observed to increase after each annealing experiment, the largest change occurring after heat treatment at 700°C, to a value twelve per cent greater than the cold-worked resistance. Mes'kin et al[140] measured an increase in resistance of eleven per cent for an alloy of similar composition. Smaller changes are observed after annealing at higher temperatures; the total cumulative resistance increase after annealing at 1000°C is approximately thirteen per cent.

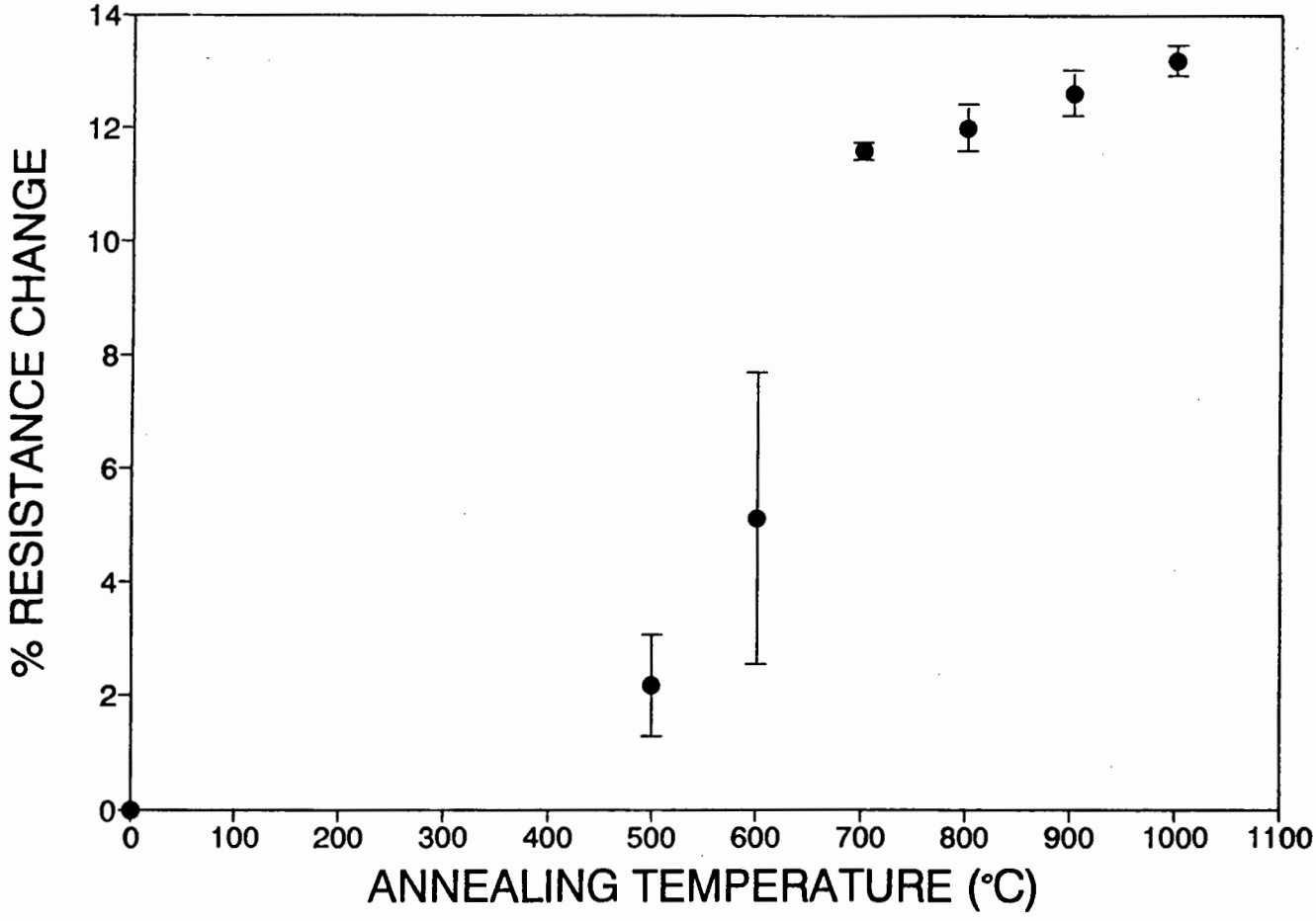

Figure 4.6: Graph of percentage change in resistance of palladium 9.7 at.% molybdenum vs. annealing temperature.

The electrical resistivity of cold-worked palladium 16.0 at.% molybdenum at 22°C was 138 μΩ-cm, ten times as great as that of cold-worked pure palladium. The effect of annealing on resistance is shown in fig. 4.7. A substantial increase in resistance is observed due to annealing at 600°C and 700°C, resulting in a cumulative increase in resistance of seven per cent. Heat treatments at higher temperatures produce no significant change in resistance.

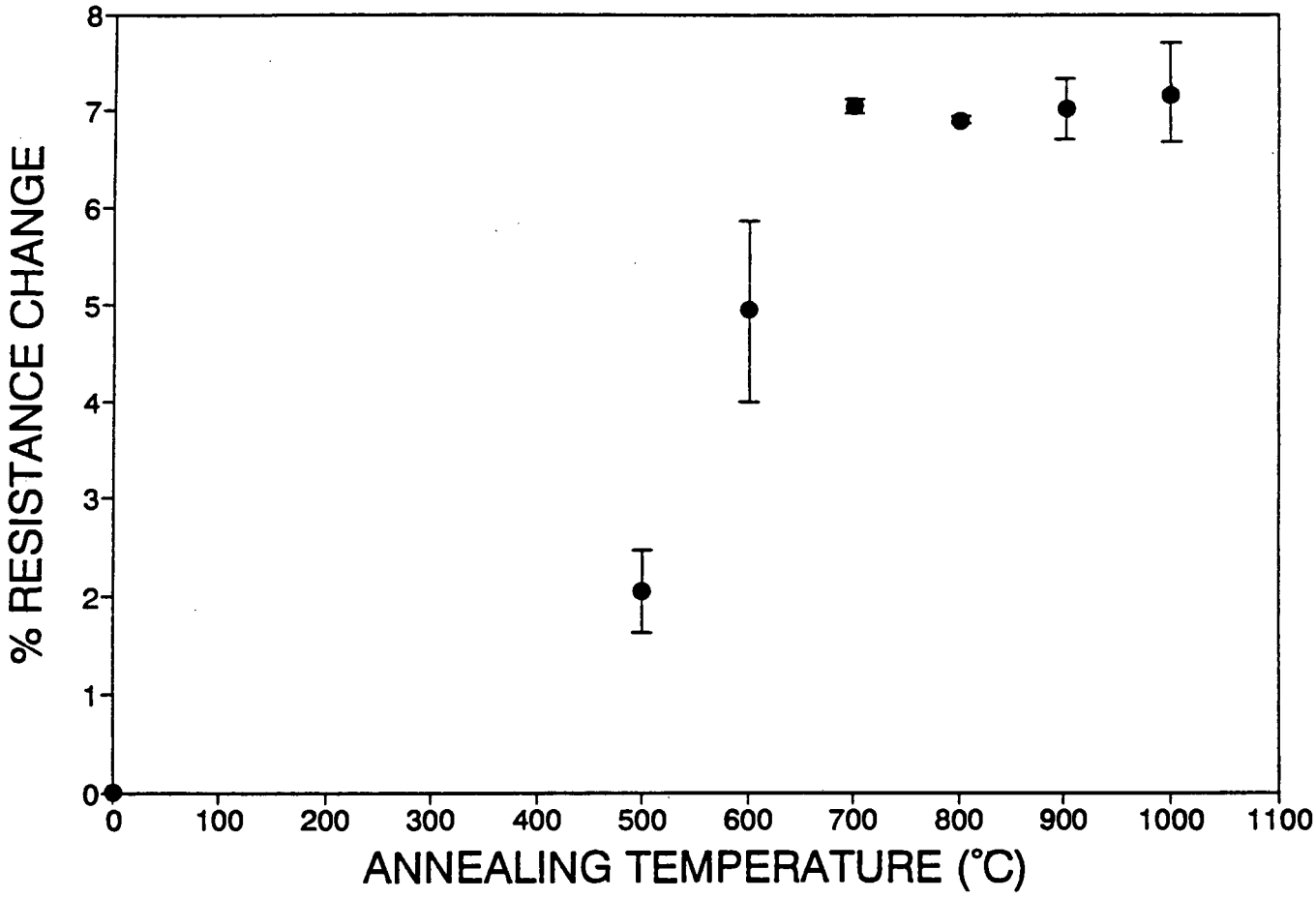

Figure 4.7: Graph of percentage change in resistance of palladium 16.0 at.% molybdenum vs. annealing temperature.

4.1.2 THE EFFECT OF SOLUTE CONCENTRATION ON ELECTRICAL RESISTIVITY

The results of the present work show the electrical resistivity of palladium to increase significantly with the addition of tungsten or molybdenum, by an order of magnitude in the composition ranges investigated. Figure 4.8 shows the measured resistivity of cold-worked palladium-tungsten and palladium-molybdenum at 22°C as a function of solute concentration.

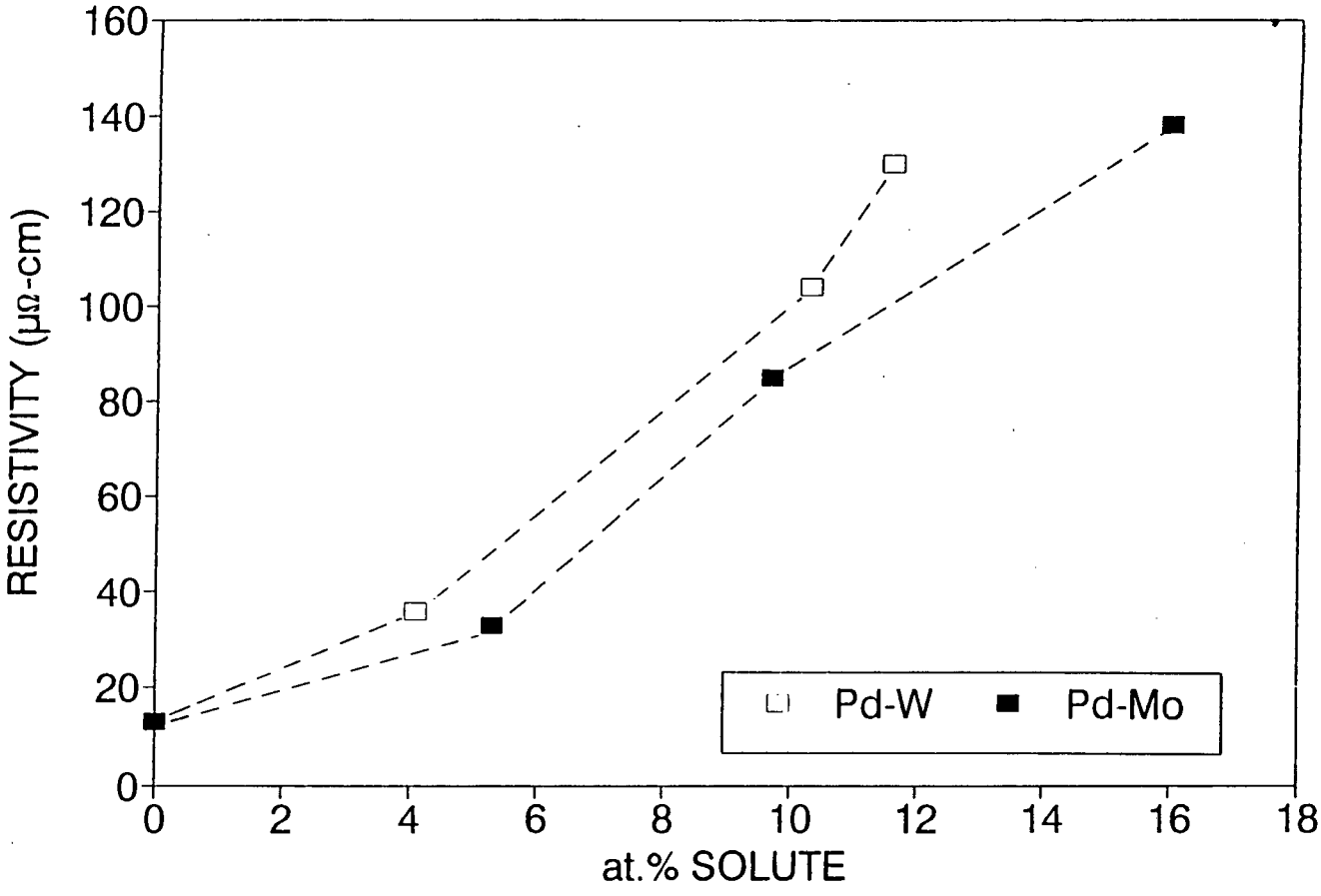

Figure 4.8: Graph of resistivity vs. solute concentration for cold-worked palladium-tungsten and palladium-molybdenum.

In all palladium-tungsten alloys a marked change in resistance is observed after annealing at temperatures up to 700°C. This change is negative for palladium 4.1 at.% tungsten; however, the magnitude of the decrease is larger than might be expected to occur due to a decrease in dislocation density during recovery. Both palladium 10.3 at.% tungsten and palladium 11.6 at.% tungsten exhibit an

increase in resistance after annealing at 700°C, the magnitude of the increase being greater for the higher solute concentration. The change in resistance of palladium-molybdenum alloys due to annealing follows a similar trend to palladium-tungsten alloys. After annealing at temperatures up to 700°C, palladium 5.3 at.% molybdenum shows a decrease in resistance, whereas palladium 9.7 at.% molybdenum and palladium 16.0 at.% molybdenum show an increase in resistance; the percentage increase in resistance after annealing at 700°C is larger for palladium 9.7 at.% molybdenum than for palladium 16.0 at.% molybdenum. Figure 4.9 shows the dependence on composition of the resistivity change after annealing at 700°C for palladium-tungsten and palladium-molybdenum. These results are in general consistent with those of Mes'kin et al[140], although the latter suggest the existence of a maximum in the resistance increase between 10 at.% tungsten and 12 at.% tungsten.

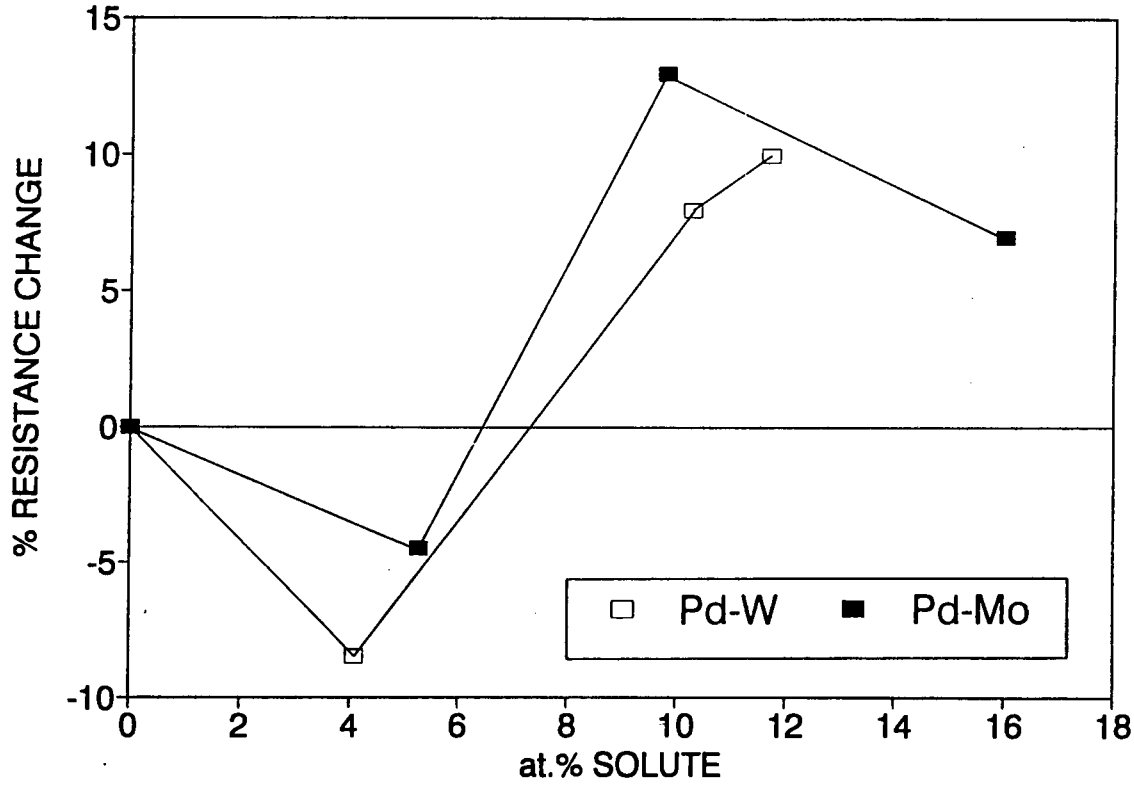

Figure 4.9: Graph of percentage change in resistance after annealing at 700°C vs. solute concentration for palladium-tungsten and palladium-molybdenum.

4.2 CRYSTAL STRUCTURE

Selected area zone-axis electron diffraction patterns from all the materials, in the cold-worked and annealed conditions, were investigated for evidence of changes due to annealing. Electron diffraction patterns of the high symmetry [001], [110], [111] and [112] zone axes, at exposure times of up to 30 minutes, were taken in each case. Obtaining diffraction patterns from materials in the cold-worked condition presented some difficulty, since foil regions which were sufficiently thin for electron diffraction exhibited local bending due to the high dislocation density. With the exception of some split matrix reflections as a result of this, diffraction patterns of all the cold-worked alloys reveal a normal fcc crystal structure with no unexpected features. A set of zone-axis electron diffraction patterns for palladium 10.3 at.% tungsten, shown in figs. 4.10 and 4.11, is representative of alloys in the cold-worked condition.

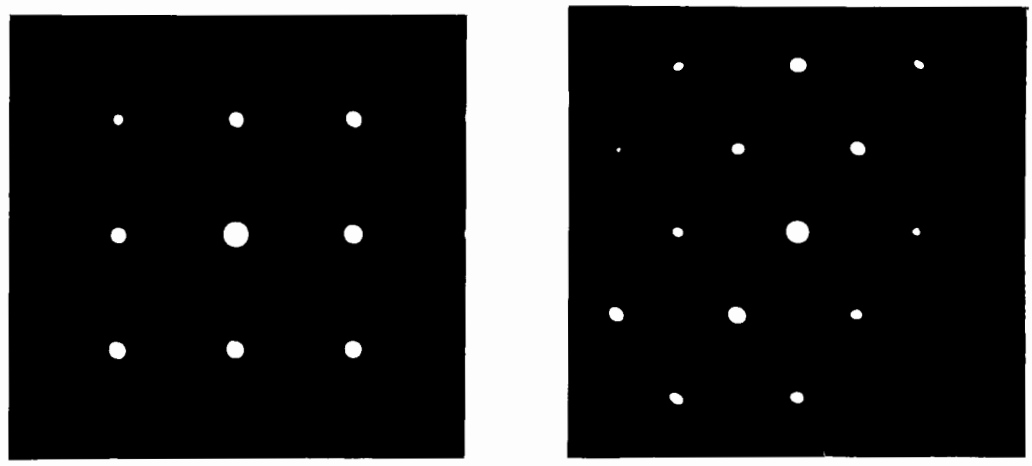

(a) (b)

Figure 4.10: Electron diffraction patterns from palladium 10.3 at.% tungsten in the cold-worked condition: (a) [001] zone axis (b) [110] zone axis.

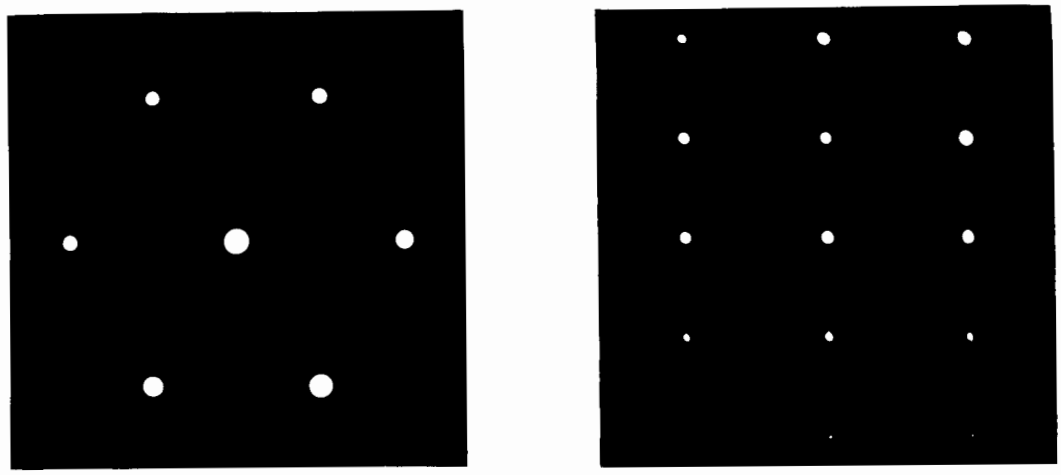

(a) (b)

Figure 4.11 Electron diffraction patterns from palladium 10.3 at.% tungsten in the cold-worked condition: (a) [111] zone axis (b) [112] zone axis.

Figures 4.12 and 4.13 show zone axis electron diffraction patterns of palladium 5.3 at.% molybdenum after annealing at 700°C. Sharp additional reflections are observed in the [111] and [112] zone axis diffraction patterns, at the $1/3$242-type and $1/2$131-type positions respectively, as shown in fig. 4.13. (The convention $1/3$242 or $1/2$131 is used to signify a position in reciprocal space with particular reference to the fcc structure). In order to determine the microstructural features from which these additional reflections arise, dark-field images were recorded with the objective aperture placed over the centered additional reflection. Figure 4.14 shows a bright-field image and a dark-field image obtained by using the $1/3$242-type reflection arrowed in fig. 4.13 (a). The region shown in the bright-field image, fig. 4.14 (a), is observed in the dark-field image to contain precipitate-like features, as shown in fig. 4.14 (b). Figure 4.15 shows a bright-field image and a dark-field image obtained by using the $1/2$131-type reflection arrowed in fig. 4.13 (b). A bright-field image containing precipitate-like features is shown in fig. 4.15 (a); in the dark-field image, shown in fig. 4.15 (b), a distribution of fine precipitates is brought into contrast.

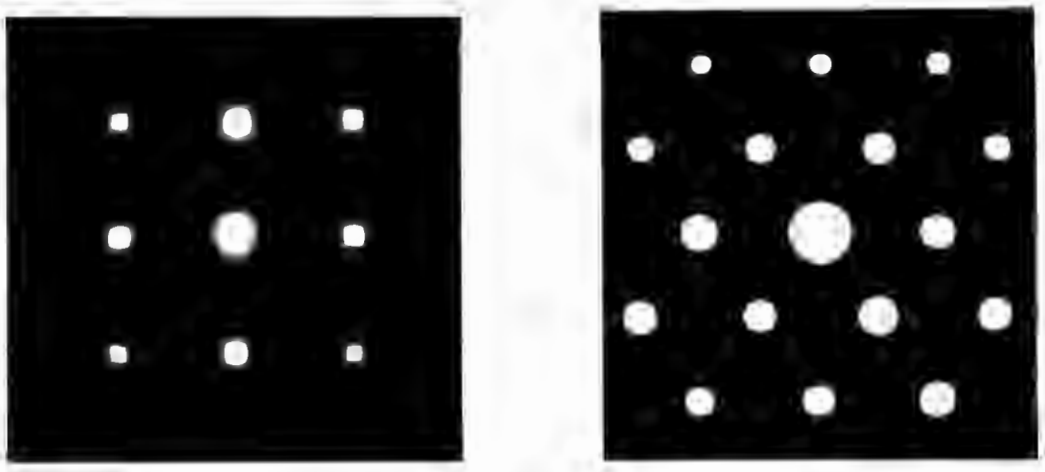

(a) (b)

Figure 4.12: Electron diffraction patterns from palladium 5.3 at.% molybdenum after annealing at 700°C: (a) [001] zone axis (b) [110] zone axis.

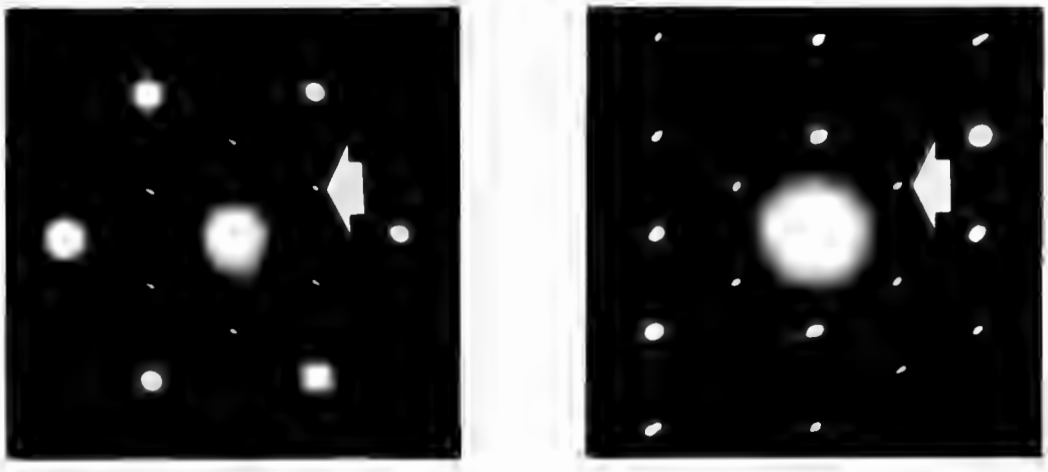

(a) (b)

Figure 4.13: Electron diffraction patterns from palladium 5.3 at.% molybdenum after annealing at 700°C: (a) [111] zone axis showing additional reflections at $1/3$242-type positions (b) [112] zone axis, showing additional reflections at $1/2$131-type positions.

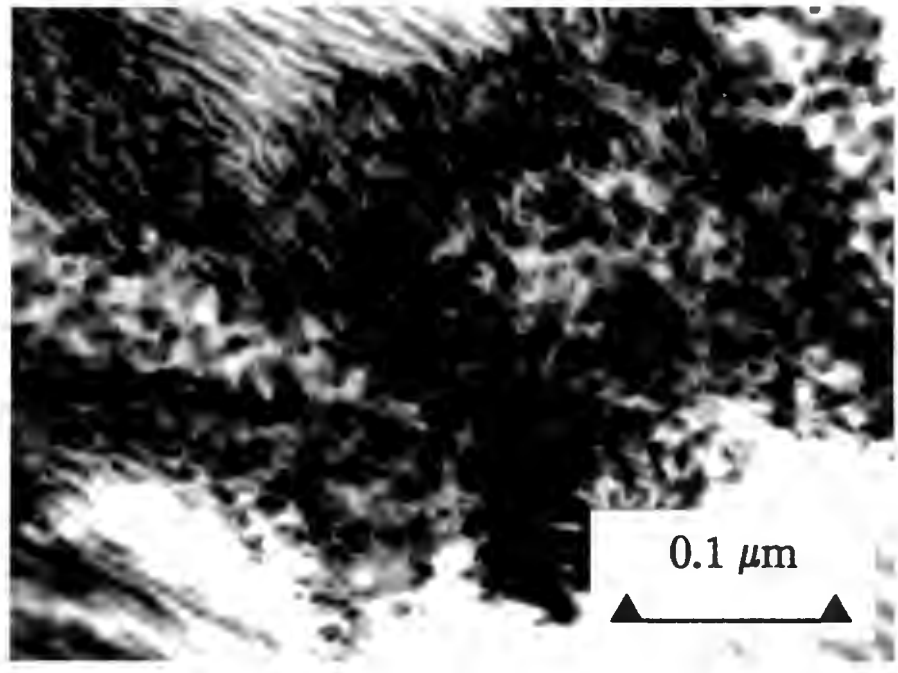

(a)

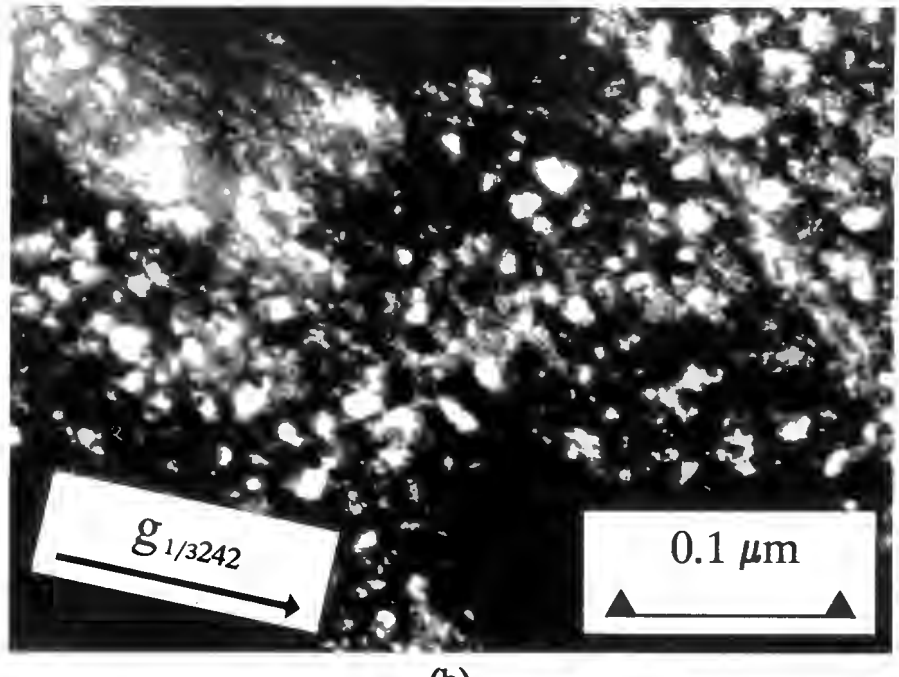

(b)

Figure 4.14: Palladium 5.3 at.% molybdenum after annealing at 700°C: (a) bright-field image (b) dark-field image using $_{1/3}$242-type reflection arrowed in fig. 4.13 (a), showing precipitates.

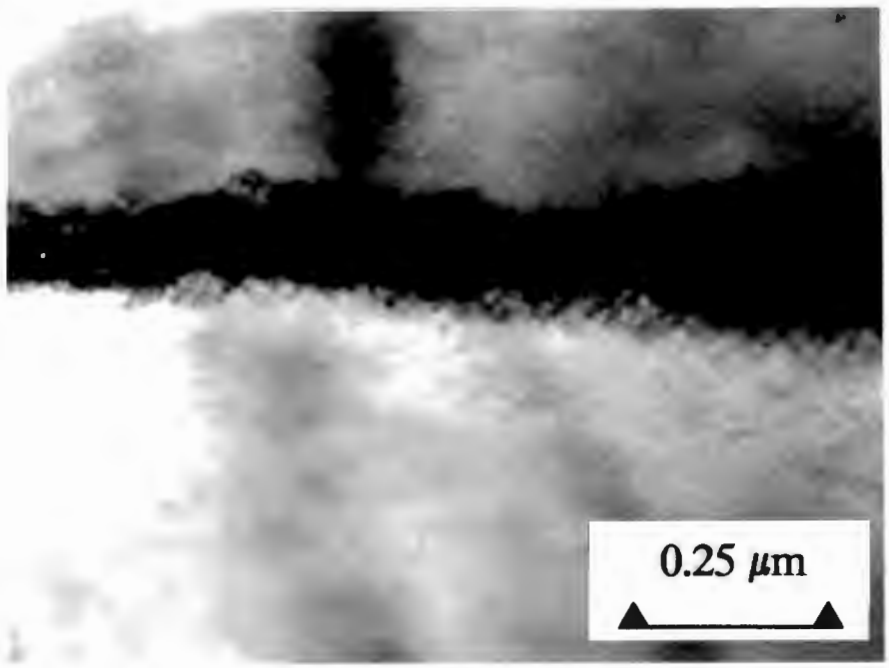

(a)

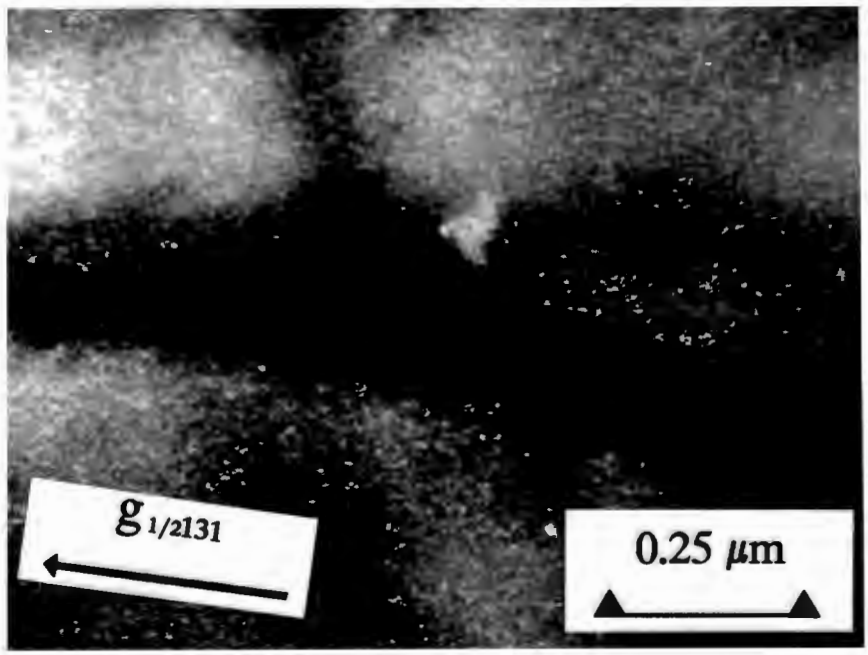

(b)

Figure 4.15: Palladium 5.3 at.% molybdenum after annealing at 700°C: (a) bright-field image (b) dark-field image using $1/2$131-type reflection arrowed in fig. 4.13 (b), showing distribution of precipitates.

The presence of *sharp* additional reflections in zone axis electron diffraction patterns after annealing at 700°C is observed only in palladium 5.3 at.% molybdenum. However, in the remaining five alloys faint or diffuse reflections are visible at $1/3$242-type positions in [111] zone axis electron diffraction patterns, and at $1/2$131-type positions in [112] zone axis electron diffraction patterns. These reflections remain visible after further annealing at temperatures up to 1000°C. After annealing palladium 5.3 at.% molybdenum at temperatures up to 1000°C, the sharp additional reflections observed in [111] and [112] zone axis electron diffraction patterns after annealing at 700°C (fig. 4.13) have become fainter and more diffuse. In all alloys after annealing at 1000°C then, reflections at $1/3$242-type positions in [111] zone axis electron diffraction patterns and at $1/2$131-type positions in [112] zone axis electron diffraction patterns are observed.

Figure 4.16 shows the high symmetry [001], [110], [111] and [112] zone-axis electron diffraction patterns of pure palladium after annealing at 500°C. The zone axis diffraction patterns reveal no features additional to the fundamental fcc lattice reflections. Figures 4.17 - 4.22 show the high symmetry zone axis diffraction patterns of the alloys investigated, after annealing at 1000°C. Electron diffraction patterns of [001] and [110] zone axes do not contain reflections other than the fundamental fcc lattice reflections. Long exposure times are required in order to record the faint additional reflections in [111] and [112] zone axis electron diffraction patterns referred to above. It is not always possible to print diffraction patterns in such a way as to make clear the information contained in the negative, since the additional reflections are faint with respect to the fundamental fcc lattice reflections on the negative.

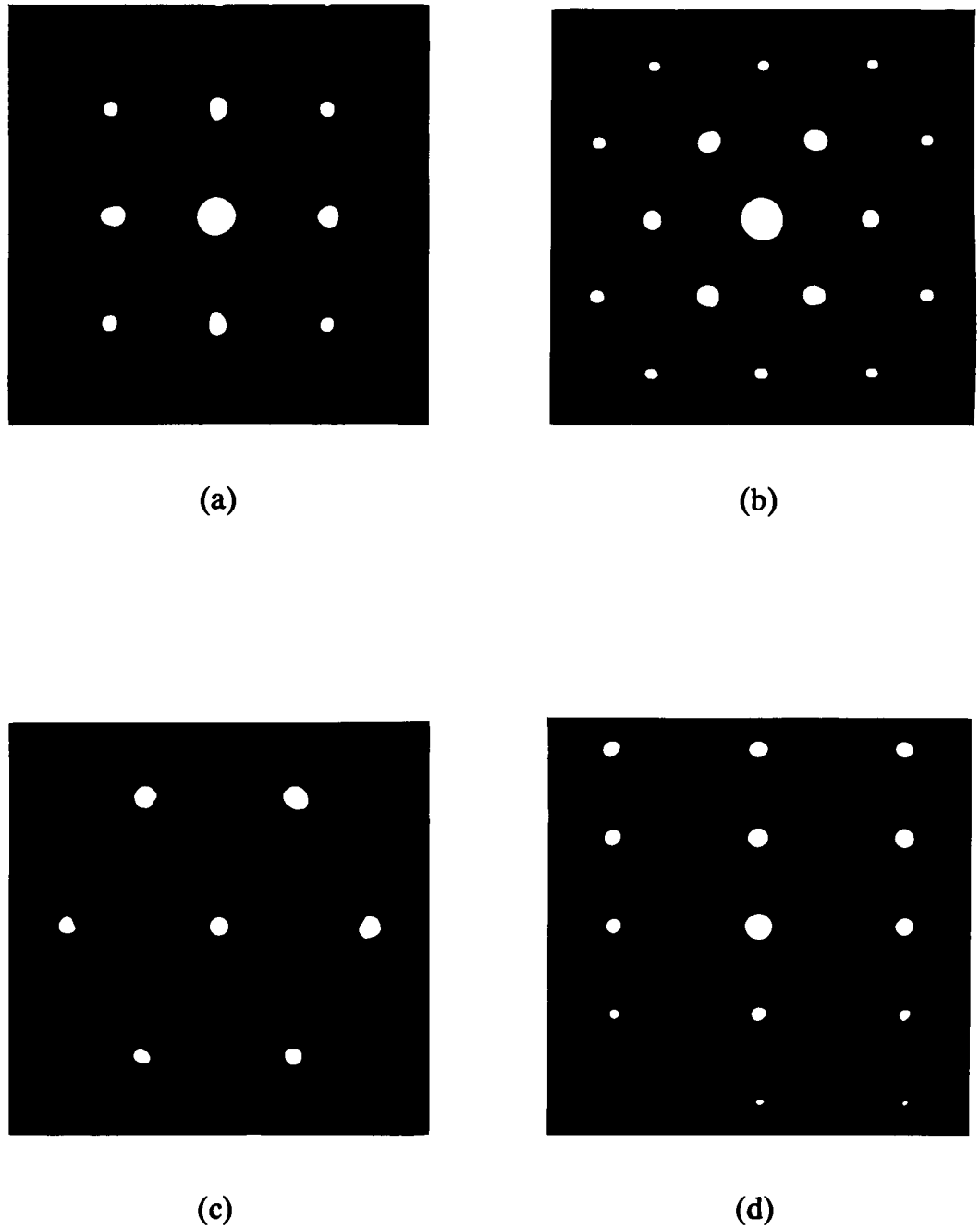

Figure 4.16: Electron diffraction patterns from palladium after annealing at 500°C: (a) [001] zone axis (b) [110] zone axis (c) [111] zone axis (d) [112] zone axis.

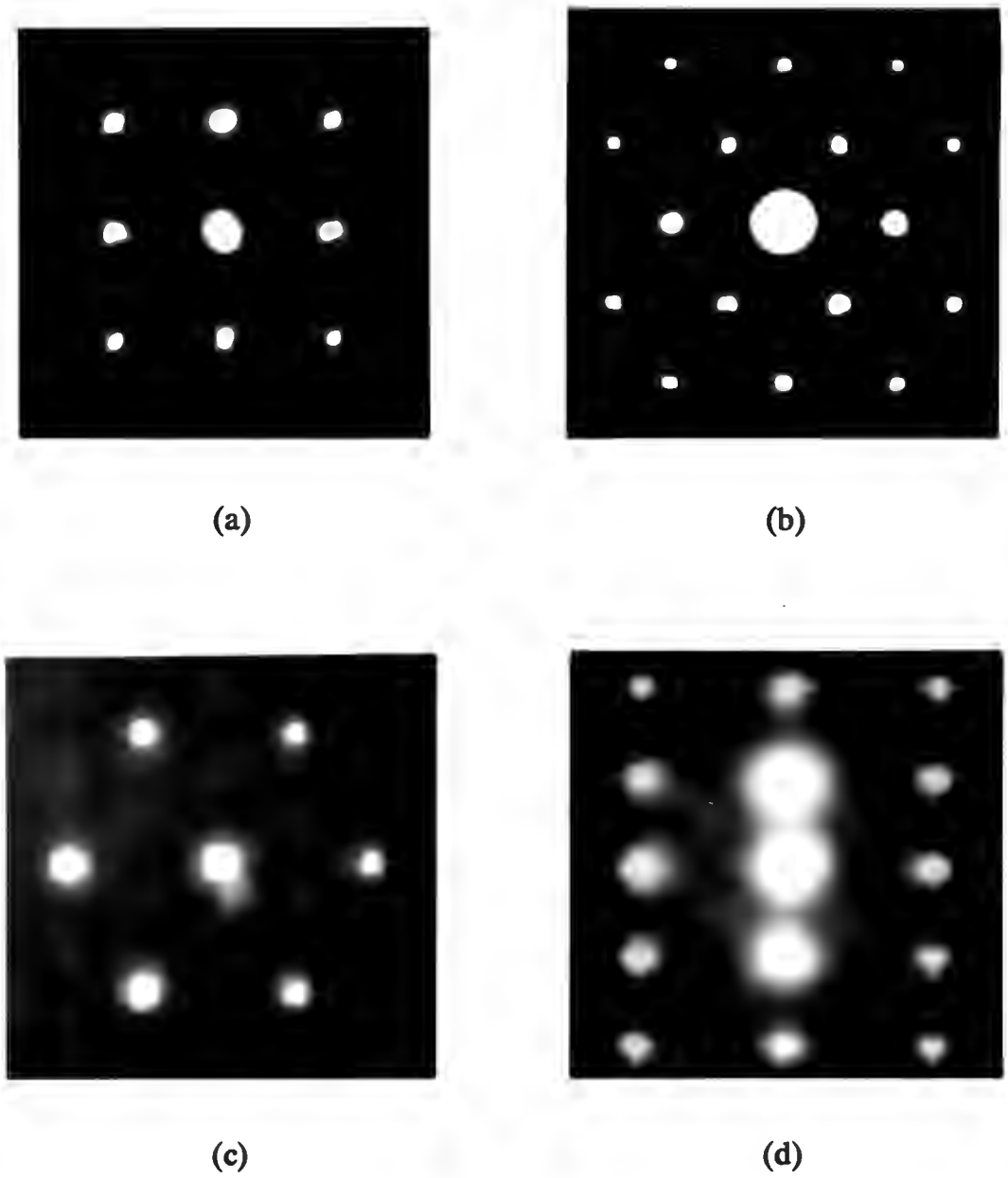

Figure 4.17: Electron diffraction patterns from palladium 4.1 at.% tungsten after annealing at 1000°C: (a) [001] zone axis (b) [110] zone axis (c) [111] zone axis, showing faint reflections at $1/3$242-type positions (d) [112] zone axis, showing faint reflections at $1/2$131-type positions.

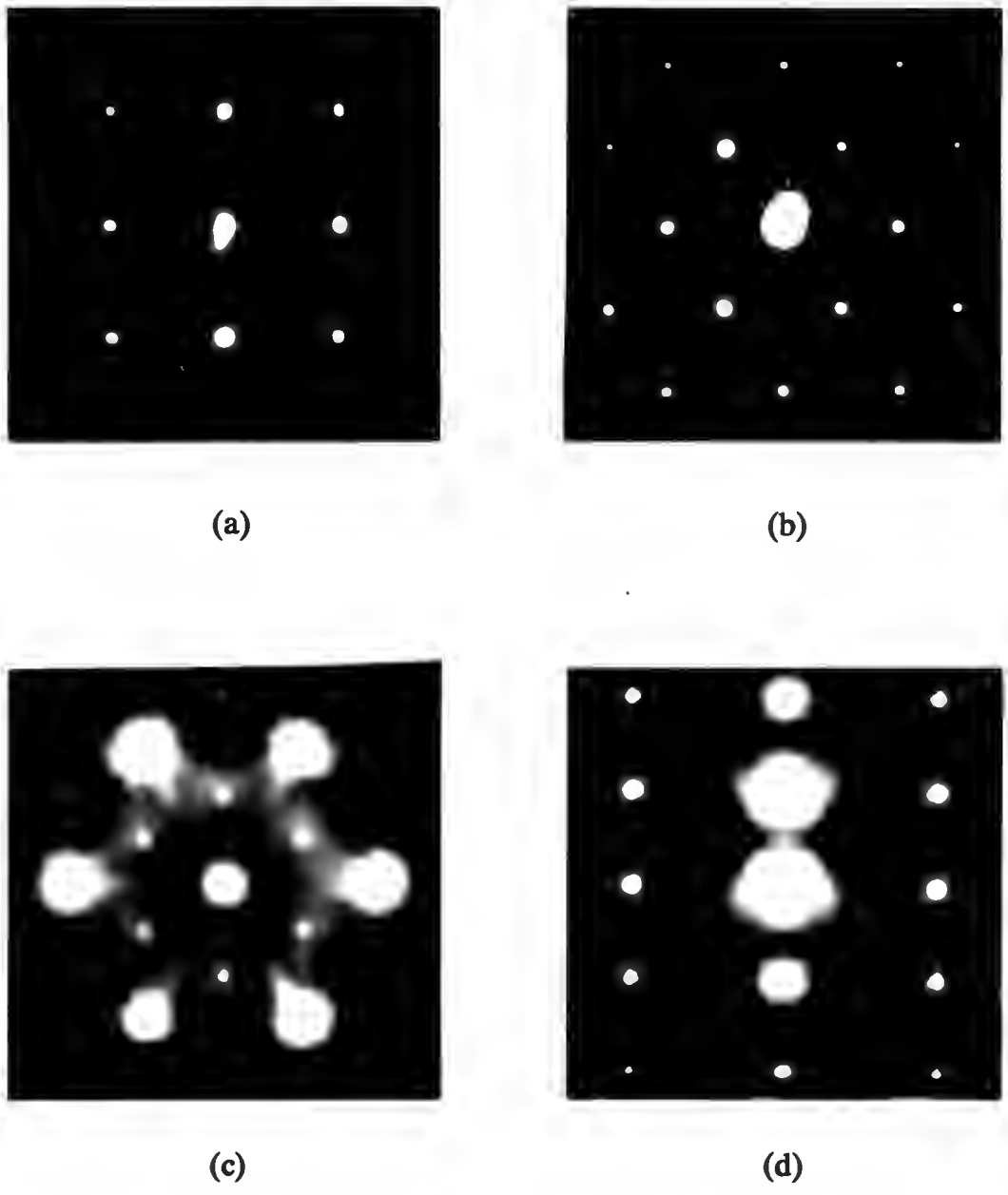

Figure 4.18: Electron diffraction patterns from palladium 10.3 at.% tungsten after annealing at 1000°C: (a) [001] zone axis (b) [110] zone axis (c) [111] zone axis, showing reflections at $1/3$242-type positions, faint with respect to fundamental fcc reflections (d) [112] zone axis, showing diffuse reflections at $1/2$131-type positions.

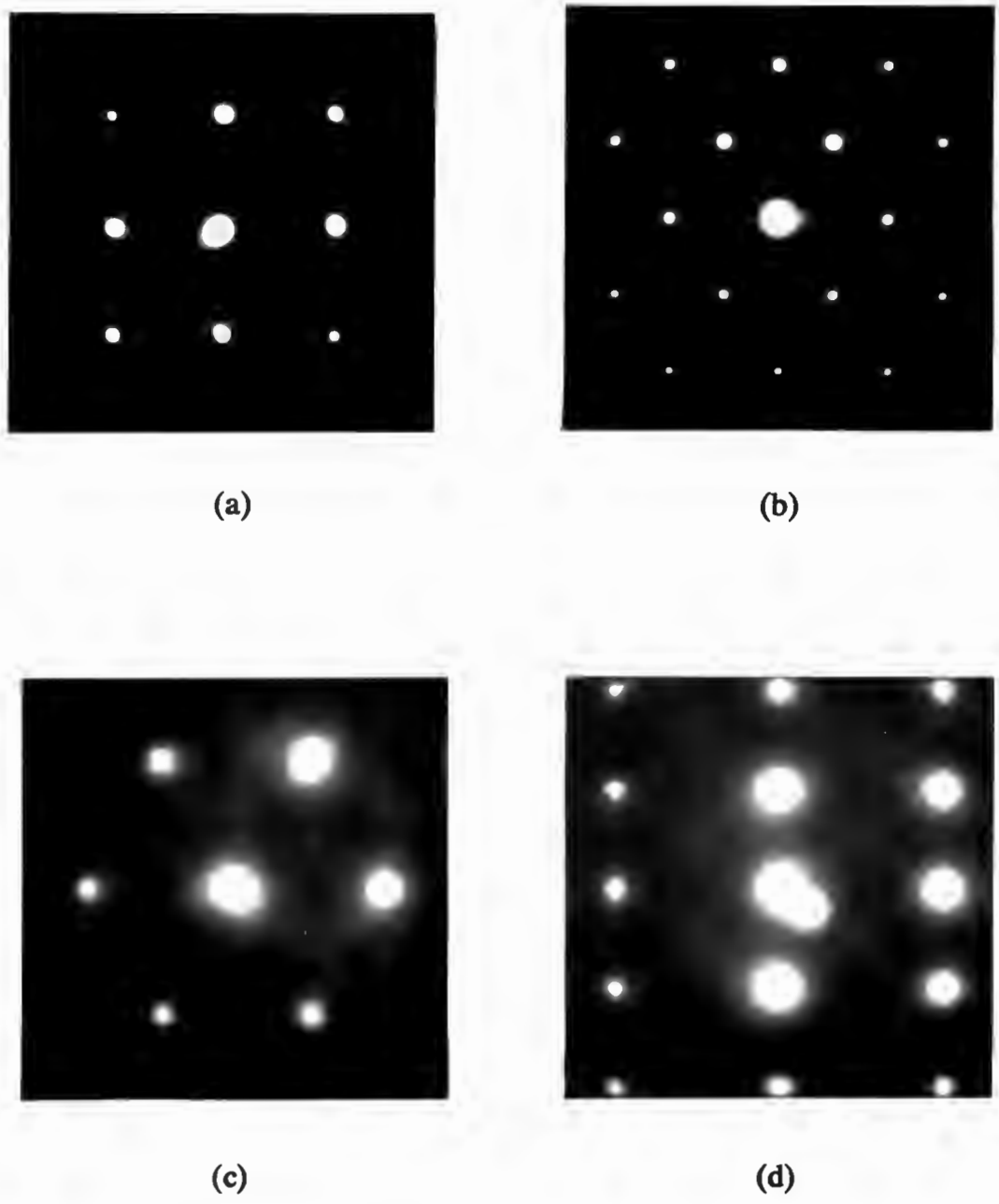

Figure 4.19: Electron diffraction patterns from palladium 11.6 at.% tungsten after annealing at 1000°C: (a) [001] zone axis (b) [110] zone axis (c) [111] zone axis, showing diffuse reflections at $1/3$242-type positions (d) [112] zone axis, showing diffuse reflections at $1/2$131-type positions.

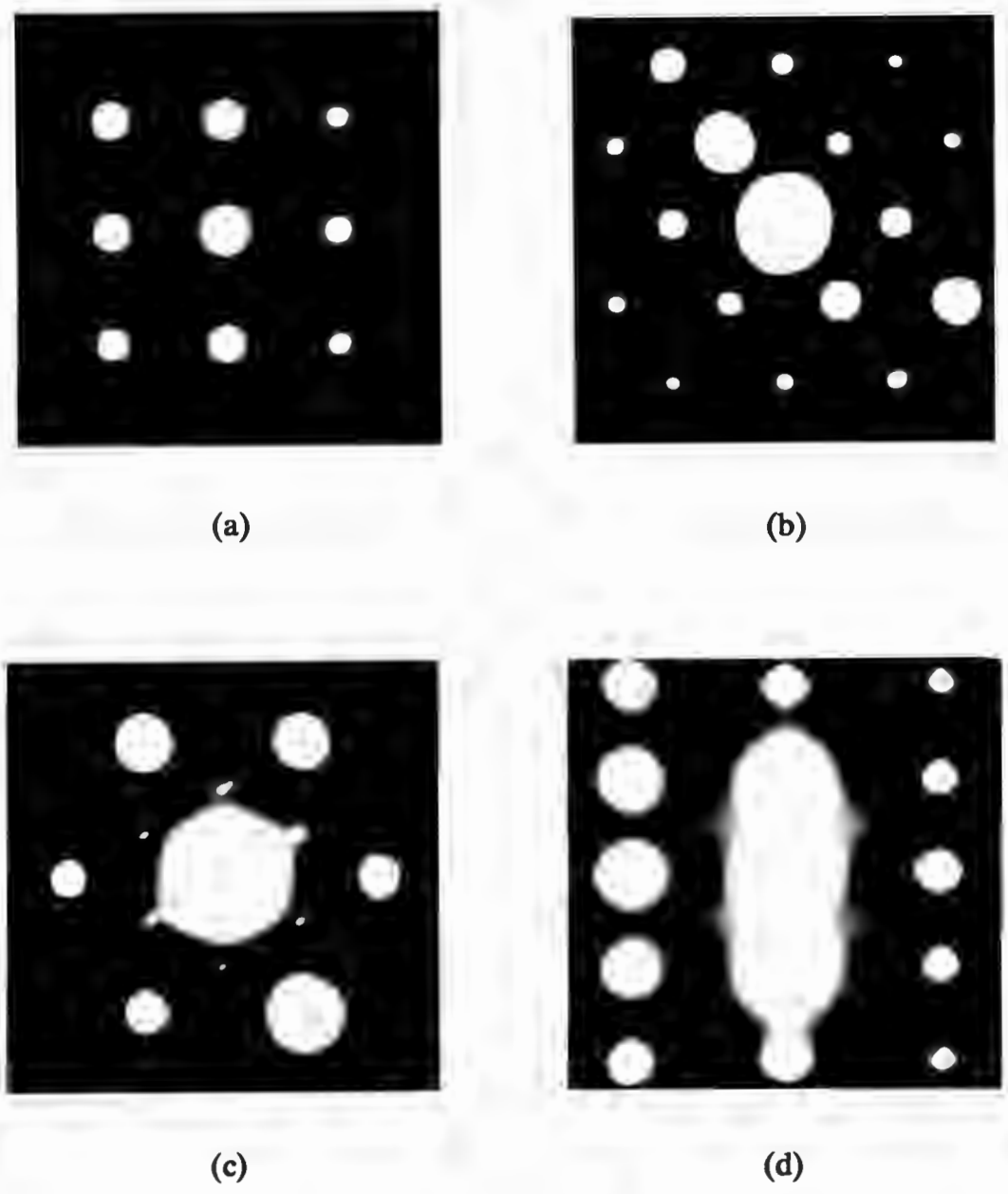

Figure 4.20: Electron diffraction patterns from palladium 5.3 at.% molybdenum after annealing at 1000°C: (a) [001] zone axis (b) [110] zone axis (c) [111] zone axis, showing reflections at $1/3$242-type positions, faint with respect to fundamental fcc lattice reflections (d) [112] zone axis, showing diffuse reflections at $1/2$131-type positions.

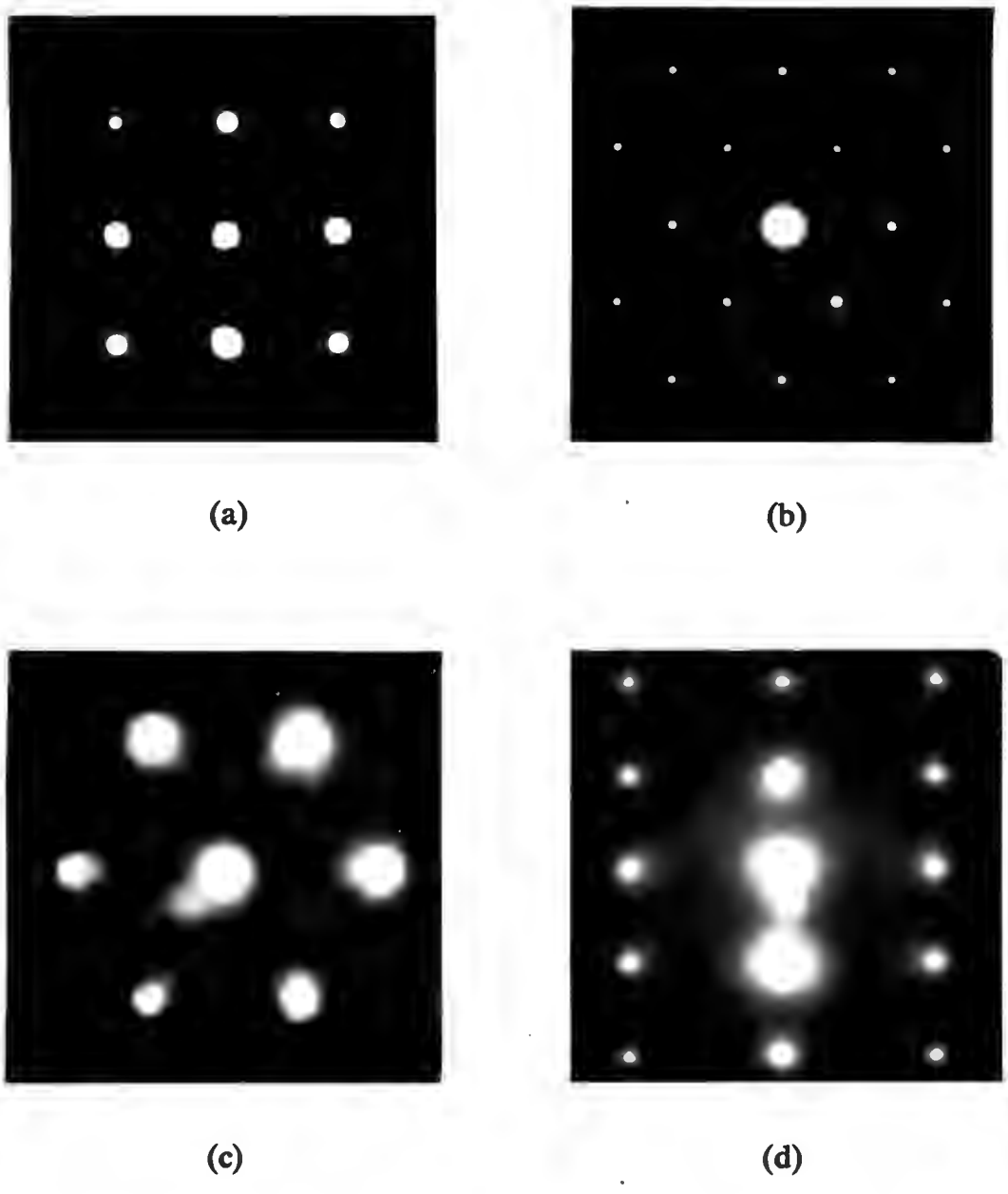

Figure 4.21: Electron diffraction patterns from palladium 9.7 at.% molybdenum after annealing at 1000°C: (a) [001] zone axis (b) [110] zone axis (c) [111] zone axis, showing diffuse reflections at $1/3$242-type positions (d) [112] zone axis, showing diffuse reflections at $1/2$131-type positions.

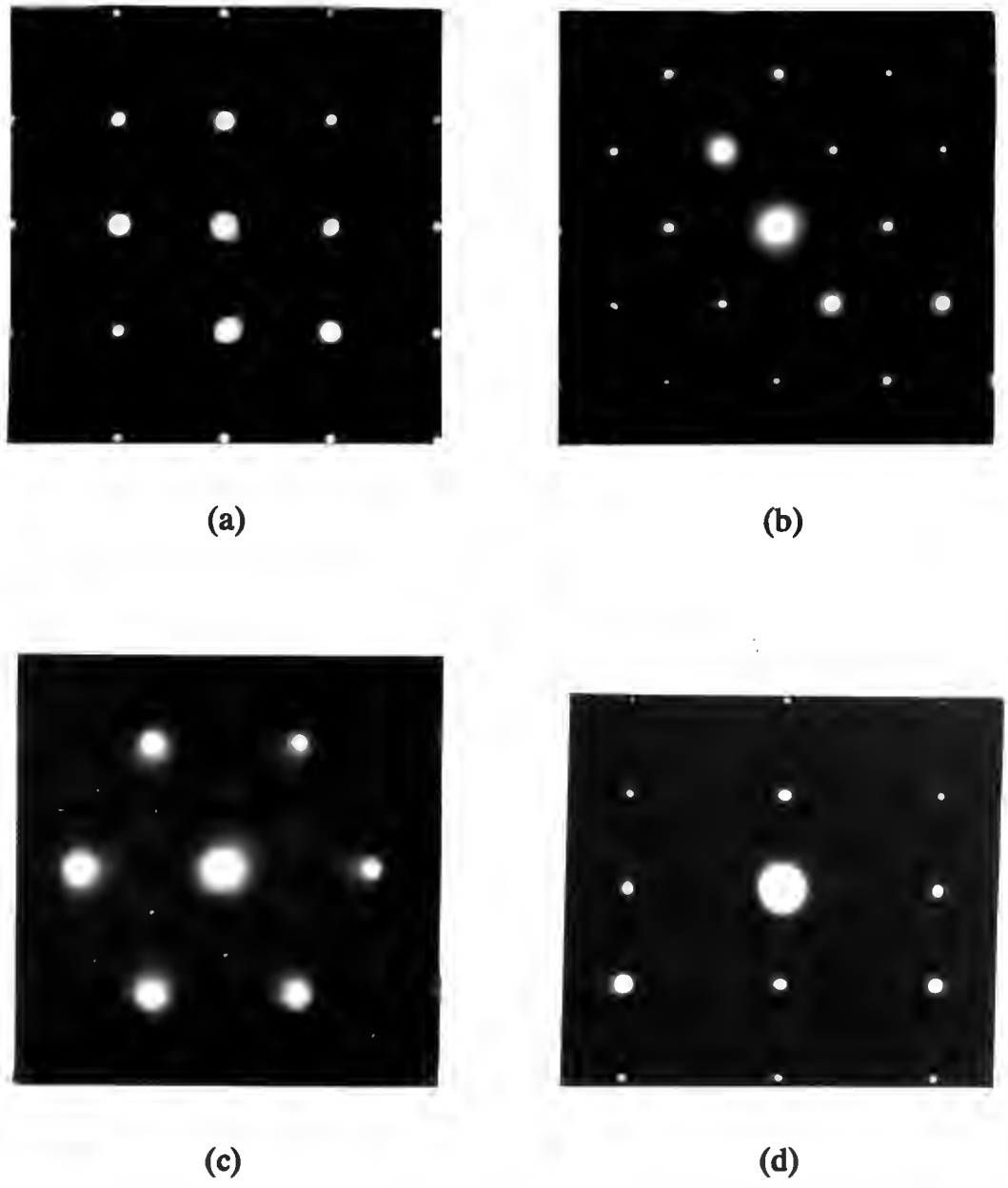

Figure 4.22: Electron diffraction patterns from palladium 16.0 at.% molybdenum after annealing at 1000°C: (a) [001] zone axis (b) [110] zone axis (c) [111] zone axis, showing faint reflections at $1/3$242-type positions (d) [112] zone axis; very diffuse reflections at $1/2$131-type positions on the negative are not visible in the print.

4.3 MICROSTRUCTURE

4.3.1 TRANSMISSION ELECTRON MICROSCOPY

Palladium

Transmission electron micrographs of pure palladium before and after annealing are shown in figs. 4.23 - 4.25. In the cold-worked condition, shown in fig. 4.23, a high dislocation density is observed, as expected due to the high degree of deformation associated with the cold-rolling process; a cellular dislocation structure is evident. After annealing at 300°C, the nucleation of recrystallised grains is observed, as shown in fig. 4.24. Recrystallisation is complete after annealing at 500°C; isolated dislocations are observed in the recrystallised grains, as shown in fig. 4.25.

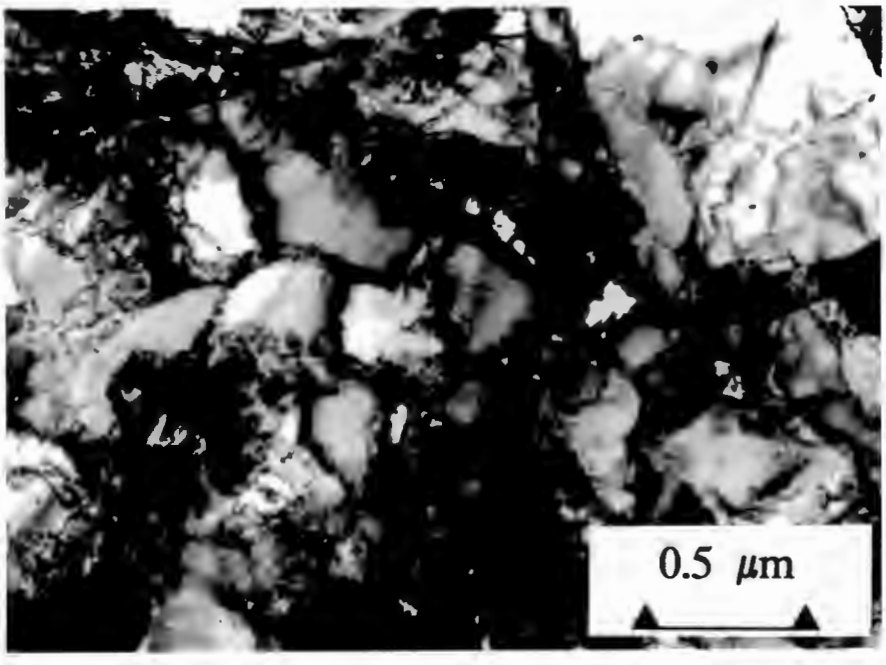

Figure 4.23: Bright-field transmission electron micrograph of palladium in the cold-worked condition, showing dislocation cells.

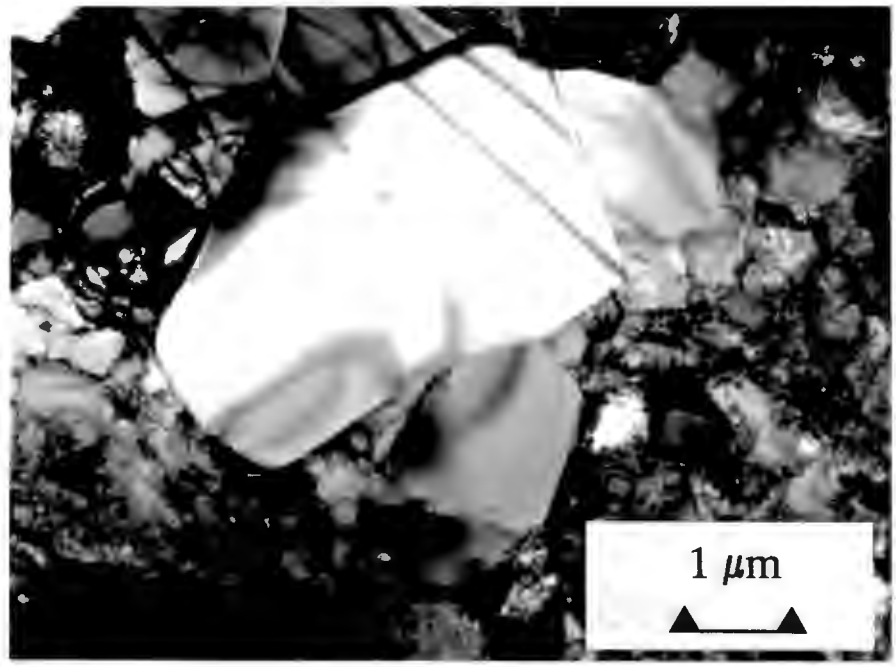

Figure 4.24: Bright-field transmission electron micrograph of palladium after annealing at 300°C, showing recrystallised grains surrounded by dislocations.

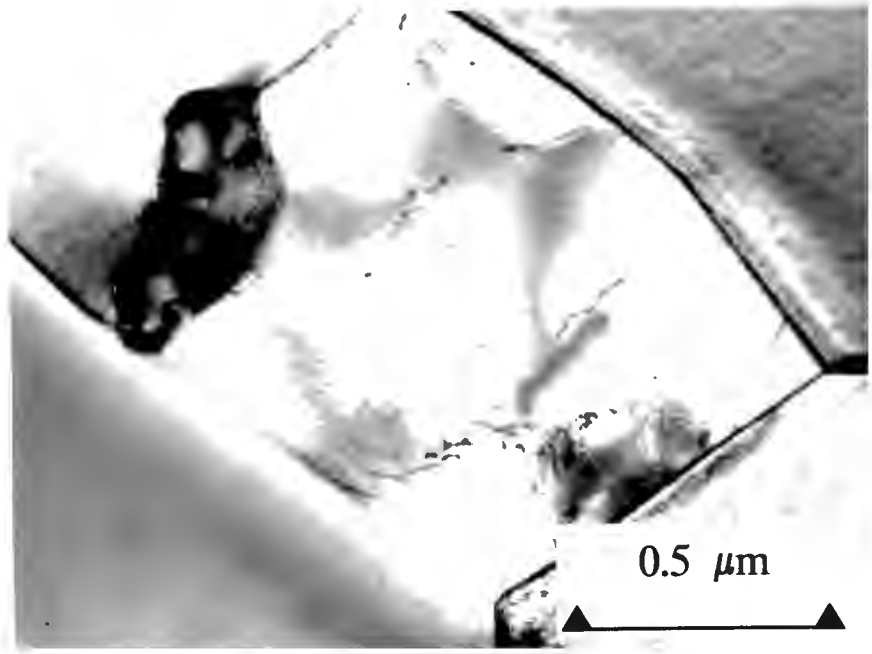

Figure 4.25: Bright-field transmission electron micrograph of palladium after annealing at 500°C, showing fully recrystallised microstructure containing isolated dislocations.

Palladium-tungsten

Figures 4.26 - 4.29 show transmission electron micrographs of palladium 4.1 at.% tungsten before and after annealing. Figure 4.26 illustrates the microstructure of the deformed alloy before annealing. Annealing at temperatures up to 700°C, the temperature at which nucleation of recrystallised grains occurs, does not result in a significant decrease in dislocation density; however some rearrangement of dislocations into low-angle boundary arrays is observed, as shown in figs. 4.27 (a) and (b). Annealing at 800°C results in the growth of recrystallised grains into the surrounding regions of high dislocation density; the microstructure is fully recrystallised after annealing at 900°C. The fully recrystallised microstructure is characterised by the presence of annealing twins, as illustrated in fig. 4.28.

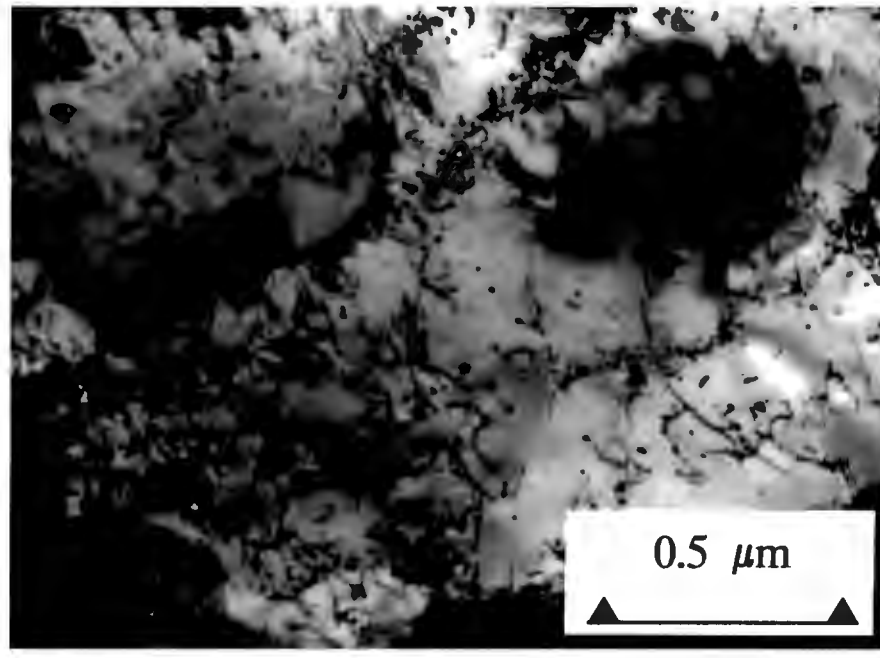

Figure 4.26: Bright-field transmission electron micrograph of palladium 4.1 at.% tungsten in the cold-worked condition.

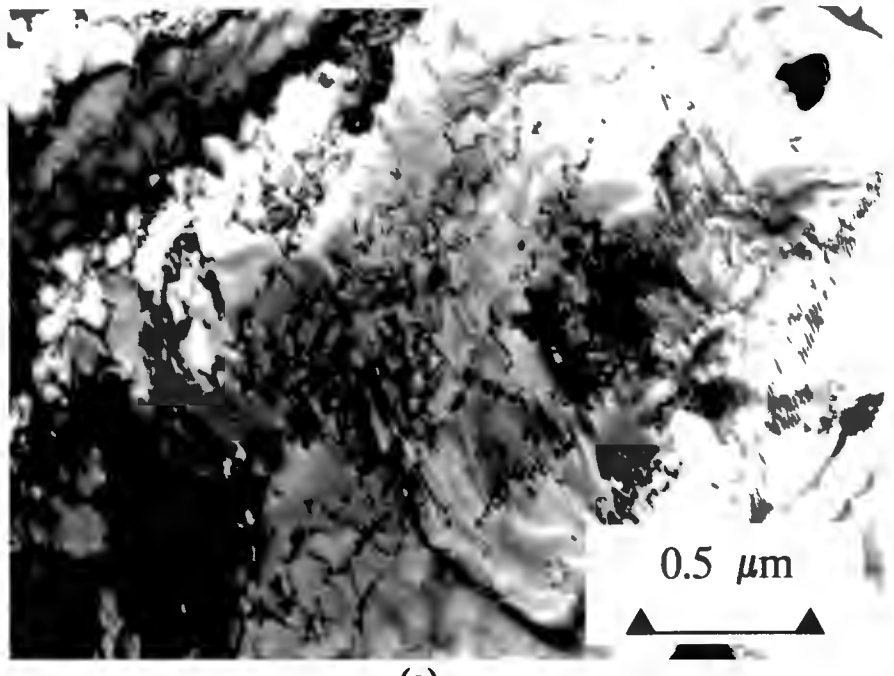

(a)

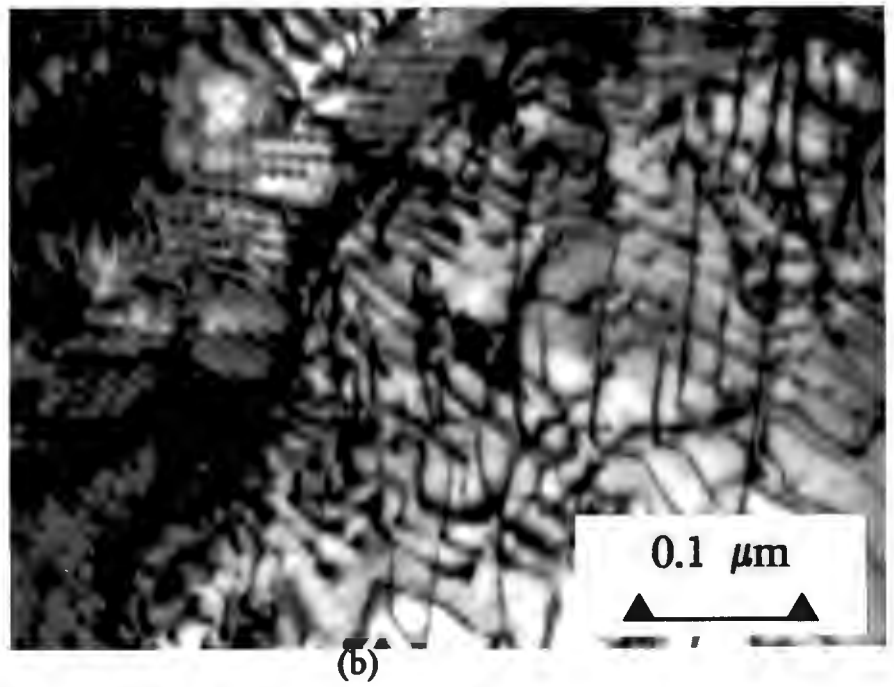

(b)

Figure 4.27: Bright-field transmission electron micrograph of palladium 4.1 at.% tungsten after annealing at 700°C: (a) showing evidence of low-angle boundary formation; (b) showing detail of dislocation structure.

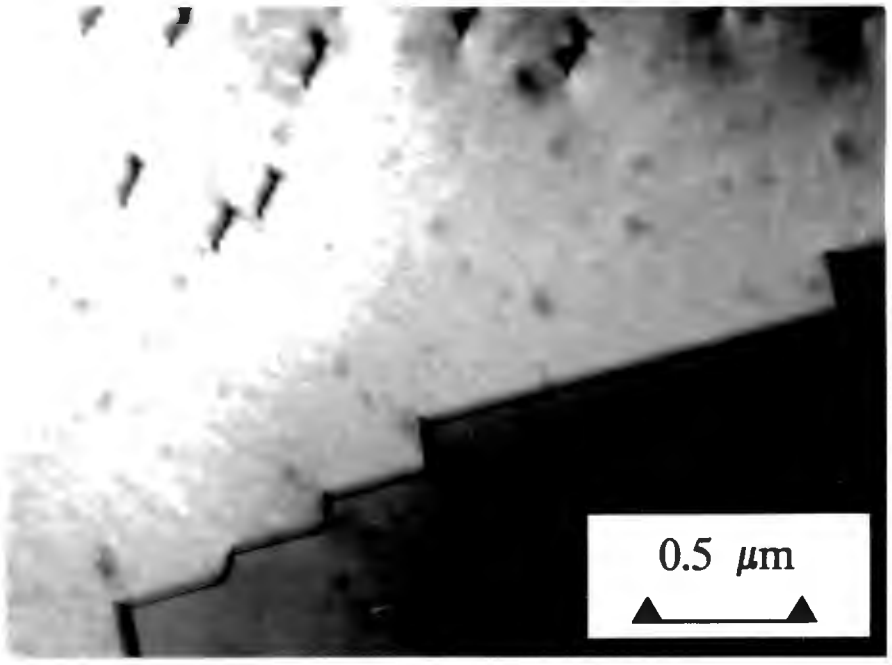

Figure 4.28: Bright-field transmission electron micrograph of palladium 4.1 at.% tungsten after annealing at 1000°C, showing a recrystallised grain containing a twin boundary.

Transmission electron micrographs of palladium 10.3 at.% tungsten before and after annealing are shown in figs. 4.29 - 4.31. In the cold-worked condition, a high dislocation density is observed, as shown in fig. 4.29. After annealing at 600°C nucleation of recrystallised grains has occurred, as shown in fig. 4.30; some rearrangement of dislocations in the regions surrounding the recrystallised grains is observed. Annealing at 700°C results in growth of the recrystallised grains into the surrounding regions of high dislocation density; recrystallisation is complete after annealing at 800°C. After annealing at 1000°C the material exhibits a strain-free microstructure, illustrated in fig. 4.31, containing numerous annealing twins and few dislocations.

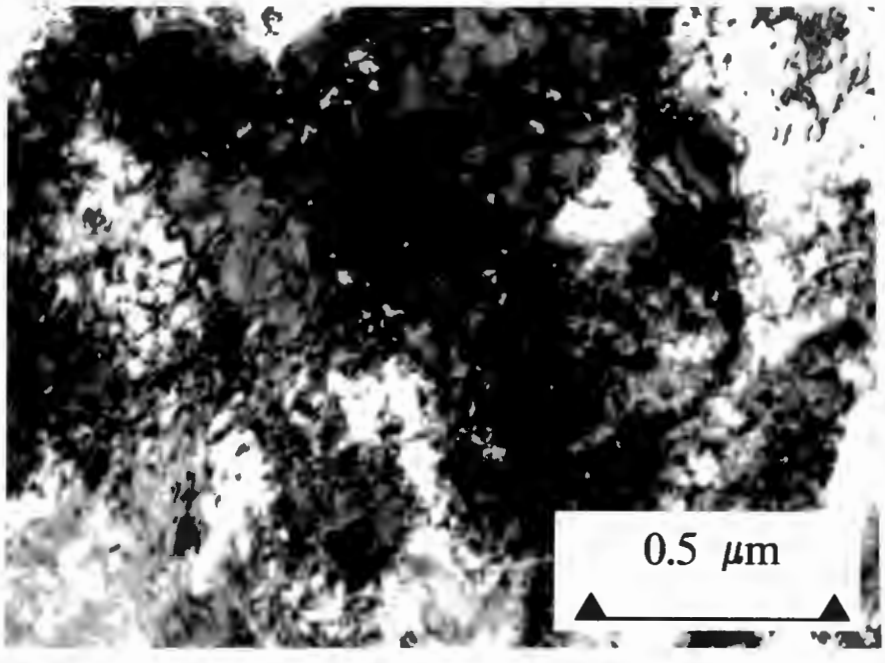

Figure 4.29: Bright-field transmission electron micrograph of palladium 10.3 at.% tungsten in the cold-worked condition.

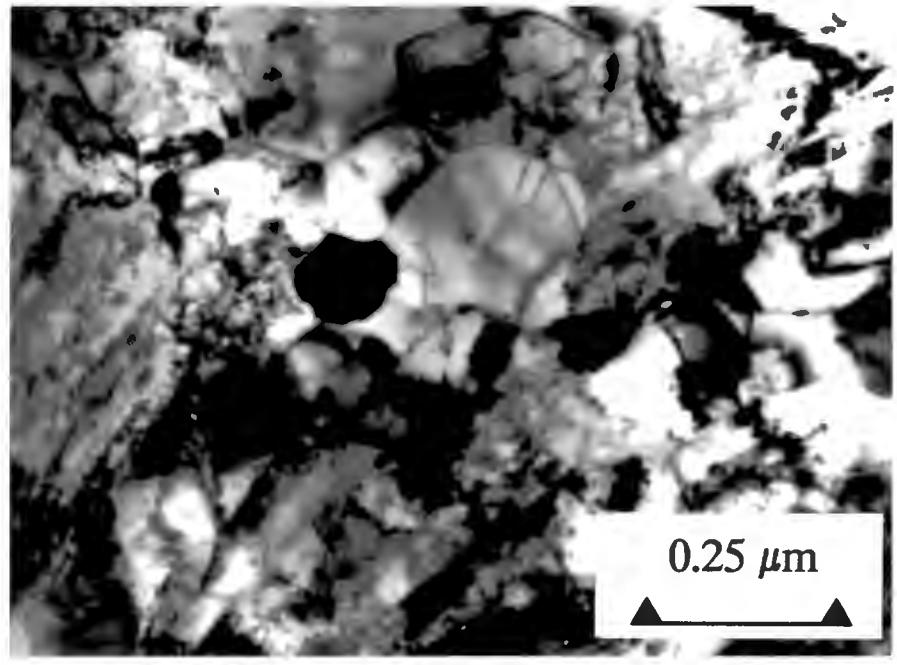

Figure 4.30: Bright-field transmission electron micrograph of palladium 10.3 at.% tungsten after annealing at 600°C, showing recrystallised grains.

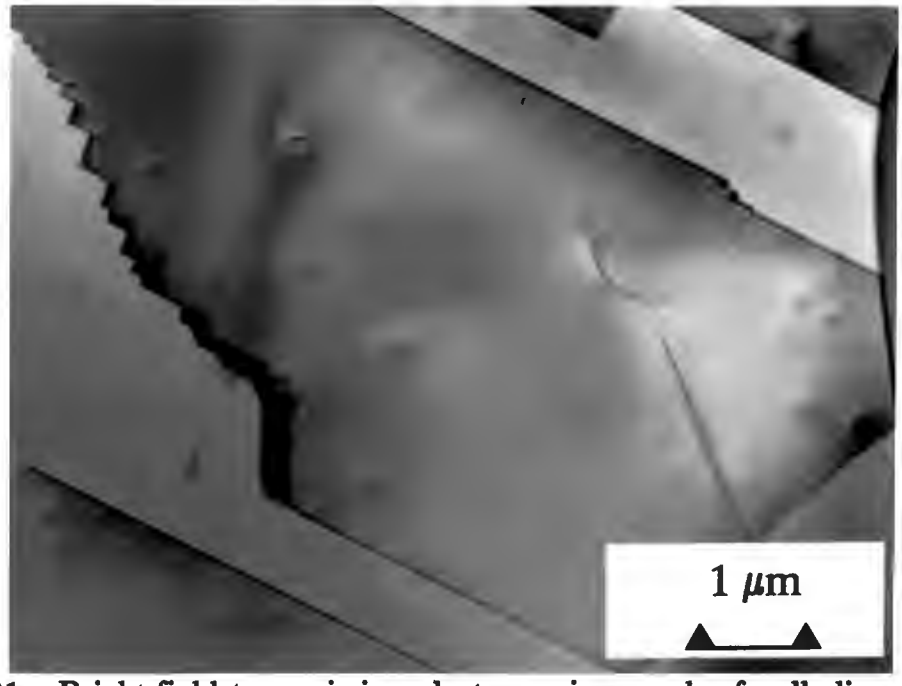

Figure 4.31: Bright-field transmission electron micrograph of palladium 10.3 at.% tungsten after annealing at 1000°C, showing a fully recrystallised microstructure containing annealing twins and isolated dislocations.

Figures 4.29 - 4.31 illustrate the effect of annealing on the microstructure of palladium 11.6 at.% tungsten. In the cold-worked condition, shown in 4.32, a high dislocation density is observed. No significant recovery takes place as a result of annealing at temperatures up to 700°C: dislocation density remains high, as shown in fig. 4.33. The nucleation of recrystallised grains has occurred after annealing at 800°C, and recrystallisation is complete after annealing at 900°C. The fully recrystallised condition, illustrated in fig. 4.34, is characterised by the presence of annealing twins.

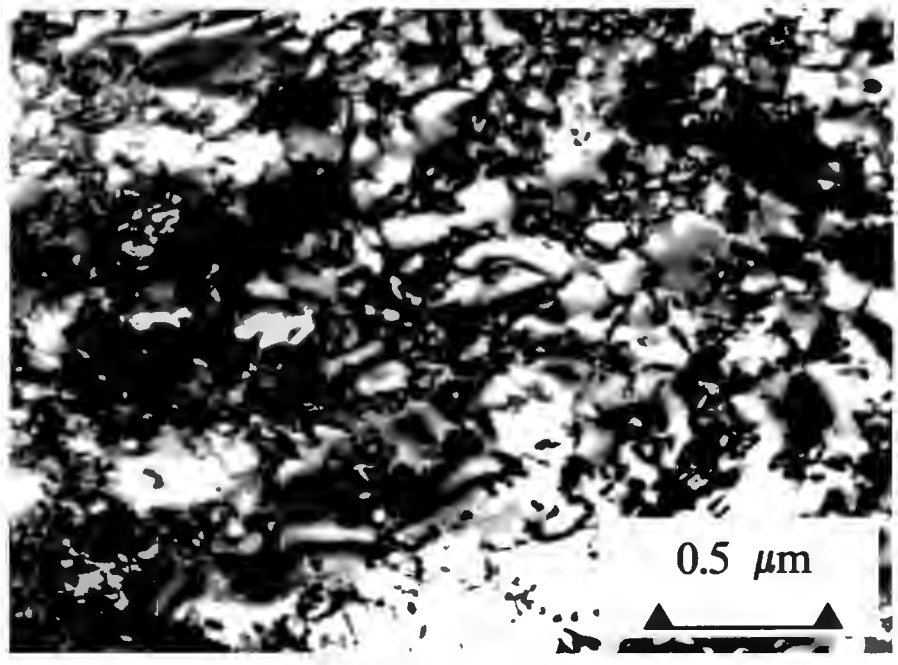

Figure 4.32: Bright-field transmission electron micrograph of palladium 11.6 at.% tungsten in the cold-worked condition.

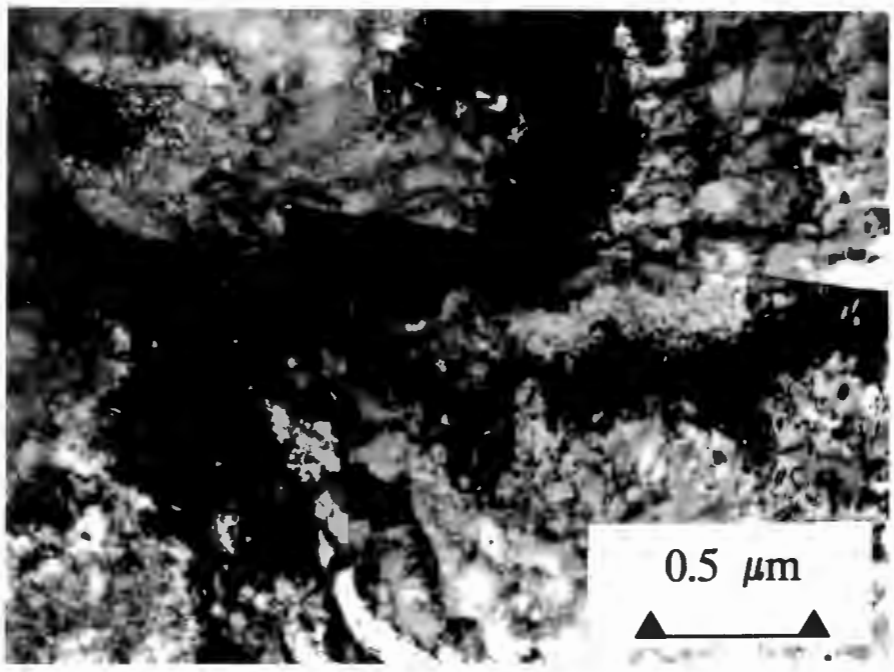

Figure 4.33: Bright-field transmission electron micrograph of palladium 11.6 at.% tungsten after annealing at 700°C, showing no significant decrease in dislocation density due to annealing.

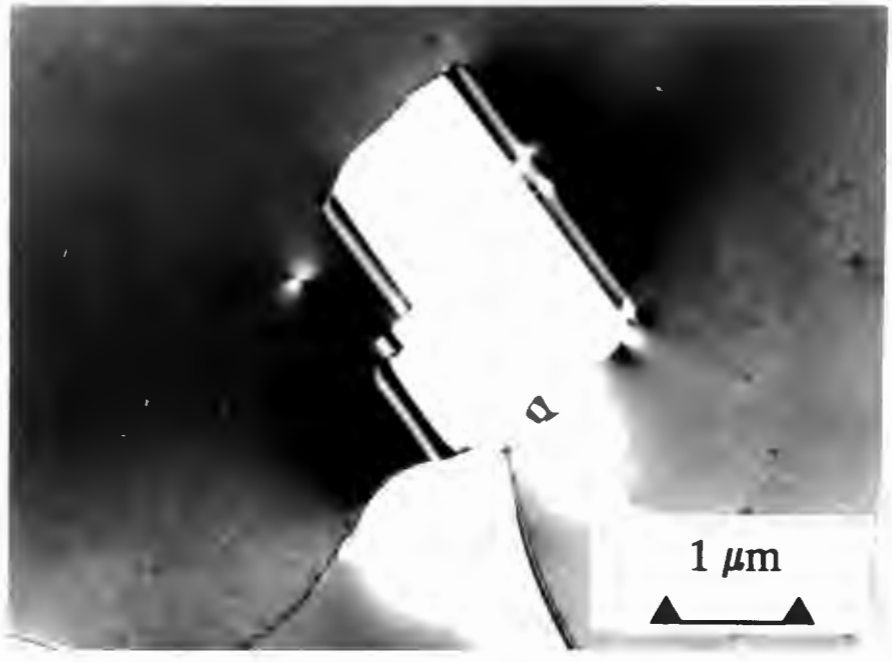

Figure 4.34: Bright-field transmission electron micrograph of palladium 11.6 at.% tungsten after annealing at 1000°C, showing a fully recrystallised microstructure containing a twinned region.

Palladium-molybdenum

The microstructure of palladium 5.3 at.% molybdenum after annealing is illustrated in figs. 4.35 - 4.37. Dislocation density is high after annealing at 500°C, as shown in fig. 4.35; annealing at 600°C results in the nucleation of recrystallised grains in regions of high dislocation density. A fully recrystallised microstructure is observed after annealing at 700°C, containing small-scale precipitate-like features, as shown in fig. 4.36. Dark-field images of these features were presented in section 4.2. After annealing at 1000°C, these features are no longer visible even under high magnification, as shown in fig. 4.37.

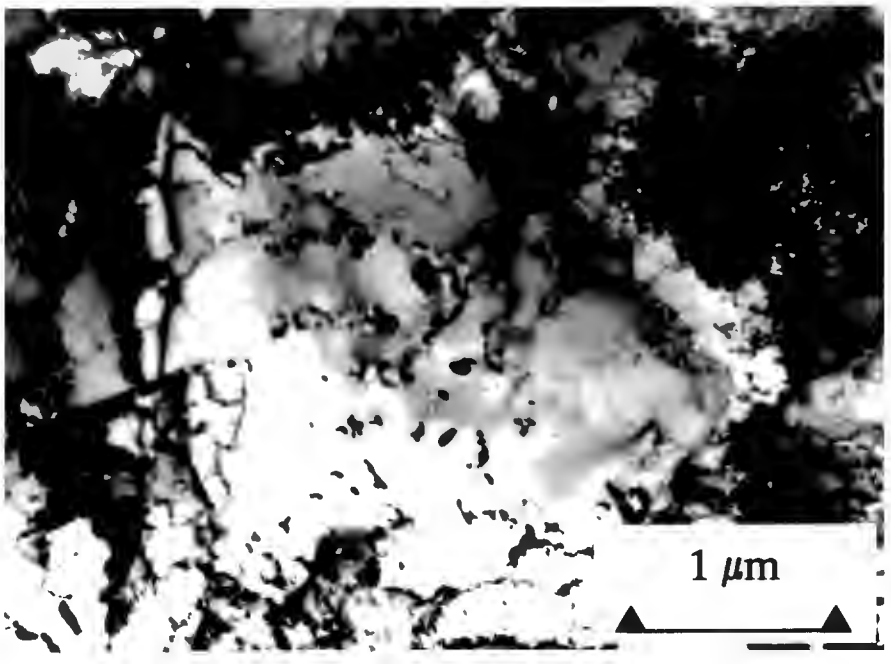

Figure 4.35: Bright-field transmission electron micrograph of palladium 5.3 at.% molybdenum after annealing at 500°C, showing no significant recovery prior to recrystallisation.

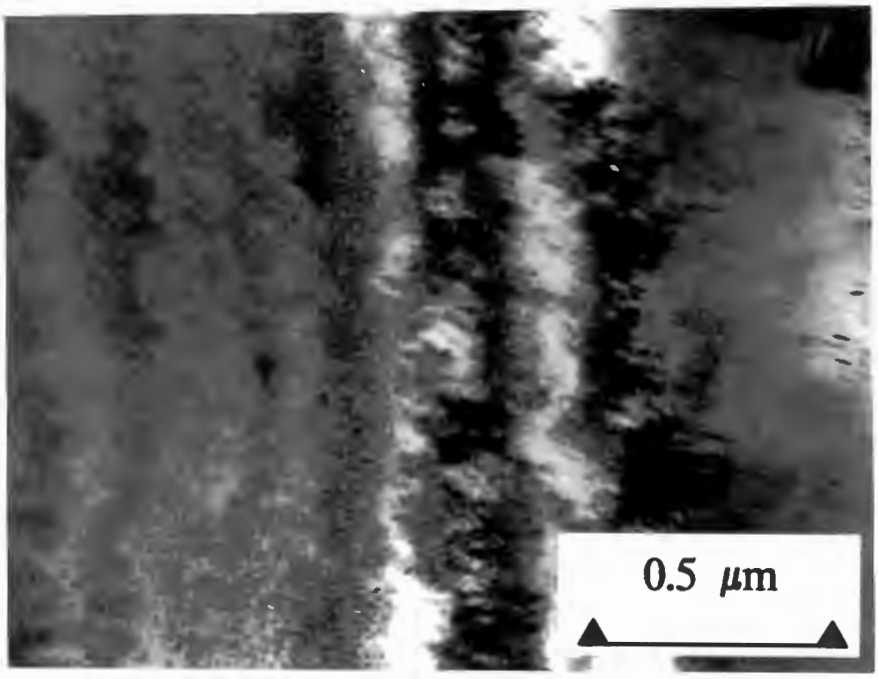

Figure 4.36: Bright-field transmission electron micrograph of palladium 5.3 at.% molybdenum after annealing at 700°C, showing fine microstructural features in recrystallised grain.

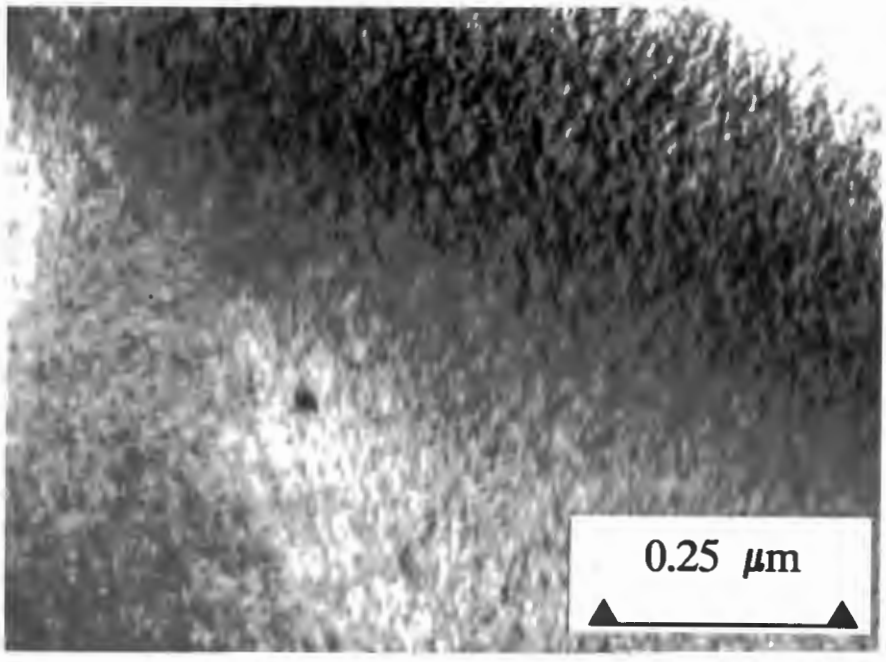

Figure 4.37: Bright-field transmission electron micrograph of palladium 5.3 at.% molybdenum after annealing at 1000°C, showing a recrystallised microstructure free of the features observed in fig. 4.36.

The microstructure of palladium 9.7 at.% molybdenum before and after annealing is shown in fig.s 4.38 - 4.40. Figure 4.38 shows the high dislocation density observed in the cold-worked condition. No significant recovery occurs as a result of annealing, and recrystallisation initiates after annealing at 600°C. Extensive recrystallised regions, containing numerous annealing twins, are evident after annealing at 700°C as shown in fig. 4.39. Recrystallisation is complete after annealing at 800°C. The fully recrystallised microstructure, illustrated in fig. 4.40, is characterised by extensive twinning.

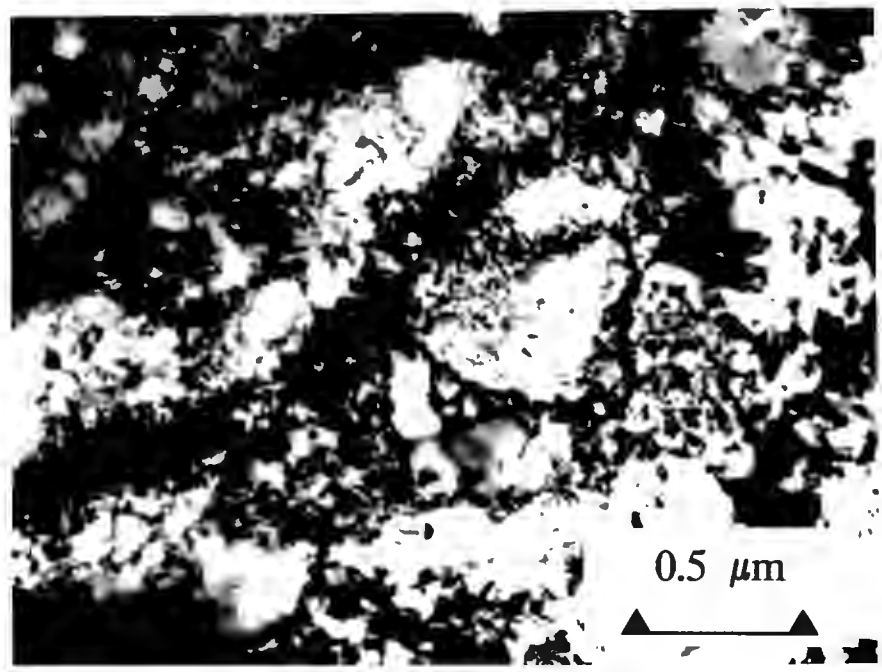

Figure 4.38: Bright-field transmission electron micrograph of palladium 9.7 at.% molybdenum in the cold-worked condition.

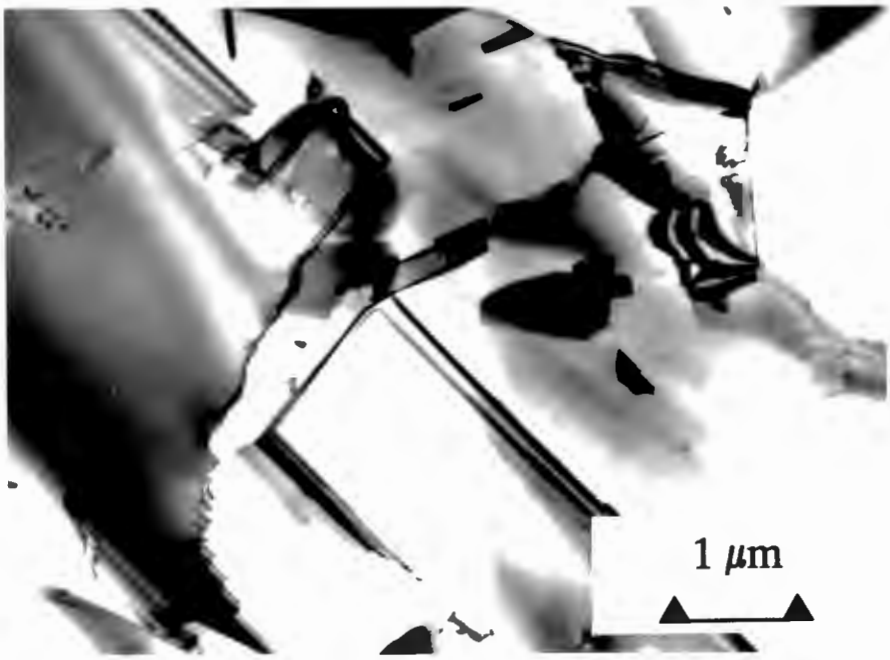

Figure 4.39: Bright-field transmission electron micrograph of palladium 9.7 at.% molybdenum after annealing at 700°C, showing recrystallised region containing annealing twins.

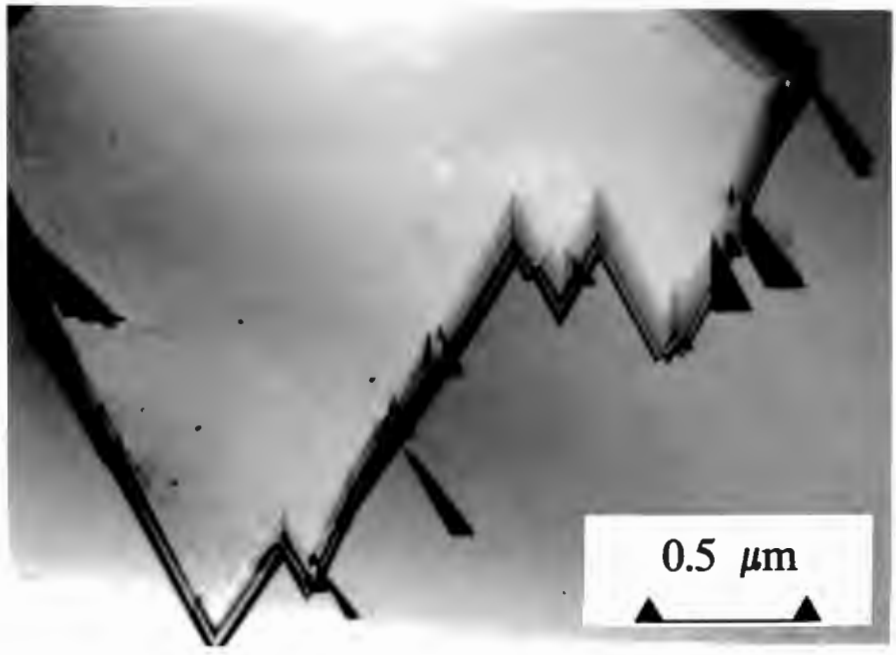

Figure 4.40: Bright-field transmission electron micrograph of palladium 9.7 at.% molybdenum after annealing at 1000°C, showing twin boundaries in a recrystallised grain.

The microstructure of palladium 16 at.% molybdenum before and after annealing is shown in figs. 4.41 - 4.43. No significant decrease in dislocation density relative to the cold-worked condition, shown in fig. 4.41, occurs as a result of annealing at 500°C. Recrystallisation initiates as a result of annealing at 600°C, and progresses rapidly during annealing at 700°C. Figure 4.42 shows a recrystallised region after annealing at 700°C, containing dislocations and numerous annealing twins. After annealing at 1000°C, dislocations remain present in a fully recrystallised and exensively twinned microstructure.

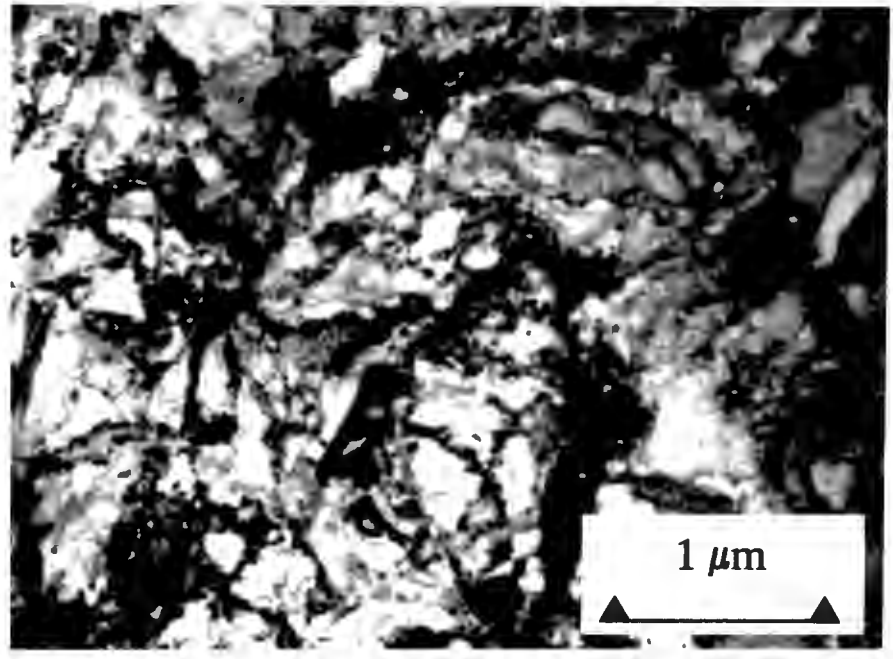

Figure 4.41: Bright-field transmission electron micrograph of palladium 16.0 at.% molybdenum in the cold-worked condition.

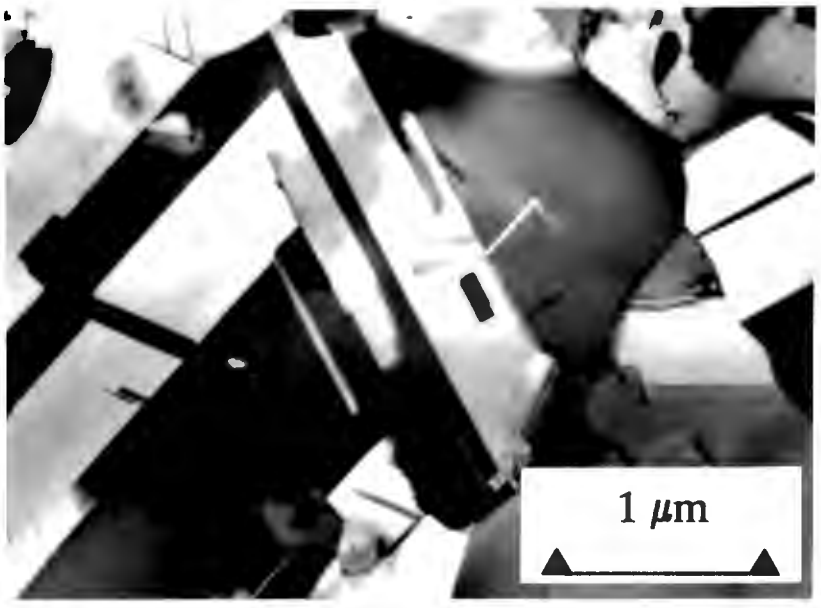

Figure 4.42: Bright-field transmission electron micrograph of palladium 16.0 at.% molybdenum after annealing at 700°C, showing an extensively recrystallised region containing annealing twins.

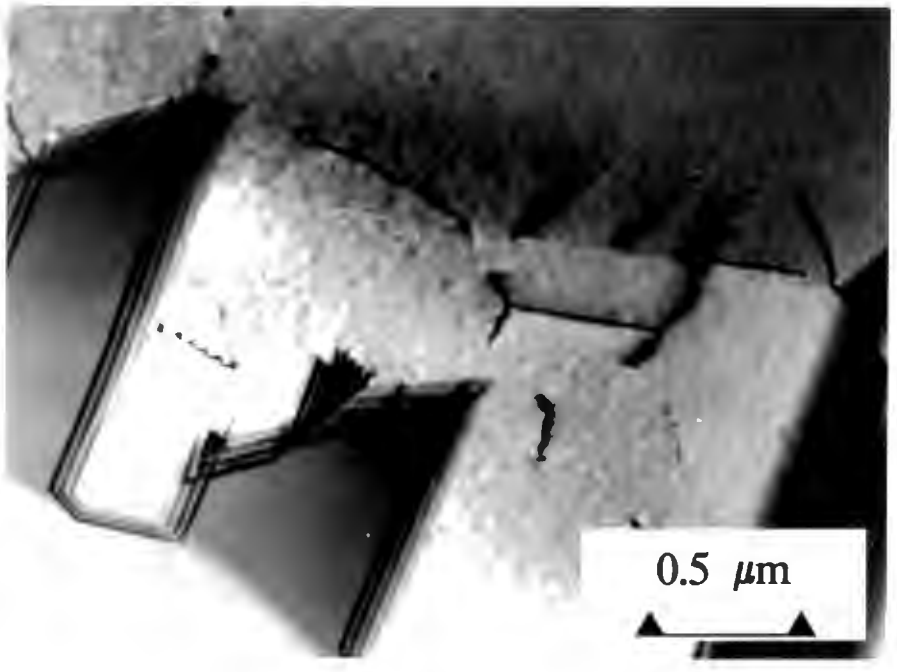

Figure 4.43: Bright-field transmission electron micrograph of palladium 16.0 at.% molybdenum after annealing at 1000°C, showing a fully recrystallised microstructure containing dislocations and twin boundaries.

4.3.2 GRAIN SIZE

The grain size of alloys after a full series of annealing experiments was determined by optical metallography and the mean intercept method. Pure palladium, which is fully recrystallised after annealing at 500°C, exhibits significant grain growth after annealing at temperatures up to 800°C. After annealing at 1000°C, palladium 4.1 at.% tungsten and palladium 5.3 at.% molybdenum have grain size of approximately 20 μm; a smaller grain size is measured in the remaining alloys of higher solute concentration

TABLE 4.1: Grain size of specimens after completion of annealing experiments in the temperature ranges 300°C - 800°C (pure palladium) and 500°C - 1000°C (palladium-tungsten and palladium-molybdenum).

SPECIMEN	GRAIN SIZE (μm)
Palladium	46.3 ± 10.6
Palladium 4.1 at.% tungsten	22.1 ± 5.19
Palladium 10.3 at.% tungsten	7.02 ± 0.59
Palladium 11.7 at.% tungsten	13.7 ±3.41
Palladium 5.3 at.% molybdenum	21.1 ± 4.48
Palladium 9.8 at.% molybdenum	16.1 ± 2.34
Palladium 16 at.% molybdenum	7.5 ± 0.69

4.3.3 THE EFFECT OF SOLUTE CONCENTRATION ON RECOVERY AND RECRYSTALLISATION

The recrystallisation temperature of a pure metal decreases with increasing purity and with an increase in prior cold work. In the present work, the nucleation of recrystallised grains is observed in palladium by transmission electron microscopy after annealing at 300°C; since the samples used (99% pure) were not of high purity, the low recrystallisation temperature is probably due to the high degree of prior cold work due to the preparation of specimens by cold-rolling. The addition of tungsten or molybdenum to palladium increases the recrystallisation temperature, as might be expected in association with the increase in melting point due to these solute additions. Recrystallisation initiates in the palladium alloys under investigation after annealing at temperatures from 600°C - 800°C. Although the melting point increases with increasing solute concentration, in palladium 10.3 at.% tungsten recrystallisation initiates at a lower temperature than in either palladium 4.1 at.% tungsten or palladium 11.7 at.% tungsten. After recrystallisation, the microstructure of the alloys is characterised by the presence of annealing twins.

4.4 MICROHARDNESS

4.4.1 MICROHARDNESS CHANGES DUE TO ANNEALING

Palladium

The effect of annealing on the microhardness (HV_{50g}) of pure palladium is shown in fig. 4.43. The 100gf microhardness of cold-worked palladium was 141 HV_{100g}, showing little difference from the 50gf measurement. After annealing, however, microhardness indentations using a 100g load became large with respect to specimen thickness; a 50g load was accordingly selected for measurements of pure palladium. The microhardness is observed to decrease after each heat treatment in the range 300°C - 500°C, the greatest decrease occurring after annealing at 500°C. Annealing above this temperature produces little further change.

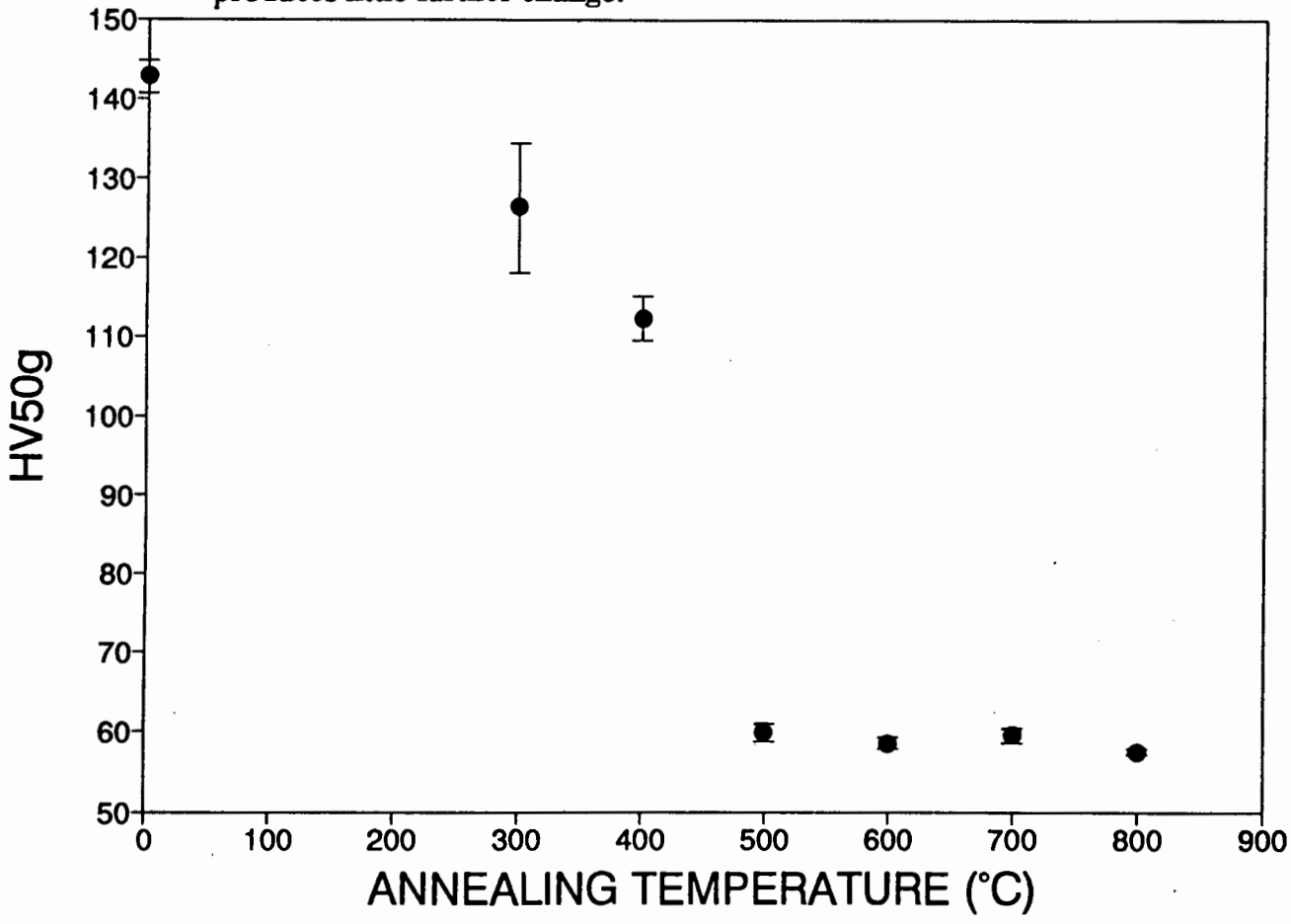

Figure 4.43: Graph of microhardness of pure palladium vs. annealing temperature.

Palladium-tungsten

The microhardness of palladium 4.1 at.% tungsten after annealing in the temperature range 500°C - 1000°C is shown in fig. 4.44. A gradual decrease from the cold-worked value of 247 HV_{100g} occurs due to successive annealing from 500°C to 700°C. Larger decreases are observed after annealing at 800°C and 900°C, to a microhardness of 120 HV_{100g}; annealing at 1000°C has little effect on this value.

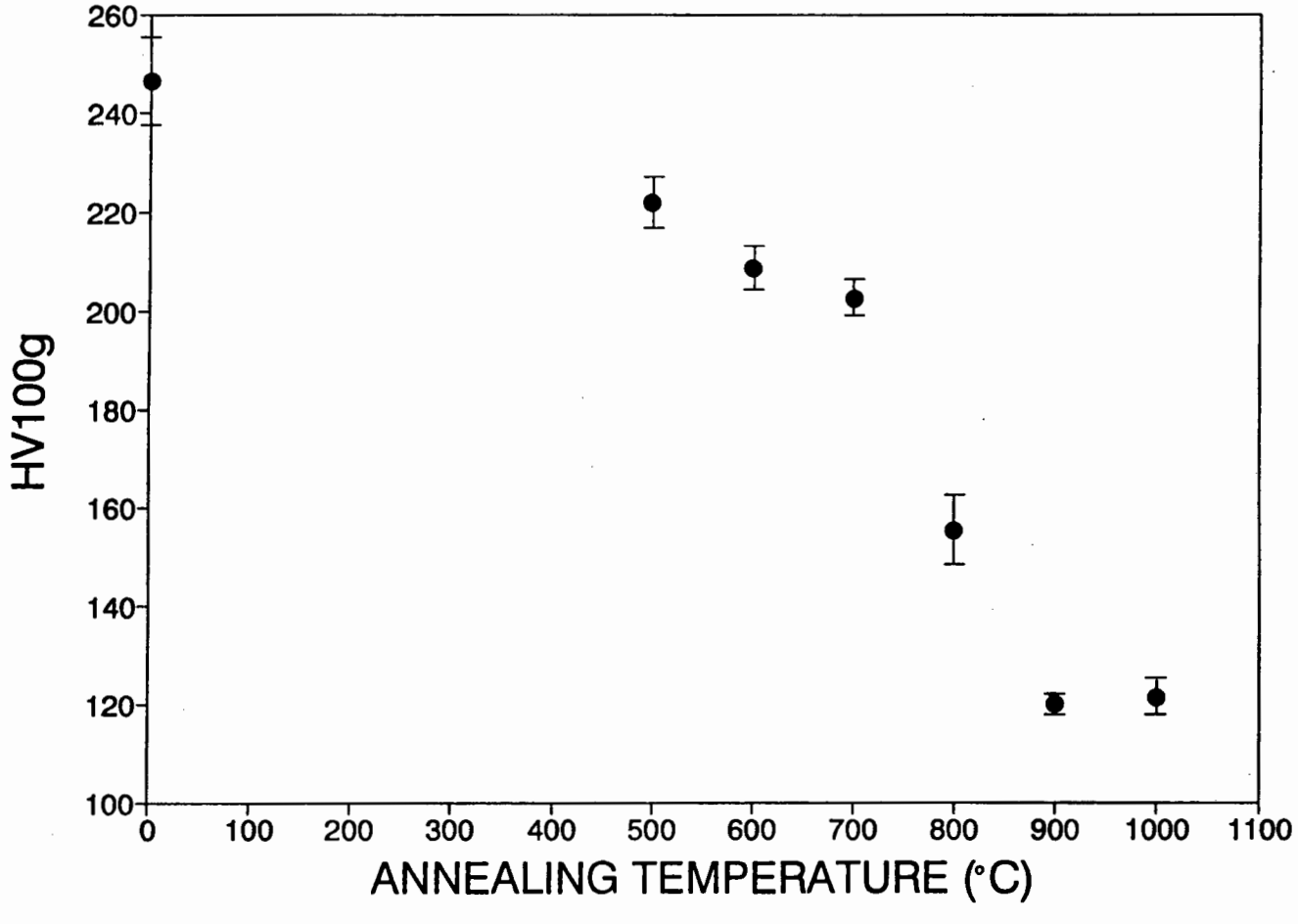

Figure 4.44: Graph of microhardness of palladium 4.1 at.% tungsten vs. annealing temperature.

The microhardness of palladium 10.3 at.% tungsten, shown in fig. 4.45, shows little variation from the cold-worked value of 400 HV_{100g} after successive annealing up to a temperature of 700°C. Large decreases in microhardness are observed after annealing at 800°C and 900°C, to a minimum value of 120 HV_{100g}; annealing at 1000°C produces no further change.

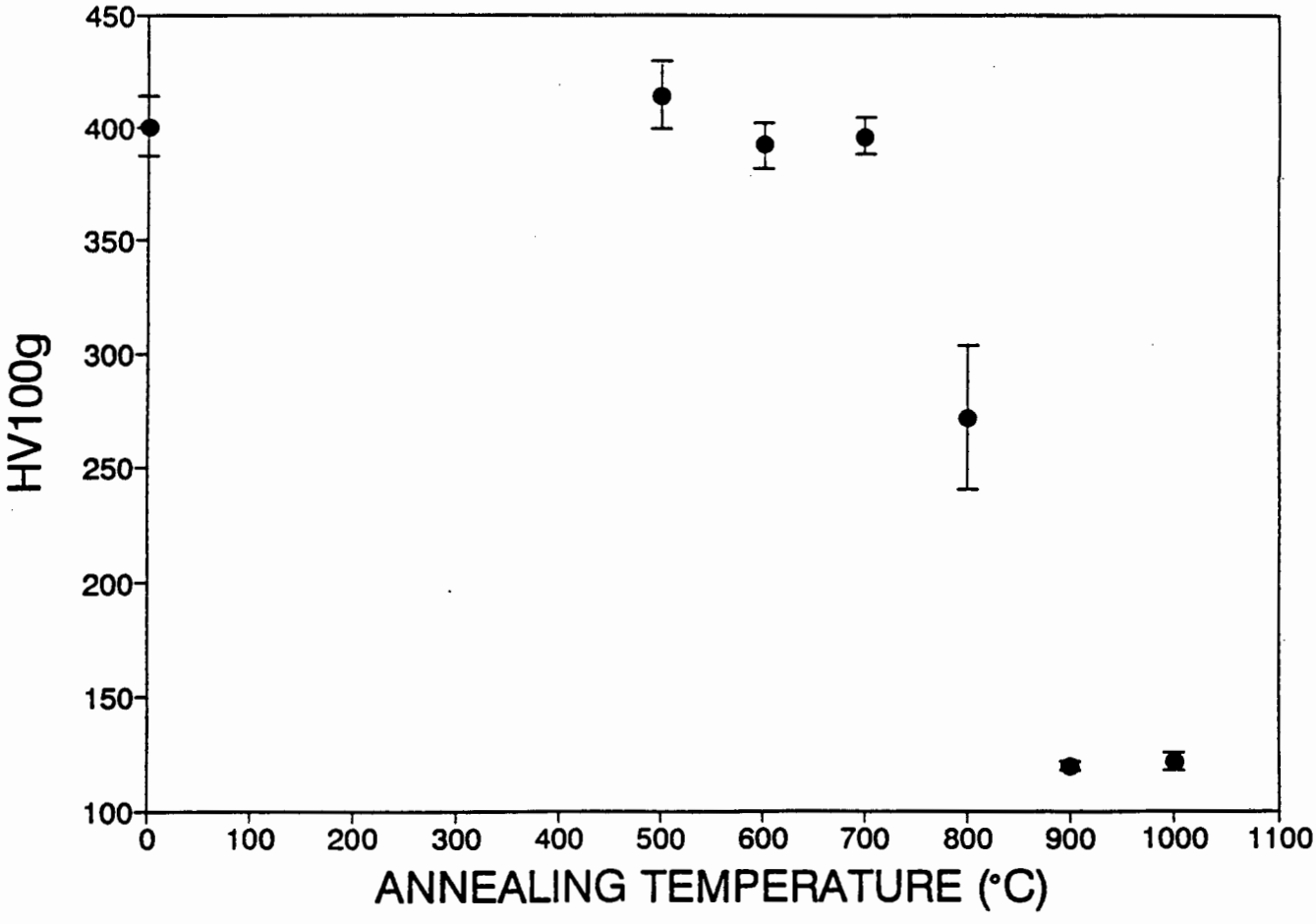

Figure 4.45: Graph of microhardness of palladium 10.3 at.% tungsten vs. annealing temperature.

The microhardness of palladium 11.6 at.% tungsten after annealing is shown in fig. 4.46. Successive annealing at temperatures up to 800°C produces a cumulative decrease in microhardness of approximately 50 HV_{100g}. The largest change in microhardness occurs after annealing at 900°C; annealing at 1000°C results in a decrease to approximately 220 HV_{100g}.

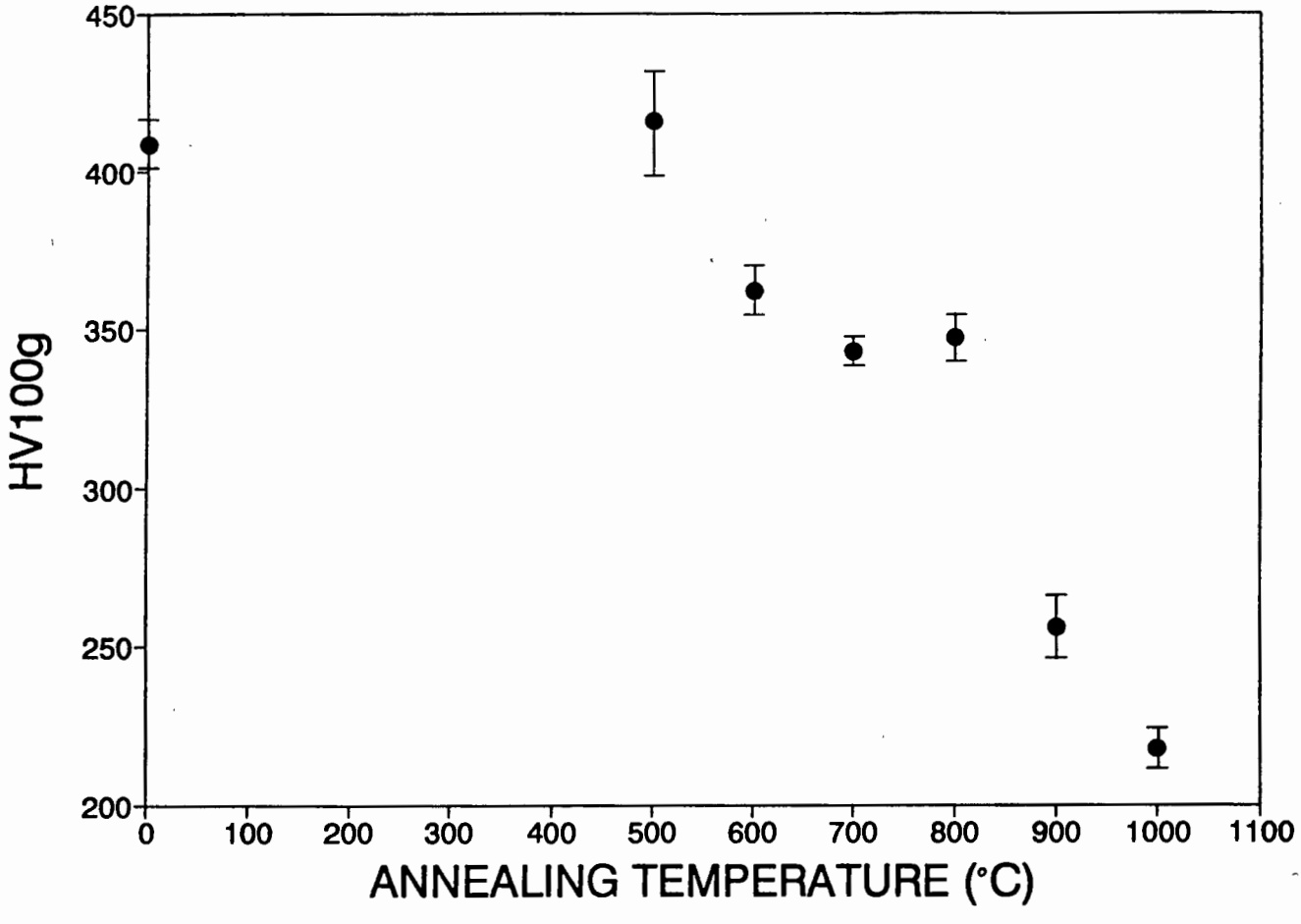

Figure 4.46: Graph of microhardness of palladium 11.6 at.% tungsten vs. annealing temperature.

Palladium-molybdenum

The microhardness of palladium 5.3 at.% molybdenum, shown in fig. 4.47, shows little change after annealing at 500°C. Annealing at 600°C and 700°C results in a steady decrease in microhardness; however, annealing in the range 800°C - 1000°C produces an unexpected increase in microhardness. The final microhardness after the full series of heat treatments, 190 HV_{100g}, returns to the value produced by annealing at 600°C.

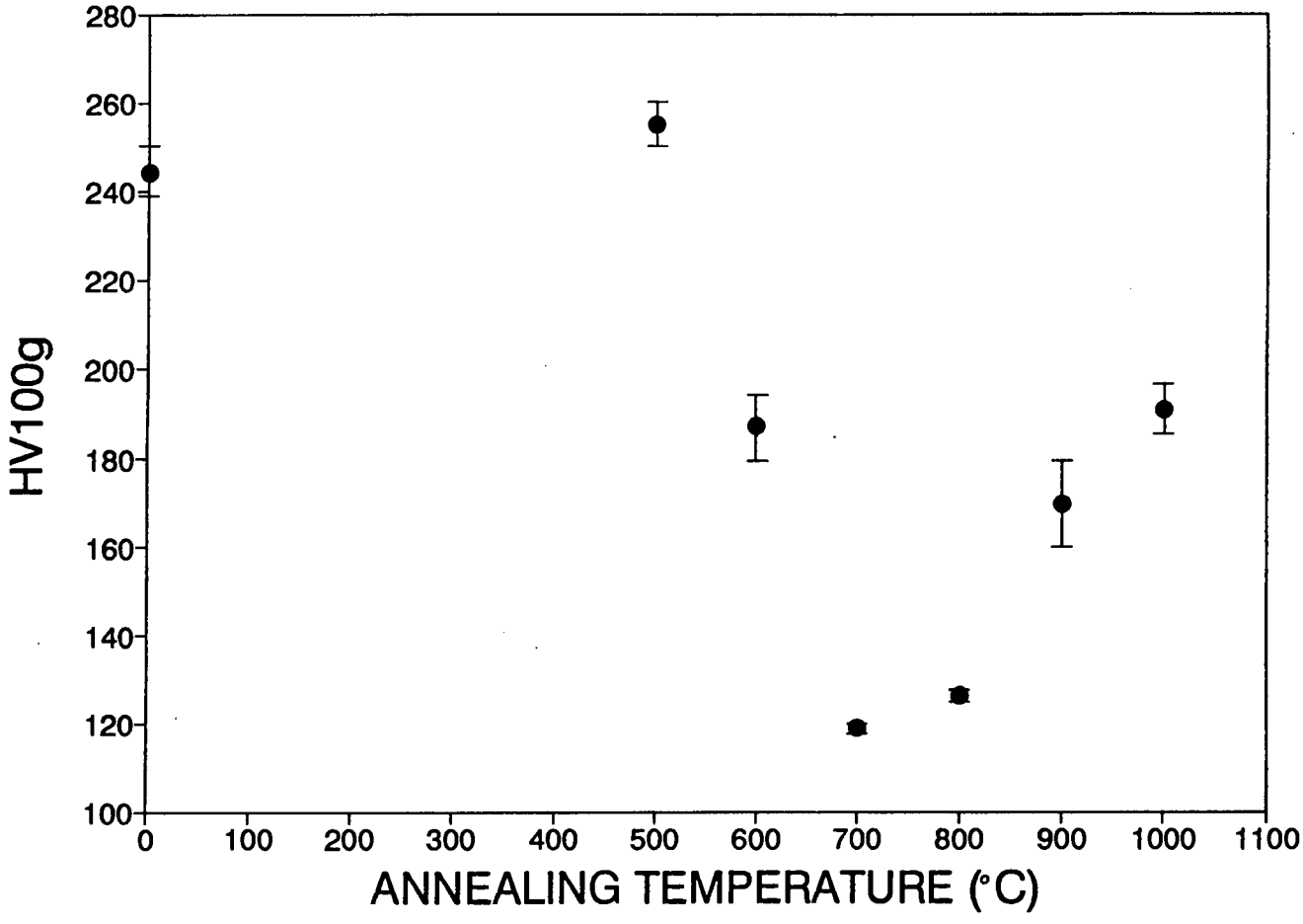

Figure 4.47: Graph of microhardness of palladium 5.3 at.% molybdenum vs. annealing temperature.

The effect of annealing on the microhardness of palladium 9.7 at.% molybdenum is shown in fig. 4.48. The microhardness decreases only slightly from the cold-worked value of 338 HV_{100g} after annealing at 500°C and 600°C. Annealing at 700°C results in a large decrease; successive annealing at higher temperatures results in a small further decrease, to a final value of 178 HV_{100g}.

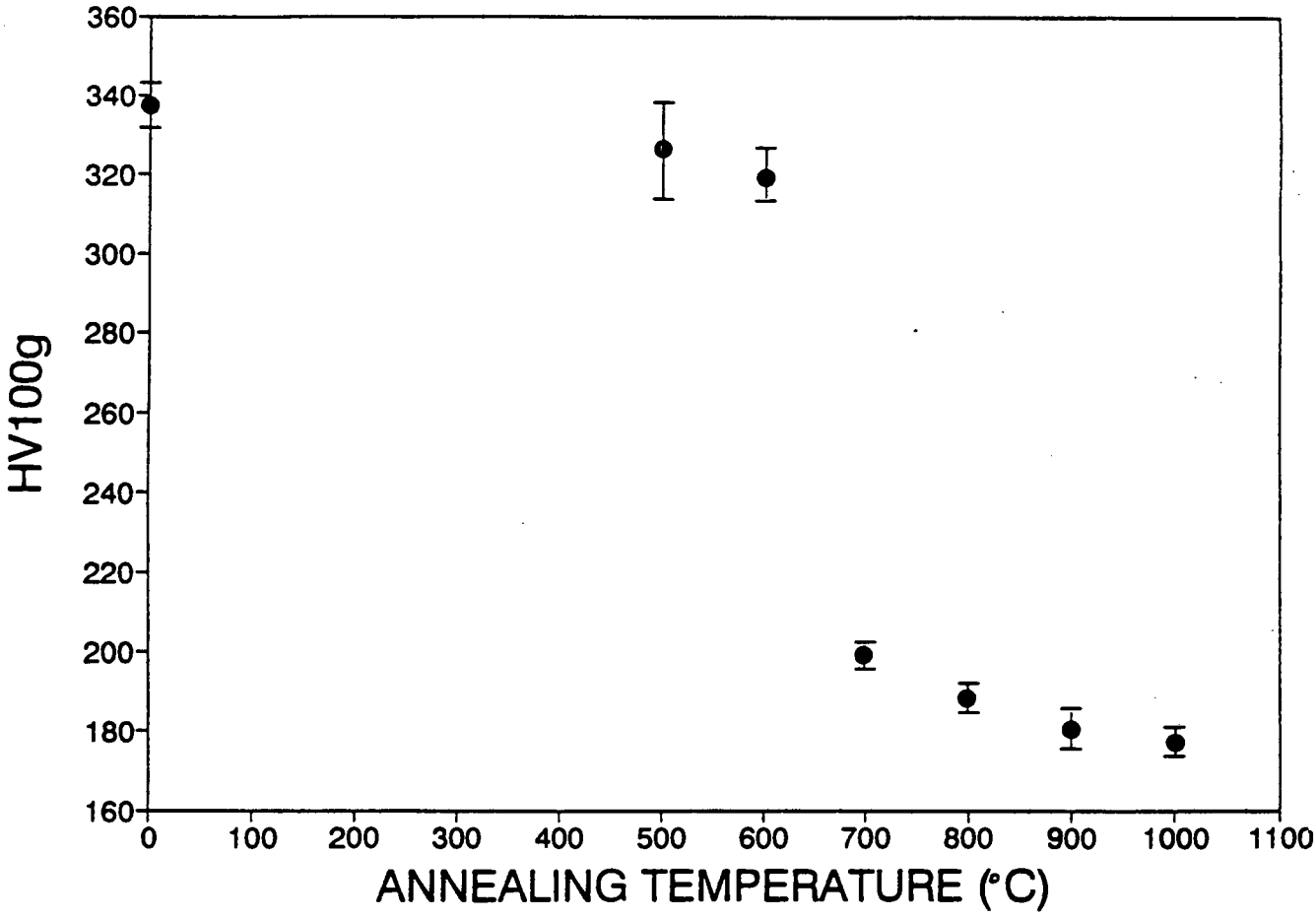

Figure 4.48: Graph of microhardness of palladium 9.7 at.% molybdenum vs. annealing temperature.

The microhardness of palladium 16.0 at.% molybdenum after annealing in the range 500°C - 1000°C is shown in fig. 4.49. Little change in microhardness from the cold-worked value of 455 HV_{100g} is observed after successive annealing at 500°C and 600°C. A large decrease occurs due to annealing at 700°C, with a further decrease after annealing at 900°C. The microhardness after the full series of annealing experiments is 230 HV_{100g}.

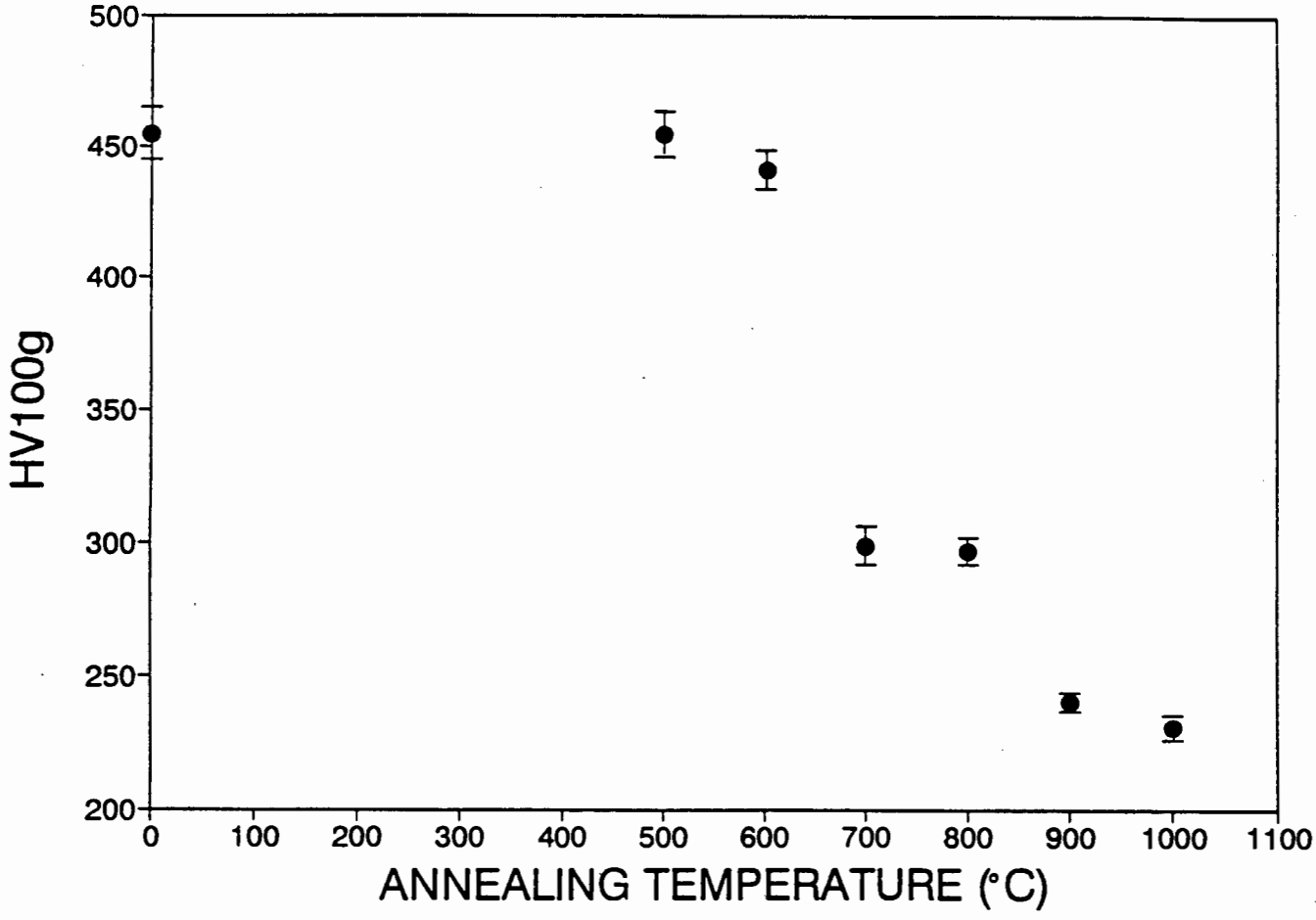

Figure 4.49: Graph of microhardness of palladium 16.0 at.% molybdenum vs. annealing temperature.

4.4.2 THE EFFECT OF SOLUTE CONCENTRATION ON MICROHARDNESS

In the cold-worked condition, the microhardness of palladium increases steeply with the addition of tungsten or molybdenum in the concentration ranges investigated. Successive annealing of cold-worked palladium alloys in the range 500°C - 1000°C results in a nett decrease in microhardness; with the exception of palladium 5.3 at.% molybdenum, microhardness has reached a minimum after the 900°C anneal, no significant change occurring after heat treatment at 1000°C. Figure 4.50 shows the microhardness of palladium-tungsten and palladium-molybdenum alloys in both the cold worked and fully recrystallised (1000°C annealed) condition.

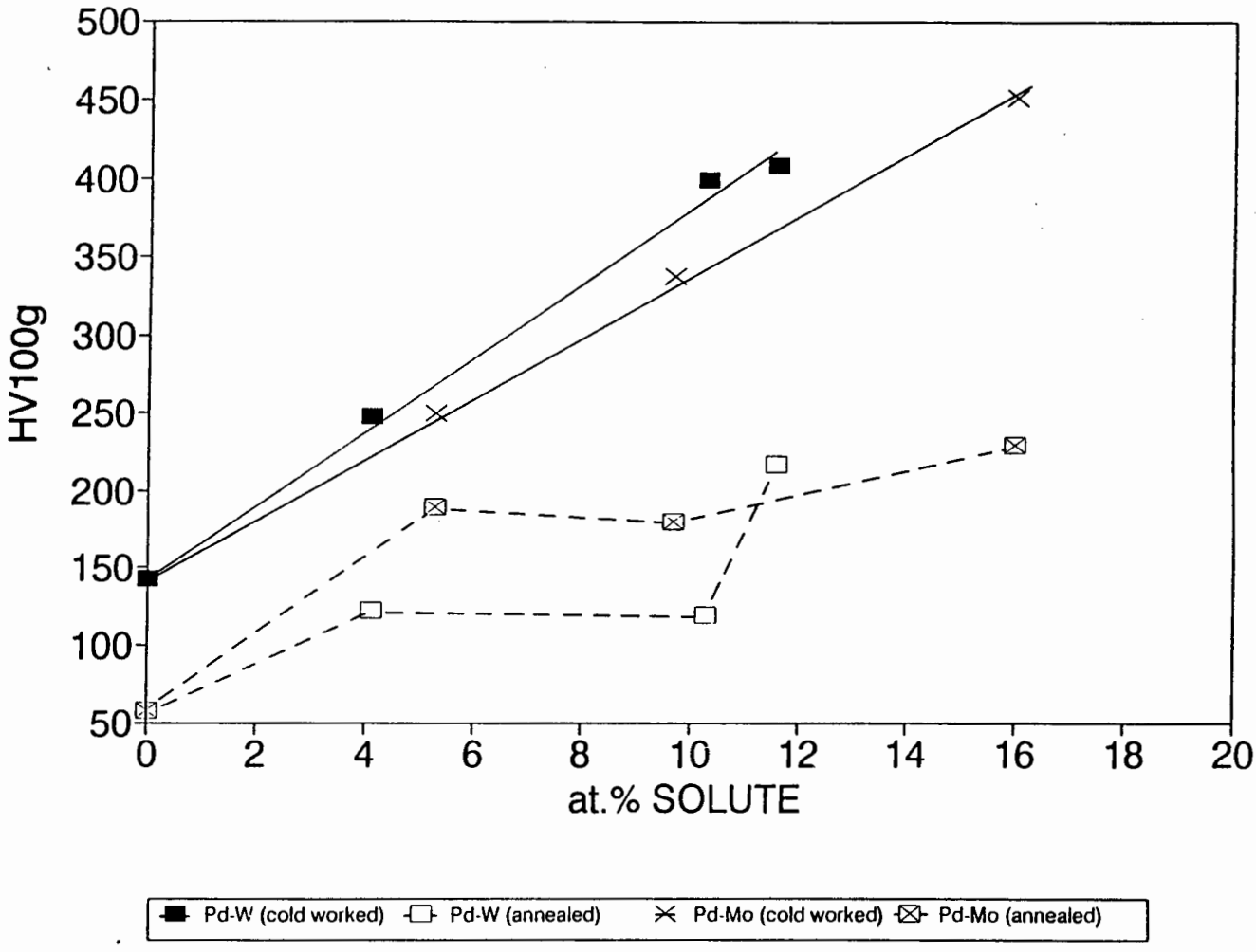

Figure 4.50: Graph of microhardness vs. solute concentration for palladium-tungsten and palladium-molybdenum.

After annealing at 1000°C, there is little variation with solute concentration in the microhardness of palladium-molybdenum alloys. Palladium 4.1 at.% tungsten and palladium 10.3 at.% tungsten have a similar microhardness after annealing at 1000°C; the microhardness of palladium 11.6 at.% tungsten is however much greater. The dependence of microhardness on solute concentration in annealed alloys is unexpected in view of the linear increase in microhardness with concentration observed for alloys in the cold-worked condition, and suggests that a mechanism additional to recovery and recrystallisation occurs during annealing of these alloys.

4.5 THE EFFECT OF ANNEALING ON STRUCTURE AND PROPERTIES

The experimental results show a wide variation in the response of structure and properties to annealing; the dependence of this response on solute concentration has been assessed for each experimental procedure. In this section, the changes observed in structure and properties as a result of annealing are discussed and graphically consolidated for each material.

Palladium

Microhardness measurements of pure palladium show a decrease after each heat treatment in the range 300°C - 500°C. Subsequent annealing at temperatures above 500°C produces no significant change in microhardness, suggesting that no further decrease in dislocation density occurs. This is confirmed by examination of transmission electron micrographs of annealed palladium, which show the the onset of recrystallisation to occur after annealing at 300°C, and the material to be fully recrystallised after annealing at 500°C. The effect of annealing temperature on the electrical resistance of pure palladium was not accurately measurable by the apparatus used. A decrease in residual resistivity is expected to occur after annealing a pure metal due to a decrease in the number of dislocations; the residual resistivity of a pure metal is, however, small in comparison to the temperature-dependent resistivity at room temperature (22°C) and changes in residual resistivity are hence difficult to resolve. Although the measurements of the electrical resistance of palladium can not, therefore, supply quantitative information regarding the effect of annealing temperature on resistivity, the results show qualitatively that the transition from the cold-worked to the fully annealed condition results in a decrease in resistivity, of less than 130 nΩ-cm in magnitude. This is consistent with measurements of the change in residual resistivity of palladium due to plastic deformation by Rowlands and Woods[99] and Zwart and Schroeder[100], who obtained a maximum value of 25 nΩ-cm.

Palladium alloys

Figures 4.51 and 4.52 show the effect of annealing on the properties of the alloys under investigation. For each alloy, the temperature range in which recrystallisation is observed is indicated by an arrow, which extends from the temperature at which recrystallisation initiates to the maximum annealing temperature of 1000°C. Although a significant decrease in dislocation density is not observed in any alloy prior to recrystallisation, an arrow marked "recovery" indicates the range of annealing temperatures in which a deformed microstructure is observed. The overlap of these arrows thus shows the temperature range in which recrystallised grains are observed in a deformed matrix.

Palladium 4.1 at.% tungsten

The effect of annealing on the properties of palladium 4.1 at.% tungsten is shown in fig. 4.51 (a). Microhardness measurements of palladium 4.1 at.% tungsten suggest that a decrease in dislocation density occurs after each annealing experiment in the range 500°C - 900°C, with the largest decreases occurring after the 800°C and 900°C heat treatments. Transmission electron microscope observations show little significant decrease in dislocation density up to 700°C. Recrystallisation initiates after annealing at 800°C and is complete after annealing at 900°C. The electrical resistance decreases after each annealing experiment in the range 500°C - 700°C, the largest decrease occurring after the 700°C heat treatment; little further change in resistance occurs as a result of annealing at 800°C. A decrease in resistance due to annealing is expected behaviour for metals and alloys as a consequence of decreasing dislocation density, although the magnitude of the total decrease for this alloy - nine per cent of the room temperature resistance - is larger than might be expected as a result of recovery and recrystallisation alone.

The effect of annealing temperature on properties is nevertheless not entirely consistent with observed changes in dislocation density. Annealing at 700°C results in a large decrease in resistance concurrent with the onset of recrystallisation, but only a small decrease in microhardness is measured.

Conversely, the greatest decrease in microhardness occurs after the 800°C heat treatment with the growth of recrystalled grains, but little change in electrical resistance is observed. The results of annealing at 900°C show a further discrepancy: a small increase in electrical resistance is associated with a large decrease in microhardness accompanying complete recrystallisation of the material. Although the overall effect of the complete series of annealing experiments on structure and properties does not appear unusual then, the effect of annealing temperature on resistance may not be related to the evolution of microstructure in a simple manner. Selected area electron diffraction of this alloy after annealing from 800°C - 1000°C show faint additional reflections at $1/3$242-type positions in [111] and at $1/2$131-type positions in [112] zone-axis diffraction patterns, which suggests that the microstructure is no longer a homogeneous solid solution.

Palladium 10.3 at.% tungsten

The effect of annealing on the properties of palladium 10.3 at.% tungsten is shown in fig. 4.51 (b). Microhardness measurements of palladium 10.3 at.% tungsten show little variation after annealing in the temperature range 500°C - 700°C; large decreases however occur after annealing at 800°C and 900°C. Transmission electron microscopy shows recrystallisation to initiate after annealing at 600°C, and to reach completion after annealing at 900°C. The observed decrease in dislocation density due to the early stages of recrystallisation after annealing at 600°C and 700°C is thus not reflected in microhardness measurements, although the progress to complete recrystallisation after annealing at 800°C and 900°C results in a large decrease in microhardness.

The electrical resistance shows an increase after successive annealing in the range 500°C - 800°C, with the largest increase occurring after the 700°C heat treatment; the cumulative resistance increase due to annealing is approximately nine per cent of the resistance of the cold-worked specimen. Neither the direction nor the magnitude of the resistance changes measured may readily be associated with changes in dislocation density. The large increases in electrical resistance measured after annealing in the range 500°C - 700°C occur during recovery and the beginning of recrystallisation in the alloy;

the smaller changes in resistance after annealing in the range 800°C - 1000°C are concurrent with the completion of recrystallisation. Neither the microhardness nor the resistance measurements are thus consistent with the microstructures observed after annealing. Faint or diffuse reflections observed after annealing, at $1/3$242-type positions in [111] and at $1/2$131-type positions in [112] zone-axis diffraction patterns, suggest that a structural change has taken place which may influence the properties of annealed alloys.

Palladium 11.6 at.% tungsten

The effect of annealing on the properties of palladium 11.6 at.% tungsten is shown in fig. 4.51 (c). Little change in microhardness is observed after annealing at 500°C; a decrease after annealing in the temperature range 600°C - 800°C is followed by a steep decrease after annealing at 900°C and 1000°C. The effect of annealing temperature on the resistance of palladium 11.6 at.% tungsten shows a similar trend to palladium 10.3 at.% tungsten: increases in resistance after annealing at 500°C and 600°C are followed by a large increase after annealing at 700°C. However, in palladium 11.6 at.% tungsten the resistance shows a further large increase after annealing at 800°C and continues to increase to a maximum, approximately fourteen per cent greater than the resistance of the cold-worked specimen, after annealing at 1000°C. Diffuse reflections are observed after annealing, at $1/3$242-type positions in [111] and at $1/2$131-type positions in [112] zone-axis diffraction patterns, suggesting that a structural transformation has occurred.

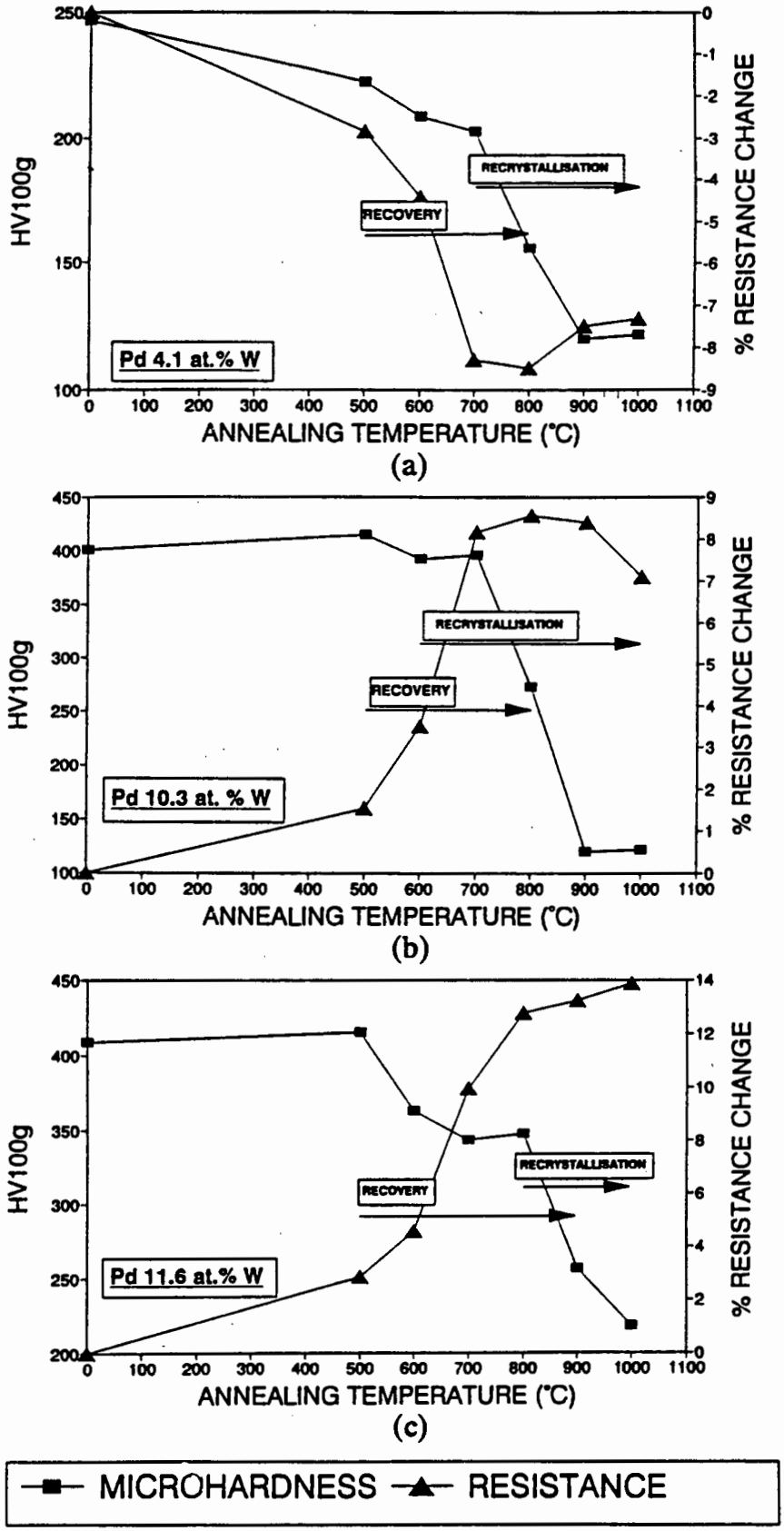

Figure 4.51: Graphs of properties vs. annealing temperature for palladium-tungsten alloys.

Palladium 5.3 at.% molybdenum

The effect of annealing on the properties of palladium 5.3 at.% molybdenum is shown in fig. 4.52 (a). The change in the microhardness of palladium 5.3 at.% molybdenum due to annealing appears normal up to an annealing temperature of 700°C: a decrease is observed after each annealing experiment. However, after annealing at higher temperatures, an unexpected increase in microhardness occurs. In this regard, the change in resistance is of particular interest, since the trend followed appears to be the same: annealing in the temperature range 500°C - 700°C results in a steady decrease in resistance, as expected for normal metals and alloys as a result of a decrease in dislocation density due to annealing, but annealing at higher temperatures results in an increase in resistance. This distinct reversal of the sign of the resistance change, during the course of a series of annealing experiments, is also an unexpected phenomenon and was not observed in any of the other alloys under investigation, although there is a suggestion of similar behaviour in palladium 4.1 at.% tungsten.

Transmission electron microscopy shows the initiation of recrystallisation to occur due to annealing at 600°C, progressing to completion after annealing at 700°C; both the resistance and microhardness measurements are thus consistent with observed changes in dislocation density due to annealing up to this temperature. However, annealing above 700°C results in no further decrease in dislocation density: that both resistance and microhardness show a significant increase suggests that a structural change occurs in the temperature range 800°C - 1000°C. Zone-axis electron diffraction patterns of this alloy after annealing at 700°C contain additional sharp reflections at $1/3$242-type positions ([111] zone axis) and at $1/2$131-type positions ([112] zone-axis) which may be used to produce dark-field images showing the presence of precipitates; after annealing at higher temperatures these reflections become faint and dark-field images are not obtainable. The decrease in resistance, dislocation density and microhardness up to an annealing temperature of 700°C is thus coincident with a structural transformation; the unexpected increase in resistance and microhardness at higher temperatures is associated with a decrease in intensity of the additional reflections in zone-axis diffraction patterns.

Palladium 9.7 at.% molybdenum

The effect of annealing on the properties of palladium 9.7 at.% molybdenum is shown in fig. 4.52 (b). The results of microhardness tests on palladium 9.7 at.% molybdenum show little decrease due to annealing at temperatures up 600°C; a large decrease occurs after annealing at 700°C. These microhardness measurements are consistent with transmission electron microscopy observations: little recovery of the material occurs after annealing at 500°C and 600°C, whereafter recrystallisation initiates after annealing at 700°C and progresses to completion with annealing at higher temperatures. An increase in resistance occurs after each annealing experiment in the range 500°C - 1000°C, with the largest increase occurring after the 700°C anneal. The appearance of diffuse reflections at $1/3$242-type positions in [111] and at $1/2$131-type positions in [112] zone-axis diffraction patterns of the annealed alloy suggests that this unexpected behaviour has its origin in a structural transformation.

Palladium 16.0 at.% molybdenum

The effect of annealing on the properties of palladium 16.0 at.% molybdenum is shown in fig. 4.52 (c). The microhardness of palladium 16.0 at.% molybdenum does not change significantly after annealing at 500°C and 600°C; a large decrease however occurs after annealing at 700°C, coincident with recrystallisation of the alloys. Microhardness continues to decrease due to annealing at temperatures up to 1000°C. The effect on electrical resistance of annealing in the temperature range 500°C - 1000°C is similar to that observed in palladium 9.7 at.% molybdenum: annealing at temperatures up to 700°C results in large increases in resistance, whereas annealing at higher temperatures produces little further change. Faint additional reflections are observed after annealing, at $1/3$242-type positions in [111] and at $1/2$131-type positions in [112] zone-axis diffraction patterns, suggesting that a similar structural transformation takes place in this alloy due to annealing.

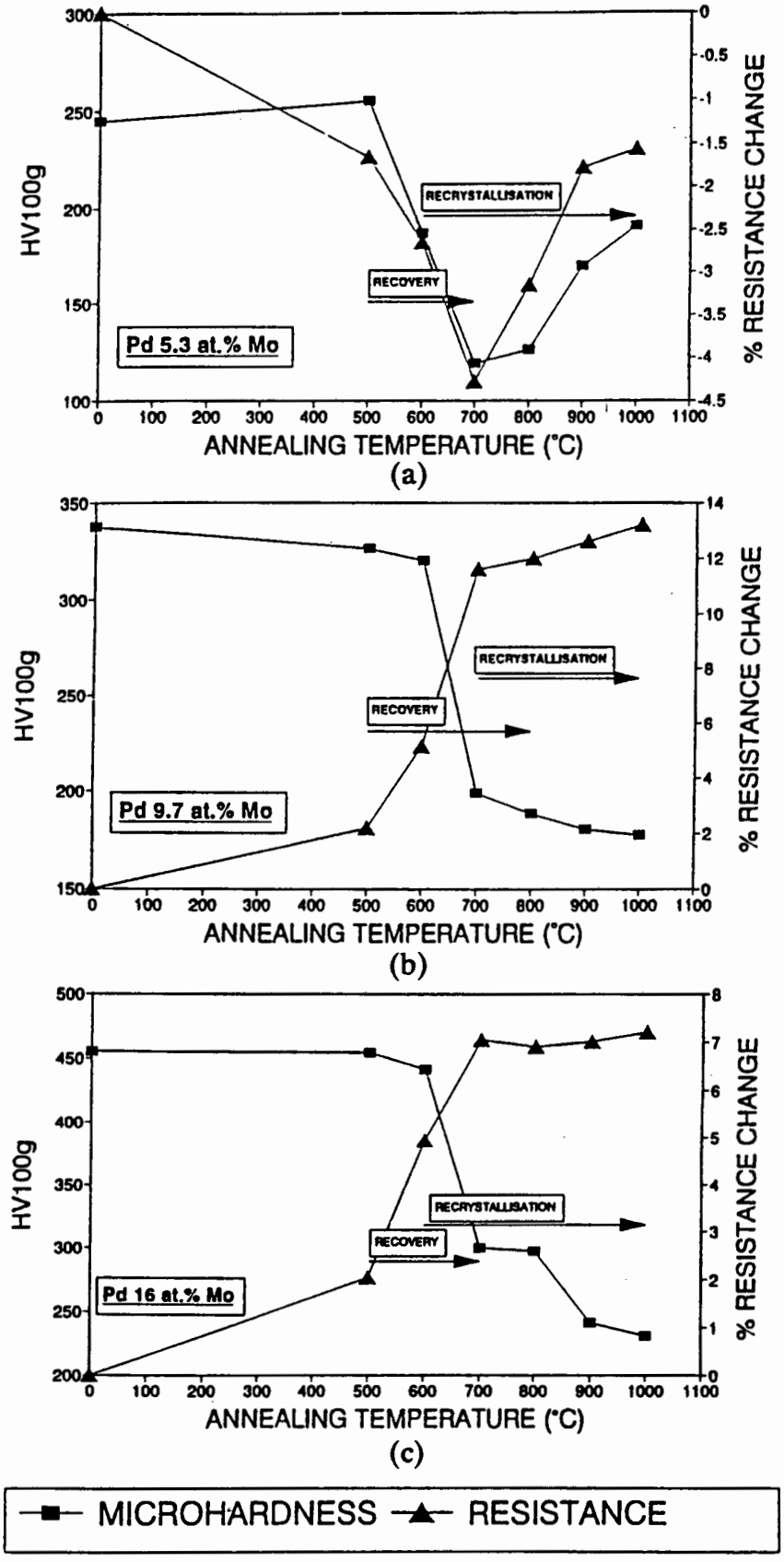

Figure 4.52: Graphs of properties vs. annealing temperature for palladium-molybdenum alloys.

Overview

Microhardness measurements of palladium-tungsten and palladium-molybdenum after annealing in the range 500°C - 1000°C show a general decrease with increasing annealing temperature (with the exception of palladium 5.3 at.% molybdenum and palladium 4.1 at.% tungsten), as observed in pure palladium. However, the effect of annealing temperature on the microhardness of the alloys is not in all cases consistent with the effect of annealing temperature on dislocation density as observed by means of transmission electron microscopy.

In all the alloys tested, the first annealing experiment at 500°C results in a small change in resistance; subsequent annealing at 600°C produces a greater change, and annealing at 700°C a large further change of up to six per cent of the resistance of the cold-worked specimens. The first three heat treatments, then, result in a similar trend in the *magnitude* of resistance changes for all the alloys. However, the resistance of alloys of lower solute concentration (palladium 4.1 at.% tungsten and palladium 5.3 at.% molybdenum) *decreases* as a result of these heat treatments whereas the resistance of alloys of higher solute concentration *increases*. Annealing at temperatures in the range 800°C - 1000°C results in an increase in the resistance of palladium 5.3 at.% molybdenum and palladium 4.1 at.% tungsten; the cumulative effect of annealing in the range 500°C - 1000°C is nevertheless a decrease in resistance. The four alloys of higher solute concentration show a smaller difference between the resistance after annealing at 700°C and the resistance after annealing in the range 800°C - 1000°C.

The expected relationship between microstructure, microhardness and electrical resistance - a decrease in dislocation density due to annealing leading to a decrease in both microhardness and resistance - is thus not evident in the alloy systems under investigation. The appearance of additional reflections at $1/3$242-type positions in [111] and at $1/2$131-type positions in [112] zone-axis diffraction patterns as a result of annealing suggests that a structural transformation occurs at elevated temperatures, which may influence both resistance and microhardness.

CHAPTER 5

DISCUSSION

The results of the present work show that palladium-tungsten and palladium-molybdenum alloys exhibit unusual changes in electrical resistance as a result of annealing. In the alloys containing more than 6 at.% solute, an increase in resistance has been measured after heat treatment although a decrease in resistance is normally to be expected as a result of recovery and recrystallisation processes. An increase of this nature is exhibited by many transition metal alloys due to the development at elevated temperatures of structural order (the "k-state"), which may result in a large increase in resistance. In the alloys containing less than 6 at.% solute however, a minimum in resistance with respect to annealing temperature has been observed, suggesting that additional influences on the resistivity are present.

In section 5.1 of this chapter the electrical resistivity of the alloys under investigation is discussed. The experimental approach to resistivity measurement is reviewed in section 5.1.1; in section 5.1.2, mechanisms whereby changes in resistance may occur in binary alloys are considered with reference to the alloys under investigation. It is concluded that a change in the atomic configuration of the alloys is the only mechanism consistent with the experimental observations of the present work. The influence of short-range order on resistivity is then considered in sections 5.1.3 and 5.1.4. Section 5.2 concerns the development of structural order and its effects on the properties of the alloys. The electron diffraction investigation in the present work is considered in section 5.2.1; the presence of structural order in annealed alloys is discussed in section 5.2.2. In section 5.3 the evolution of microstructure as a result of annealing after cold work is discussed.

Section 5.3.1 concerns the transmission electron microscope investigation; the evolution of microstructure and the development of short-range order are discussed in section 5.3.2. Section 5.4 addresses the mechanical properties of the alloys under investigation, and the dependence of mechanical properties on microstructure and structural order.

The effect of structural order on the properties of palladium-tungsten and palladium-molybdenum is discussed in section 5.5: alloys of low solute concentration are considered in section 5.5.1 and alloys of high solute concentration in section 5.5.2. On this basis, the type of short-range order present and its development during annealing is considered in section 5.5.3. The final section of this chapter comprises an overview of the issues discussed.

5.1 ELECTRICAL RESISTIVITY

5.1.1 RESISTANCE MEASUREMENTS

In the present work, the purpose of the electrical resistance measurements was to detect changes in resistivity brought about by annealing, and to relate these changes to microstructure. The electrical resistivity of a metal is sensitive to microstructural changes, since any deviation from periodicity in the crystal lattice causes electron scattering. Although there is a number of factors which may influence resistivity (discussed in section 5.2), it was anticipated at the outset that the annealing experiments would bring about predominantly two processes: recovery/recrystallisation, and a change in atomic configuration.

The residual resistivity ρ_0 is the resistivity in the absence of thermal vibrations, i.e. at T = 0 K. However if ρ_0 alone undergoes a change, the temperature dependence of resistivity remaining constant, the resistance measuring temperature T_m need not be restricted to low temperatures. For a given measuring temperature, the change in residual resistivity ($\rho_{0f} - \rho_{0i}$) is given by the difference between final and initial measured resistivity, provided that the ideal resistivity $\rho(T_m)$ remains constant:

$$\begin{aligned} \rho_f - \rho_i &= (\rho_{0f} + \rho(T_m)) - (\rho_{0i} + \rho(T_m)) \\ &= \rho_{0f} - \rho_{0i} \end{aligned} \qquad (5.1)$$

Clearly, the accuracy of such measurements is dependent upon the capacity of the measuring apparatus to resolve the change in residual resistivity, which may be very small compared with the total resistivity.

The presence of lattice defects, including dislocations, makes a positive contribution to the residual resistivity; a reduction in defect density due to annealing will consequently decrease this contribution. The presence of structural order in the lattice may make a positive or a negative contribution to the residual resistivity. The residual resistivity due to dislocations, however, is likely to be small in comparison to the ideal resistivity except at low temperatures; the contribution to resistivity of changing defect densities is thus difficult accurately to determine at ordinary temperatures. Furthermore, information regarding lattice defects is not directly obtainable from resistivity measurements; such information is more easily obtainable from electron microscopy. However, the measurement of changes in resistivity is a favoured method of obtaining information regarding short-range order, because it offers experimental simplicity relative to alternative techniques. It is commonly assumed that the influence of ordering on the temperature coefficient of resistivity is negligible, so that the change in residual resistivity due to ordering is equal to the change in total resistivity at the measuring temperature (see fig. 2.1).

In transition metals, a change in local atomic configuration may lead to local alterations in band structure and hence to a change in the temperature coefficient of resistivity. Nevertheless, the contribution of short-range order to resistivity has been assessed on the basis of room-temperature resistance measurements, made before and after annealing, for many transition metal alloys including AgPd[113], AuPd[112] and CuPd[125], PdEu[108], and Ni-Fe-Mo-Cu[149]. This experimental procedure has been followed in the present work; the influence of structural order on the temperature coefficient of resistivity is however considered in section 5.1.3.

5.1.2 POSSIBLE CAUSES OF ANOMALOUS RESISTANCE EFFECTS

The unusual features observed in the present work are the sign (direction) and the magnitude of the measured changes in resistivity brought about by annealing. Resistance changes have been measured which are positive, and of the order of ten per cent of the room temperature resistance in magnitude. Given the high resistivity of the alloys under investigation, this represents a large change. A change in the room-temperature resistance of a specimen after annealing may be brought about by a change in the residual resistivity alone, or by a change in both the residual resistivity and the temperature dependence of resistivity. Those factors contributing to the residual or the ideal resistivity which may be altered by heat treatment are therefore assessed below for the alloys under investigation, in order to determine mechanisms whereby the observed changes in resistance may come about.

The heat treatment of a binary alloy may result in a change in defect density, which affects only the residual resistivity; or a phase transformation or a change in magnetic or structural order, which may affect both the residual and the temperature-dependent resistivity. An additional effect considered below is the decrease in temperature coefficient of resistivity reported to occur during the heating of highly resistive alloys.

The effect of annealing on the electrical resistance of palladium-tungsten and palladium-molybdenum cannot directly be related to changes in residual resistivity due to changing defect densities, since in all the alloys investigated an increase in resistance has been measured after heat treatments which are observed to result in either a decrease or no significant change in dislocation density (sections 4.1.1, 4.3.1; figs. 4.51, 4.52). A decrease in the contribution of dislocations to the residual resistivity certainly occurs as a result of annealing; however, a simultaneous increase in the contribution to residual resistivity from other sources apparently more than compensates for this, resulting in an overall increase in resistivity.

With respect to the possibility of a phase transformation, the solute concentrations of palladium-tungsten and palladium-molybdenum specimens investigated in the present work were selected as examples of single-phase

palladium-based solid solutions on the basis of published equilibrium phase diagrams[e.g.128,141]. Examination of these alloys after annealing by means of scanning electron microscopy, including energy dispersive analysis, showed no evidence of the presence of an equilibrium second phase.

It is also unlikely that magnetic effects are solely responsible for the observed variation in resistivity, since the addition of tungsten or molybdenum to palladium results in a significant decrease in magnetic susceptibility to almost zero at 10 at.% solute concentration[e.g.139,104], the composition at which the resistance increase due to annealing is particularly large. Furthermore, the magnetic susceptibility of palladium-tungsten alloys is reported to decrease after annealing at temperatures which cause an increase in resistivity[133]. It is possible that magnetic effects may contribute to the resistivity of the alloys of less than 6 at.% solute concentration; this will be considered further in sections 5.1.3 and 5.5.

Mooij[150] investigated the resistivity of a number of transition metal alloy systems and observed that, for highly resistive alloys, the temperature coefficient of resistivity tended to decrease with increasing resistivity. This was noted both when the resistivity of alloys increased as a function of increasing solute concentration, and when the resistivity increase occurred due to increased temperature for a particular alloy. It was suggested that this comes about owing to a decrease in the mean free path of conduction electrons, resulting in the contribution of phonon scattering to electrical resistivity becoming less dominant: under such circumstances a decrease in the temperature coefficient of resistance is to be expected[150]. Measurements of the temperature dependence of resistivity were not undertaken in the present work: in this regard, measurements of the resistivity of palladium-tungsten during continuous heating and cooling by Klyuyeva et al[133] are of interest (fig. 2.11): the alloys of highest resistivity (palladium 9.3 at.% tungsten and palladium 12.7 at.% tungsten) are reported to exhibit a decrease in the temperature coefficient of resistivity above 700°C. In this temperature range, palladium 12.7 at.% tungsten exhibits a negative temperature coefficient of resistivity[133]; this is reported by Mooij to be characteristic of alloys of resistivity greater than 100 $\mu\Omega$-cm[150]. The reported reduction in the temperature coefficient of resistivity of palladium-tungsten is however not completely

reversed on cooling, resulting in both a higher resistivity and a lower temperature coefficient of resistivity at room temperature than measured prior to heating[133]. The decrease in temperature coefficient of resistivity which occurs in the above alloys at high temperatures is thus brought about, at least in part, by some transformation which is not reversed by cooling, and not by an increase in resistivity due to thermal disorder alone.

In summary, it is unlikely that an equilibrium phase separation or a significant change in the degree of magnetic order occurs due to annealing in all the alloys under consideration; a change in defect density certainly occurs as a result of annealing, but its effect on residual resistivity does not explain all the measured changes in resistance; and although the palladium-tungsten alloys of more than 9 at.% solute concentration have a high resistivity, the decrease in temperature coefficient of resistivity reported to occur during heating[133] is not restricted to elevated temperatures. The remaining possibility is that a structural transformation, occurring at elevated temperatures and not reversed by slow cooling, is responsible for the resistance changes observed after annealing of palladium-tungsten and palladium-molybdenum. Such a transformation may result in an increase in residual resistivity of greater magnitude than any resistivity decrease due to decreasing defect concentrations, and may also influence the temperature coefficient of resistivity.

5.1.3 RESIDUAL RESISTIVITY DUE TO SHORT-RANGE ORDER

The contribution of short-range order to the resistivity of a concentrated transition metal alloy is more complex than in simple metal alloys; the calculation of ρ_{SRO} (the residual resistivity due to short-range order) for transition metal alloys may be expected to present more difficulties as a consequence. It is of interest, therefore, that the simple-metal methods of both Asch and Hall[46] and Rossiter and Wells[49] for calculation of ρ_{SRO} have been applied to transition metal alloys with some success. It should be noted in this regard that the addition of a second component to a transition metal may cause the Fermi surface to become more spherical, and hence closer to the simplifying approximations of the simple-metal calculations; it has also been suggested[126] that the simple-metal calculations reflect the influence of short-range order on s-s scattering in transition metal alloys.

Asch and Hall's[46] formalism requires a knowledge of the atomic fraction and atomic numbers of the alloy constituents, the lattice parameter, the short-range order parameters and the screening constant Q of the screened Coulomb potential given by:

$$v(\mathbf{r}) = Ze^2\exp(-Qr)/4\pi\epsilon_0 r \qquad (5.2)$$

Using Asch and Hall's method[46], assuming a screening constant Q between $4r_0^{-1}$ and $5r_0^{-1}$ (where r_0 is the Bohr radius), Katsnel'son et al obtained qualitative agreement with experimental results for equiatomic PdPt[114] containing heterogeneous or local order. Similar calculations for PdCo, using $Q = 5r_0^{-1}$ and $Q = 10r_0^{-1}$ were not successful[115].

The method of Rossiter and Wells[49] has been applied to transition metal alloys by, among others, Wagner et al[54] for NiMn and Stanisz et al[57] for NiCu. This method requires a knowledge of the Warren-Cowley parameters, the number of conduction electrons per atom (i.e. atomic fraction and valence of each atomic species), the lattice parameter and the scattering potential. Rossiter's expression[49] for ρ_{SRO}, the residual resistivity due to short-range order, is (see Chapter 2, section 2.2):

$$\rho_{SRO} = C(c_A c_B/k_F^3 n)\,\Sigma\, c_i\alpha_i Y_i \qquad (5.3)$$

For the case of a random alloy, this becomes

$$\rho_{dis} = C(c_A c_B/k_F^3 n) \qquad (5.4)$$

The fractional change in resistivity due to the development of short-range order is then:

$$\rho_{SRO}/\rho_{dis} = \Sigma\, c_i\alpha_i Y_i \qquad (5.5)$$

The Warren-Cowley parameters (WCP) assigned by Babanova et al[136] to annealed palladium-tungsten alloys (see Table 2.1 and Appendix) are negative

in the first co-ordination sphere, indicating that short-range order is present; the magnitude increases with increasing solute concentration. Using these WCP, together with lattice parameter measurements made by the same workers[133], the fractional change in resistivity of palladium-tungsten alloys due to short-range order may be calculated from equation (5.5). Following Rossiter and Wells'[49] use of a screened Coulomb potential, with a screening parameter $Q = 2.5k_F$, leads to a dependence on solute concentration of the ratio (ρ_{SRO}/ρ_{dis}) as shown in fig. 5.1. ($Q = 2.5k_F$ is an approximation to the screening parameter, which for palladium alloys is close to $3k_F$ using $Q = Z^{1/3}Å^{-1}$ and $k_F = 1Å^{-1}$. However, Rossiter and Wells[49] showed the integral Y not to be sensitive to the ratio Q/k_F provided that $Q/k_F > 2$. The same authors also showed that a difference in screening parameters between the constituents of an alloy has little effect on the integral Y.)

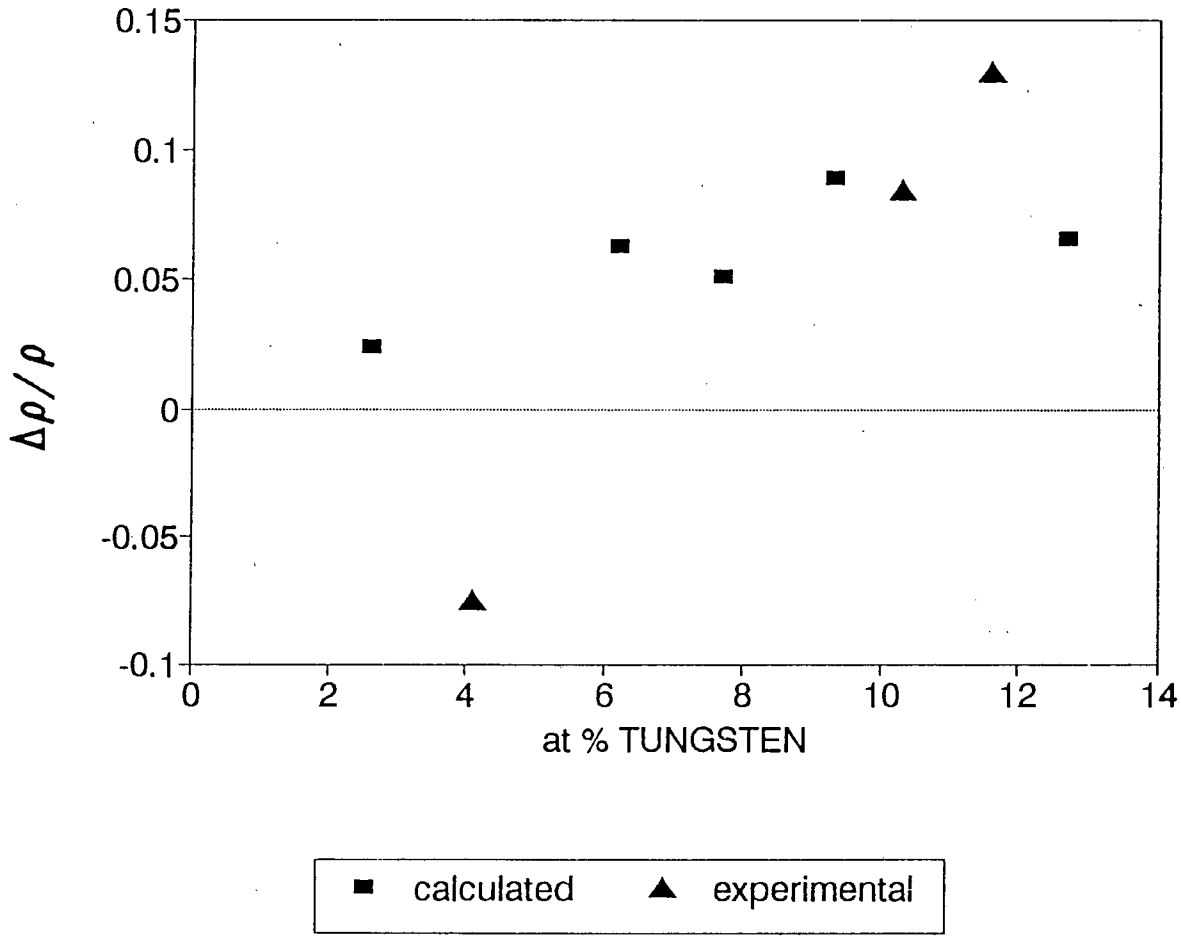

Figure 5.1: Graph of calculated ratio ρ_{SRO}/ρ_{dis}, and experimental resistivity change $\Delta\rho/\rho$, vs. solute concentration for palladium-tungsten alloys annealed at 900°C.

Figure 5.1 shows that, on the basis of Rossiter and Wells'[49] simple-metal resistivity model, the presence of short-range order in palladium-tungsten alloys should lead to an increase in resistivity. Equation 5.5 may be seen correctly to predict an increase in resistivity due to the development of short-range order during annealing, for alloys containing more than 6 at.% solute. In terms of the rigid-band model, this is the composition range in which the d band is filled and s-s scattering predominates. The calculated resistivity values, which show the influence of short-range order on s-s scattering, may therefore be expected to reflect the observed change in resistivity reasonably well.

A maximum in the calculated resistivity is observed at around 10 at.% solute concentration, similar to the trend observed for palladium-molybdenum alloys (see figs. 4.9, 4.52); and the magnitude of ρ_{SRO} (around ten per cent of the resistivity of the disordered alloy) is similar to experimental values for palladium 10.3 and 11.6 at.% tungsten (see figs. 4.9, 4.51). However, it cannot be assumed that the cold-worked specimens are fully disordered; figures as low as a 50% decrease in short-range order due to cold work have been suggested for palladium alloys[125]. The calculated resistivity due to short-range order, ρ_{SRO}, might therefore be expected to be considerably greater than the measured increase in resistivity due to annealing. Competing effects on residual resistivity are expected to be smaller: the contribution to ρ_0 of a decrease in dislocation density due to annealing is expected to be relatively small, and the influence of magnetic effects in alloys above 6 at.% solute concentration is probably negligible. Static atomic displacements are also unlikely to make a large contribution because of the similarity of atomic radii between solvent and solute. The results of the calculation of ρ_{SRO}, for alloys of more than 6 at.% solute concentration, are therefore qualitatively consistent with the measured increase in resistivity due to annealing.

For the alloys containing less than 6 at.% solute, equation (5.5) does not predict the decrease in resistance after annealing measured in the present work (figs. 4.51, 4.52) or by Mes'kin et al[140] (figs. 2.10, 2.18). However, the measurements of Klyuyeva et al[133] (fig. 2.11) show a small increase in the resistivity of alloys in this composition range, after continuous heating and cooling. This is consistent with Babanova et al's[136] WCP values which show short-range order to be present[136] in this concentration range. However, the

simple-metal approximations of equation (5.2) are inappropriate for these alloys, since only s-s scattering is assumed. In terms of the rigid-band model, the d-band of palladium is unfilled in this concentration range and s-d scattering predominates. The effect of short-range order on s-d scattering may be significant, arising from modifications to band structure brought about by changing atomic configurations, and may result in a decrease or an increase in resistivity. Although the contribution to residual resistivity of dislocations decreases as a result of annealing, this does not explain the large resistivity decrease of 8% measured for palladium 4.1 at.% tungsten. Annealing is also reported to influence the magnetic properties of palladium-tungsten alloys, resulting in a decrease the susceptibility[133]; the contribution of magnetic effects to the residual resistivity is thus also likely to decrease as a result of annealing.

In the alloys containing more than 6 at.% solute then, an increase in residual resistivity due to the development of short-range order offers a qualitative explanation for the increase in resistivity observed after annealing. In the alloys containing less than 6 at.% solute however, a change in atomic configuration due to annealing may influence a number of other factors contributing to the residual resistivity; these will be considered in more detail in section 5.5.1. For all the alloys investigated, however, the additional influence on the measured resistivity of the temperature dependence must be considered before any conclusions may be drawn.

5.1.4 THE EFFECT OF SHORT-RANGE ORDER ON IDEAL RESISTIVITY

A decrease in the temperature coefficient of resistivity α_ρ as a result of annealing was first reported by Thomas[72] for alloys containing transition metals. The resistivity/temperature curves for palladium-tungsten alloys published by Klyuyeva et al[133] during continuous heating and cooling (fig. 2.11) show a decrease in $d\rho/dT$ (after cooling to room temperature) only for palladium 12.7 at.% tungsten. Mes'kin et al[140], however, observed a change in α_ρ for a range of palladium-tungsten and palladium-molybdenum alloys due to annealing at 700°C for one hour. A change in α_ρ which occurs at elevated temperatures and is not reversed during cooling will have an effect on the

resistance measured at room temperature: the measured change in resistance will be smaller than the change in residual resistivity (extrapolating to 0K), as shown in fig. 5.2.

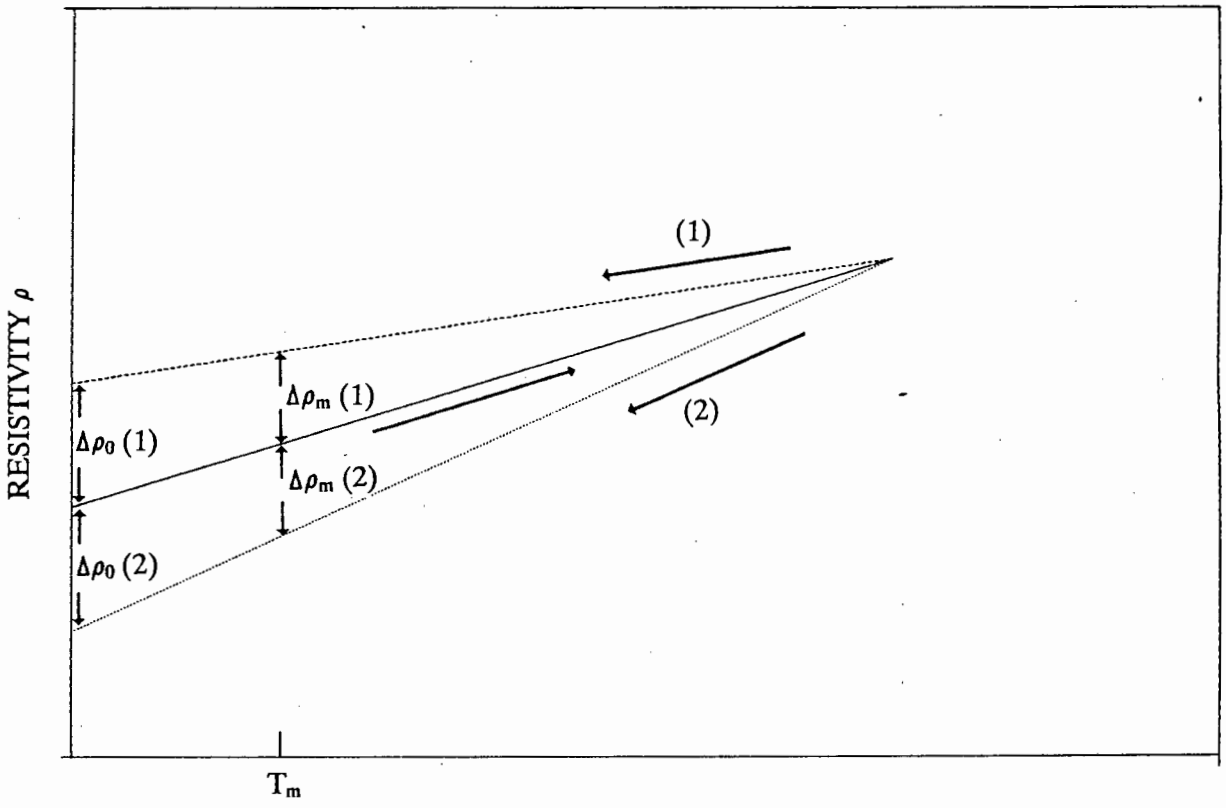

Figure 5.2: Idealised schematic diagram showing the effect of change in α_ρ during annealing on the measured change in resistivity for (1) a decrease in α_ρ and (2) an increase in α_ρ.

Mes'kin et al[140] report a decrease in α_ρ due to annealing of nearly forty per cent for palladium 10 at.% molybdenum, and between twenty and forty per cent for palladium containing 9 at.% - 12 at.% tungsten (figs. 2.18, 2.10). The temperature dependence of resistivity is very low for alloys in this composition range (e.g. $d\rho/dT$ = 0.02 $\mu\Omega$-cm/°C for palladium 10.4 at.% molybdenum[104]) so that the absolute change in α_ρ is not large. Nevertheless allowance must be made for the effect on measured resistance: the measured change in resistance will be smaller than the change in residual resistivity. For palladium-molybdenum alloys containing around 10 at.% solute, the results of Mes'kin et al[140] together with the data of Kudielka-Artner and Argent[104] suggest that the

measured change in resistivity may underestimate the change in residual resistivity by as much as 5% of the room-temperature resistivity. For palladium-tungsten and palladium-molybdenum alloys up to 7 at.% solute concentration, Mes'kin et al[140] report an increase in α_ρ of around ten per cent. This will also result in a measured change in resistivity which is smaller than the change in residual resistivity; in this case, the change in measured resistivity is a decrease, so that a greater actual decrease in residual resistivity is indicated. The effect of the changes in α_ρ for all palladium-tungsten and palladium-molybdenum alloys is thus to reduce the measured change in resistivity relative to the change in residual resistivity.

The measured resistivity at room temperature after annealing is thus affected by both ρ_0 and $\rho(T)$. The development of structural order in the lattice as a result of annealing influences both ρ_0 and α_ρ, and is thus the dominant contributing factor to the changes in resistivity measured in palladium-tungsten and palladium-molybdenum.

5.2 STRUCTURAL ORDER

In both long-range and short-range ordered structures there is a tendency for like atoms to separate and unlike atoms to be neighbours; however, long-range order concerns correlations in the distribution of atoms on sublattices of the structure as a whole, whereas short-range order concerns correlations in the local environment of an atom. Short-range order and clustering (clustering is a localised tendency for like atoms to be neighbours) concern only the atomic distribution in the vicinity of an atom and are not measured in terms of the occupation of particular sites in particular directions, but rather in terms of pairwise correlations which may vary with separation of the sites. The Warren-Cowley short-range order parameters α_{ij} may be expressed by[50]

$$\langle \sigma_i \sigma_j \rangle = c_A c_B \alpha_{ij} \qquad (5.6)$$

where $\langle \sigma_i \sigma_j \rangle$ is the average site occupation over all two-site pairs
and $\alpha_{ij} = 0$ for random occupation, $i \neq j$.

If $<\sigma_i\sigma_j>$ is negative and i and j are adjacent sites, then the number of unlike neighbours exceeds random probability, and short-range order is present. Conversely, if $<\sigma_i\sigma_j>$ is positive then the number of like neighbours exceeds the random probability, and clustering of like atoms is present. It is important to note that long-range or short-range ordering does not necessarily effect the locally averaged composition.

X-ray diffraction may be used to detect the presence of short-range order, which gives rise to maxima in diffuse X-ray intensities: the position of these maxima give the position of the superlattice reflections of the corresponding ordered lattice, and the relative intensity shows the degree of short-range order present. The short-range order parameters α_i were defined by Cowley[42] for convenience in considering X-ray diffraction effects, since the α_i are the coefficients of the Fourier series expressing the scattering power due to short-range order as a function of the reciprocal lattice coordinates[42]. Alimov and Katsnel'son[137] measured an increase in diffuse X-ray scattering intensity as a result of annealing palladium 11.3 at.% tungsten, which showed that the degree of short-range order increases after annealing. Babanova et al [136] investigated a wider range of palladium-tungsten compositions, showing that the degree of short-range order present after annealing increases with solute concentration, and suggested that the X-ray measurements showed a (100) superstructure peak (see Appendix).

Ardell et al[131,144] used electron diffraction to investigate palladium-tungsten and palladium-molybdenum alloys after proton irradiation, identifying the long-range ordered structures Pd_8W and Pd_8Mo. Schematic zone-axis electron diffraction patterns of Pd_8W, simulated on the basis of the data of Cheng and Ardell[132], are shown in figs. 5.3 and 5.4. It should be noted that there is no evidence of the (100) superstructure peak, suggested for the short-range ordered alloys[136], in electron diffraction patterns of the long-range ordered structure.

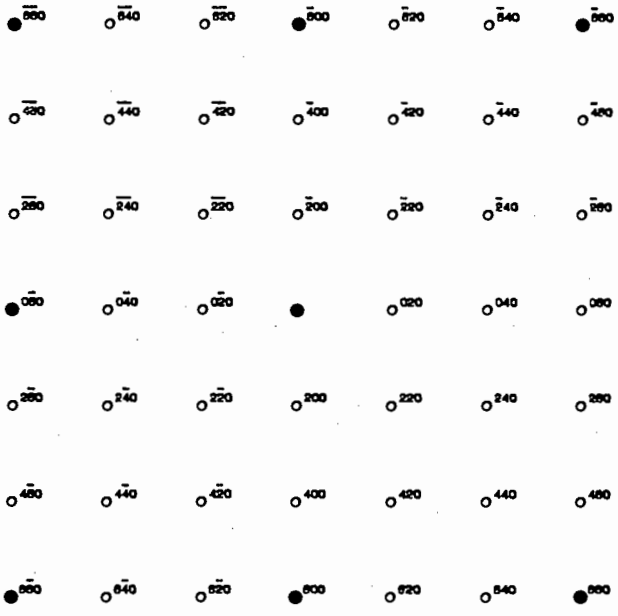

Fig. 5.3: Simulated schematic [001] zone-axis diffraction pattern for Pd_8W; (●) disordered fcc reflections.

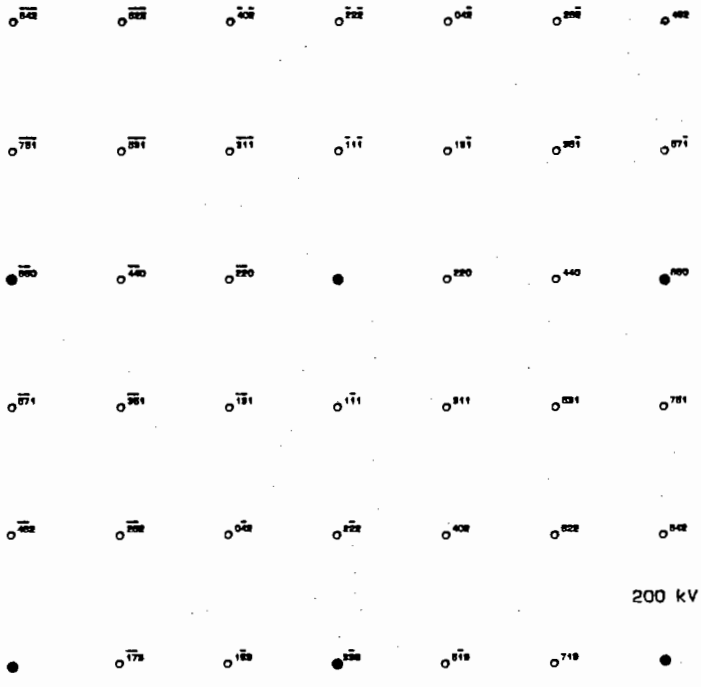

Fig. 5.4: Simulated schematic [$\bar{1}$12] zone-axis diffraction pattern for Pd_8W; (●) disordered fcc reflections. .

5.2.1 ELECTRON DIFFRACTION INVESTIGATIONS

The presence of short-range order may result in additional scattering in electron diffraction patterns; the nature of this scattering is dependent on the type of short-range order from which it arises. A distinction may be drawn between heterogeneous short-range order, characterised by microdomains having a particular ordered structure, and homogeneous short-range order in which there is a statistical probability that atoms have unlike nearest neighbours[50]. For heterogeneous short-range order, the presence of ordered microdomains in an alloy gives rise to additional scattering - discrete reflections or diffuse scattering - at superlattice reflection sites in electron diffraction patterns[e.g.151]. For homogeneous short-range order, two models have been proposed: a concentration wave approach, in which a series of static concentration waves characterises the local variation in the probability of finding a particular atomic type on a specific lattice site[152]; and a cluster variation approach based on cluster configurations of minority atoms[153]. The concentration wave model[152] provides a reciprocal-space representation in which each static concentration wave produces a superlattice reflection in electron diffraction patterns, the intensity of which is related to the amplitude of the concentration wave.

The intensity of diffuse scattering due to short-range order may be calculated from the Warren-Cowley parameters of an alloy if kinematical scattering, as occurs in X-ray diffraction, is assumed. For electron diffraction, account must be taken of dynamical effects which may modify the relative intensities of diffuse scattering[154,155]. The foils used for electron diffraction in the present work were prepared with some difficulty and were of greater than optimum thickness; the diffraction conditions therefore cannot be assumed to be kinematical. A calculation to determine the relative diffuse intensities was therefore, under the experimental conditions, inappropriate.

The purpose of the electron diffraction experiments in the present work was to investigate the presence of short-range order in annealed palladium-tungsten and palladium-molybdenum alloys, by means of a systematic investigation of high-symmetry zone-axis electron diffraction patterns. Long-exposure electron diffraction patterns were obtained for each alloy, in the cold-worked and in all

heat treatment conditions; and were inspected for scattering in the positions of the superlattice reflection sites of the long-range ordered structure Pd_8W (and Pd_8Mo)[131,144] and at the site of the (001) superstructure peak suggested by Babanova et al[136]. The results of this investigation showed that electron diffraction patterns do not exhibit scattering in the positions suggested by the works cited above. The only features noted, other than the fundamental fcc reflections, were the additional reflections observed at $1/3$242-type positions in [111], and $1/2$131-type positions in [112] zone axis diffraction patterns for all the alloys after annealing (fig. 4.13). Such zone axis diffraction patterns are characteristic of the presence of hcp precipitates or twinning in face-centred cubic (fcc) crystals[156]. However, care was taken to use selected areas distant from visible twin interfaces for all electron diffraction patterns. In addition, both twinning and hcp precipitates are expected to give rise to additional reflections in [110] zone axis diffraction patterns; such reflections were not observed in the present work.

The additional $1/3$242 and $1/2$131 reflections observed in [111] and [112] zone-axis electron diffraction patterns were sharpest for palladium 5.3 at.% molybdenum after annealing at 700C. Annealing this alloy at temperatures from 800°C - 1000°C caused the additional reflections to decrease in intensity relative to the fundamental fcc reflections (fig. 4.20 (c) and (d)). In palladium 4.1 at.% tungsten, after annealing at temperatures from 800°C - 1000°C, reflections in the $1/3$242 and $1/2$131 positions are observed to be diffuse (fig. 4.17 (c) and (d)). In the remaining four annealed alloys (palladium 10.3 at.% tungsten, palladium 11.6 at.% tungsten, palladium 9.7 at.% molybdenum and palladium 16 at.% molybdnenum), these reflections are visible only very faintly, if at all, in the electron microscope, requiring long exposure times before becoming visible in diffraction patterns (figs. 4.18, 4.19, 4.21, 4.22).

In order to identify the features which give rise to the additional reflections observed in [111] and [112] zone-axis electron diffraction patterns, dark-field images were recorded by centering, and placing the objective aperture over, the diffracted beam of interest. In palladium 5.3 at.% molybdenum after annealing at 700°C (the alloy and condition for which the strongest additional reflections were observed) this technique, using the reflections arrowed in figs. 4.13, brings into contrast a distribution of small features (figs 4.14 (b) and 4.15 (b)).

In this alloy in other heat treatment conditions and in the remaining alloys, this technique failed to produce dark-field images in which any features were discernible.

The additional $1/3$242 and $1/2$131 reflections in [111] and [112] zone-axis electron diffraction patterns were observed in all the alloys after annealing, and in none of the alloys in the cold-worked condition. This suggests that the additional reflections are not the result of an artifact such as a surface film. The consistency with which the reflections are observed, in [111] and [112] diffraction patterns for all annealed alloys, suggests that they arise from a microstructural feature of the annealed condition; however, the feature is not readily resolvable with the instrument used.

5.2.2 STRUCTURAL ORDER IN PALLADIUM-TUNGSTEN AND PALLADIUM-MOLYBDENUM

The systematic electron diffraction investigation described in section 5.2.1 yields no direct evidence for the presence of short-range order in annealed palladium-tungsten and palladium-molybdenum. The work of Babanova[136] and Alimov and Katsnel'son[137] on palladium-tungsten alloys thus remains the only direct investigation which shows short-range order to be present in either system: the presence of short-range order in palladium-molybdenum has been suggested[140] but not previously investigated. However, the results of resistance measurements in the present work give strong indirect evidence for the presence of short-range order in annealed alloys of more than 6 at.% solute concentration, in both alloy systems (section 5.3). The resistivity behaviour of the alloys containing less than 6 at.% solute will be shown, in section 5.5, also to be consistent with the presence of structural order.

Other indirect evidence for the presence of order after annealing may be obtained from published lattice parameter measurements of palladium-tungsten and palladium-molybdenum, annealed at a variety of temperatures, both of which show an unusual dependence of lattice parameter on concentration[e.g.139,146] (figs. 2.7 and 2.13). Figure 5.5 shows the atomic volume of palladium-tungsten alloys after annealing at 1000°C, together with the

expected atomic volume curves for co-ordination numbers (CN) 8 and 12, as measured and calculated by Goetz and Brophy[129]. The measured decrease in atomic volume with the addition of up to 10 at.% tungsten, when solute additions are expected to bring about lattice dilation in a random solid solution, suggests that a non-random atomic configuration is present. Above 10 at.% tungsten concentration, an increase in atomic volume with increasing solute concentration occurs; the atomic volume nevertheless remains smaller than that of pure palladium up to 15 at.% tungsten[129] (the limit of solid solubility[139]), indicating that deviations from a random solid solution are also present in the concentration range 10 at.% - 15 at.% tungsten. The lattice parameter of palladium-molybdenum alloys shows the same minimum at around 10 at.% solute, and is smaller than that of pure palladium up to 20 at.% solute concentration (fig. 2.13). A non-random atomic configuration after annealing is thus probable in palladium-tungsten and palladium-molybdenum alloys of the concentration ranges investigated in the present work.

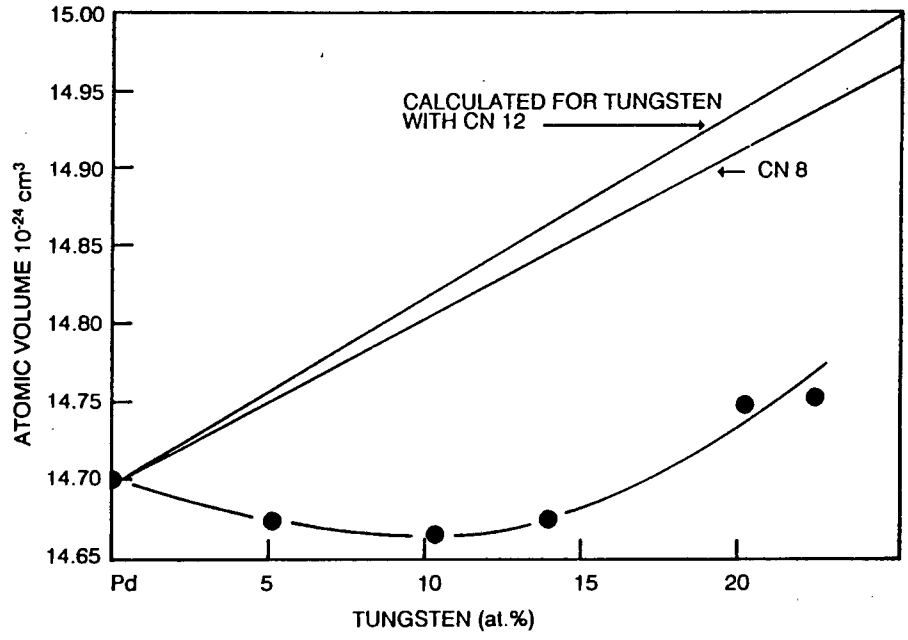

Figure 5.5: Measured and calculated atomic volume vs. solute concentration curves for palladium-tungsten (after Goetz and Brophy[129]).

In a single-phase solid solution, a non-random atomic configuration may take the form of a localised preference for like nearest neighbours (clustering) or unlike nearest neighbours (short-range ordering). Either of these non-random configurations may bring about a decrease in lattice parameter relative to the

disordered alloy. However, it seems unlikely that clustering of the oversized tungsten or molybdenum solute atoms would bring about a decrease in lattice parameter; whereas the presence of a minimum (such as is exhibited by palladium-tungsten and palladium-molybdenum at around 10 at.% solute concentration) suggests the presence of short-range order. If the presence of short-range order results in a contraction of the lattice, this minimum might be expected to indicate the composition at which short-range order is present to the greatest degree. Of particular interest in this regard is the reported formation, under proton irradiation at elevated temperatures, of the long-range ordered phases Pd_8W and Pd_8Mo at 10 at.% solute concentration[131,144]. A solute concentration of 10 at.% is close to the stoichiometric composition (11.1 at.% solute) for the long-range ordered structure; it appears that this is also a favourable composition for the development of short-range order.

The Warren-Cowley parameters calculated by Babanova et al[136], the increase in resistivity due to annealing measured in the present work, and the unusual dependence of lattice parameter on solute concentration exhibited by annealed palladium-tungsten and palladium-molybdenum alloys[e.g139,146], are consistent with the development of short-range order as a result of annealing.

5.3 MICROSTRUCTURE

The development of structural order as a result of annealing cannot be viewed in isolation from the simultaneous evolution of microstructure. The introduction, movement, presence and annealing-out of dislocations may have a significant effect on structural order in the alloys under investigation, and the relationship between microstructure and structural order accordingly requires consideration.

5.3.1 TRANSMISSION ELECTRON MICROSCOPY

The objective of the transmission electron microscope (TEM) investigation in the present work was to monitor the recovery and recrystallisation of cold-worked palladium-tungsten and palladium-molybdenum, in order to relate the changes in microstructure to the measured changes in electrical resistance.

Bright-field images were recorded for all alloys in the cold-worked and in all heat treatment conditions, allowing identification of the temperature ranges in which recovery and recrystallisation occur.

In order to monitor recovery, it is desirable to determine dislocation densities as a function of annealing temperature. Although this was attempted in the present work, it proved impracticable; where foils were sufficiently thin, the high dislocation density caused local bending of the foil, making controlled tilting to the required diffraction conditions difficult. Transmission electron microscopy was accordingly used qualitatively to assess cold work and recovery, and to determine the temperature ranges in which recrystallisation initiates and reaches completion.

Materials with a high stacking-fault energy are characterised by homogeneous deformation and the formation of dislocation cell structures due to easy cross-slip[157]. The absence of cellular dislocation structures in cold-worked alloys, compared to pure palladium (fig.4.23), suggests that the stacking-fault energy (SFE) is lower in the alloys than in the host metal. A decrease in the SFE of palladium with the addition of tungsten or molybenum is consistent with the observation that a significant decrease in dislocation density does not occur prior to recrystallisation (e.g. fig. 4.33), a characteristic of materials having low SFE. Finally, the presence of annealing twins is a feature of the recrystallised microstructure of all the alloys (e.g. fig. 4.34), indicating a low twin fault energy and hence a low SFE. The ease with which twins may form in an fcc crystal is dependent on the energy difference between the hcp and fcc crystal structures[157]: the energy of each crystal structure type is dependent on the electronic structure of the alloy under consideration, and as a consequence may be expected to be sensitive to both solute concentration[158] and atomic configuration[162] in transition metal alloys.

5.3.2 MICROSTRUCTURE AND SHORT-RANGE ORDER

An examination of the measured changes in resistivity, due to annealing of alloys containing more than 6 at.% solute, shows that the largest cumulative change in resistivity occurs as a result of annealing in the lower temperature range (500°C - 700°C); a far smaller change in resistivity is observed after

annealing in the temperature range 800°C- 1000°C. This suggests that the degree of short-range order increases rapidly during annealing in the lower temperature range. This is of interest, since a lesser degree of thermally-activated diffusion of atoms might be expected at the lower temperatures than at the higher temperatures. Khan and Raub[139] report that homogenisation of as-cast palladium-tungsten alloys, of above 5 at.% solute concentration, at 700°C required heat treatments of up to 1000 hours, indicating that the rate of atomic diffusion is extremely low.

When the resistivity measurements are considered relative to the observed evolution of microstructure, however, the results show that resistivity increases rapidly prior to recrystallisation, suggesting that short-range order develops rapidly in a plastically deformed microstructure characterised by a high dislocation density. The development of short-range order is a diffusional process and may be expected to occur by vacancy migration in fcc alloys; the rate of ordering should therefore be proportional to the concentration of vacancies[55]. The plastic deformation of a metal introduces a variety of defects, including dislocations, jogs, stacking faults, interstitials and vacancies. During subsequent annealing, the thermally-activated migration of vacancies to sinks (such as dislocations and grain boundaries) will serve to enhance the atomic rearrangement to a short-range ordered configuration. Gahn and Pitsch[159], using a Monte Carlo simulation of short-range order reactions in binary fcc alloys, found that during vacancy migration, lattice sites in volumes of low SRO were preferentially visited by vacancies, enhancing the increase in SRO. Soltys et al[160], studying the formation of short-range order in nickel 10 at.% molybdenum, concluded that the formation of short-range order is associated with the mobility of vacancies. It is also of interest to note that palladium-chromium, which forms long-range ordered structures with relative ease, is reported to have an anomalously high vacancy diffusion rate[161].

In palladium-tungsten and palladium-molybdenum alloys then, the presence of an excess of vacancies during annealing subsequent to cold work serves to enhance the development of short-range order. This bears comparison with the formation of the thermodynamically stable phases Pd_8W and Pd_8Mo under conditions of enhanced vacancy concentration and diffusion brought about by proton irradiation[131,132].

The short-range order developed during annealing of palladium-tungsten and palladium-molybdenum, however, may be considerably reduced by the subsequent introduction of dislocations by plastic deformation. Materials with a low stacking-fault energy are susceptible to planar slip and twin formation. During cold work, the passage of dislocations across a slip plane reduces the local order across this plane by about 20%[162]. The introduction of lattice defects, including large numbers of dislocations, into palladium-tungsten and palladium-molybdenum by means of cold rolling may thus be expected considerably to reduce the degree of local order present in the lattice, but not to disorder the lattice completely. This is an important distinction, since the change in structural order due to cold work followed by annealing is therefore one of degree only, rather than a process of destruction and redevelopment of order.

With regard to electrical resistivity, the scattering due to dislocations arises from electron scattering from the displaced atoms close to the dislocation core, and hence is confined to the immediate vicinity of the dislocation[35]. Plastic deformation results in an increase in dislocation density and hence in a positive contribution to the residual resistivity. However, the passage of a dislocation through an ordered crystal results in a decrease in local order across the slip plane, and hence a reduction in scattering from a volume (dependent on the distance travelled by the dislocation) considerably larger than the volume containing the displaced atoms around the dislocation itself. If the presence of structural order enhances electron scattering considerably, then a decrease in structural order may be expected to result in a decrease in resistivity which is greater in magnitude than the increase in resistivity brought about by the presence of dislocations.

In the alloys containing more than 6 at.% solute, a decrease in resistivity as a result of plastic deformation and an increase in resistivity during recovery are consistent with the interaction of dislocations, vacancies and local order described above. Although the microstructure of alloys of less than 6 at.% solute concentration follows a similar pattern of recovery and recrystallisation, the resistivity behaviour of these alloys suggests that different processes are at work; these will be discussed in section 5.5.1.

5.4 MECHANICAL PROPERTIES

The electrical resistivity of palladium-tungsten and palladium-molybdenum alloys may be affected by a number of factors (section 5.1.2) not directly measured in the present work. The mechanical properties of a material may be affected by variations in microstructure (such as changing dislocation densities) or variations in the degree of structural order, or a combination of the two. The effect of plastic deformation and annealing on the mechanical properties of palladium-tungsten and palladium-molybdenum was assessed by means of microhardness measurements; and the evolution of microstructure was observed by means of transmission electron microscopy. A comparison of the trends observed in each gives an insight into the development of structural order in these alloys.

The effect of annealing on microhardness, for all the alloys investigated, is a small decrease prior to recrystallisation. A large decrease in microhardness was measured after annealing experiments which resulted in recrystallisation, consistent with the observed decrease in dislocation density. However, the change in microhardness measured after completion of recrystallisation is not consistent with microstructural observations. Figure 4.52 shows that, for palladium 5.3 at.% molybdenum, microhardness increases significantly after annealing at 800°C - 1000°C. Annealing in this temperature range produces no significant variation in dislocation density, since the material has already recrystallised. The measured increase in microhardness must therefore be the result of a change in the degree of order in the alloy.

Mes'kin et al[140] measured the influence of annealing temperature on the microhardness of palladium 12 at.% tungsten after 50% deformation, reporting a small increase in microhardness due to annealing at 700°C. Since the dislocation density, if it changes at all, may be assumed to decrease due to annealing, this suggests that the reported increase in microhardness is also brought about by an increase in the degree of order, which is known to occur in palladium-tungsten alloys in this concentration range[136]. It is thus probable that the reported increase in microhardness comes about as a result of an increase in short-range order. If an increase in the degree of short-range order makes a positive contribution to microhardness, then the effect of annealing on

microhardness will be the outcome of competition between the processes of ordering and of recovery/recrystallisation. After recrystallisation, further heat treatments have little effect on the microstructure of the alloys under investigation; any significant change observed in microhardness must then arise from a change in the degree of structural order, as observed for palladium 5.3 at.% molybdenum. Conversely, the absence of significant changes in microhardness after completion of recrystallisation argues that there is no significant change in the degree of order.

On the basis of the foregoing, for the alloys containing more than 6 at.% solute, no significant change in the degree of order occurs after recrystallisation is complete. This is consistent with resistance measurements, which also show little change after recrystallisation (figs. 4.51, 4.52). For palladium 5.3 at.% molybdenum, microhardness measurements suggest that a large increase in the degree of order occurs after annealing above 700°C; this is also reflected in resistance measurements, which show a large increase after annealing in this temperature range.

Although an increase in the degree of order increases the microhardness of the alloys under investigation, the decrease in dislocation density during recovery and recrystallisation is accompanied by a decrease in microhardness. This suggests that, under the experimental conditions of the present work, the effect on microhardness of decreasing dislocation density outweighs any contribution from ordering effects, which may be observed only when dislocation density is constant after recrystallisation is complete.

5.5 STRUCTURE/PROPERTY RELATIONSHIPS

The results of all the experiments performed in the present work on palladium-tungsten and palladium-molybdenum alloys containing more than 6 at.% solute, show that an increase in short-range order occurs as a result of annealing; the presence of short-range order after annealing then has a significant effect on the properties of these alloys. However, the two alloys of less than 6 at.% solute concentration, palladium 4.1 at.% tungsten and palladium 5.3 at.% molydenum, do not fit this simple model. These lower

concentration alloys differ from the other alloys in other respects: the d-band is unfilled (in terms of the rigid-band model); and the magnitude of the magnetic susceptibility is not negligible.

5.5.1 PALLADIUM 4.1 at.% TUNGSTEN AND PALLADIUM 5.3 at.% MOLYBDENUM

For both palladium 4.1 at.% tungsten and palladium 5.3 at.% molybdenum, a minimum is observed in resistivity with respect to annealing temperature (fig. 4.51, 4.52). For palladium 5.3 at.% molybdenum, a minimum is also observed in microhardness with respect to annealing temperature. If the subsequent increase in microhardness observed in this alloy is a result of an increasing degree of order, then the simultaneous increase in resistivity, due to annealing in a temperature range in which microstructure is unchanged, may also be attributed to an increase in structural order. An increase in electrical resistivity as a result of an increase in the degree of structural order is consistent with the results obtained for the alloys of higher solute concentration. However, for both palladium 4.1 at.% tungsten and palladium 5.3 at.% molybdenum, a decrease in resistivity occurs after annealing at temperatures below 800°C and this must be carefully considered.

In these alloys, factors which influence resistivity and are also susceptible to change as a result of annealing include defect density, magnetic susceptibility and atomic configuration. The concentration of lattice defects decreases as a result of annealing below 800°C due to a certain degree of recovery and the onset of recrystallisation; a decrease in resistivity is therefore to be expected. However, the magnitude of the decrease in resistivity exhibited by palladium 4.1 at.% tungsten and palladium 5.3 at.% molybdenum (eight per cent and four per cent respectively) is greater than may be expected to occur as a result of decreasing defect densities alone. Although the magnetic susceptibility of palladium decreases rapidly to almost zero with the addition of tungsten[130] or molybdenum[104], the susceptibility at around 5 at.% solute is not negligible, and magnetic effects are likely to make a contribution to resistivity. Klyuyeva et al[133] report that a decrease in magnetic susceptibility occurs in palladium-tungsten alloys as a result of annealing; a decrease in resistivity may be expected to occur as a result. The combined influence of a decrease in

dislocation density and a decrease in magnetic susceptibility might be sufficient to result in a decrease in resistivity, provided that any positive contribution to resistivity which may be present, such as structural order, remains small.

The change in temperature coefficient of resistivity measured by Mes'kin et al[140] in annealed palladium-tungsten and palladium-molybdenum alloys containing around 5 at.% solute concentration (figs. 2.10, 2.18) showed that a change in electronic structure - such as might occur in transition metal alloys as a result of a changed atomic configuration - had occurred. It therefore seems likely that some increase in the degree of structural order does occur in palladium 4.1 at.% tungsten and palladium 5.3 at.% molybdenum as a result of annealing below 800°C, which has affected the band structure sufficiently to influence α_ρ. However, since there is little positive effect on resistivity, it appears that the increase in structural order is very small. Annealing above 800°C - which brings about little further change in microstructure but a significant increase in resistivity and in microhardness (for palladium 5.3 at.% molybdenum) - appears to result in a greater increase in the degree of order. Klyuyeva et al[133] noted an increased resistivity for palladium 2.6 at.% tungsten after heating to 1100°C, suggesting that structural order develops with greater ease at high temperatures.

The results of experiments for the alloys of lower solute concentration are consistent with a small increase in the degree of structural order due to annealing below 800°C, followed by a larger increase in structural order due to annealing at 800°C - 1000°C. Since the results of experiments for alloys containing more than 6 at.% solute show structural order to increase after annealing at 500°C, this suggests that the activation energy for vacancy diffusion may be greater in the alloys of low solute concentration, resulting in a significant increase in structural order only at higher temperatures. The possibility of a change in the nature of the ordering should not be ruled out.

A small decrease in the thermo-emf of palladium-tungsten and palladium-molybdenum alloys containing up to 6 at.% solute, as a result of annealing at 700°C, was reported by Mes'kin et al[140]. The thermo-emf of a metal is related to the energy derivative of the density of states, and is consequently sensitive to variations in electronic structure. The reported change in thermo-emf is

therefore likely to arise from variations in band-structure in the early stages of ordering, which also result in a change in α_ρ.

5.5.2 PALLADIUM ALLOYS CONTAINING MORE THAN 6 at.% SOLUTE

Palladium alloys containing more than 6 at.% solute concentration show a dependence of resisitivity on annealing temperature which suggests that sort-range order develops rapidly in the temperature range 500°C - 700°C. Little further change in resistivity occurs after annealing at higher temperatures, which suggests that there is no significant further increase in the degree of structural order. There is also no evidence of an increase in microhardness after annealing above 700°C such as is observed in palladium 5.3 at.% molybdenum. Since thermally activated diffusion may be expected to increase with increasing temperature, the degree of order present after annealing at 700°C (the temperature at which the resistivity increase appears to saturate (figs. 4.51, 4.52)) appears to be close to the maximum attainable by annealing for the experimental specimens.

After annealing at 700°C, the thermo-emf of palladium-tungsten and palladium-molydbenum alloys (above 6 at.% solute concentration) is reported to increase[140]. In this concentration range and temperature, a significant increase in structural order has occurred and results in an increase in resistivity. Vigier and Pelletier[52] showed that the sign of thermo-emf changes due to the development of short-range order may be expected to be the same as the sign of resistivity changes; the reported increase in thermo-emf is thus qualitatively consistent with an increase in structural order (this free-electron analysis is inappropriate for alloys containing an unfilled d-band but may, in terms of the rigid-band model, describe the alloys of higher solute concentration reasonably well).

5.5.3 THE TYPE OF STRUCTURAL ORDER PRESENT

A distinction has been drawn between heterogeneous short-range order and homogeneous short-range order (section 5.2.1). Heterogeneous short-range order is characterised by long-range ordered microdomains, of dimensions

smaller than the coherence length of the probe used. The presence and structure type of such microdomains may nevertheless be detected by means of electron diffraction. The electron diffraction investigation in the present work shows no evidence for the presence of microdomains of a long-range ordered phase; in particular there is no evidence for the presence of the ordered structures Pd_8W or Pd_8Mo.

The experimental results show that annealing results in an increase in the degree of short-range order present, manifested as an increase in electrical resistivity. In the annealing temperature range investigated, there is no evidence for a decrease in the degree of order - such as a significant decrease in resistivity - due to annealing at high temperatures. A randomisation of atomic configuration was thus not produced by heat treatment. A decrease in the degree of order occurs as a result of plastic deformation; however, this is unlikely completely to destroy the structural order present. The experimental procedures of cold work followed by repeated annealing therefore appear only to achieve a variation in the degree of order. The nature of the short-range order present in these alloys is thus more likely to be homogeneous (statistical) than associated with the nucleation and growth of an ordered phase.

This homogeneous short-range order may be a precursor to the long-range ordered phase Pd_8W (and Pd_8Mo)[131,144]. This phase is thermodynamically stable but has only been produced under the accelerated diffusion conditions resulting from proton irratiation; it has not been produced under normal annealing conditions, suggesting extremely sluggish kinetics. Under ordinary circumstances, then, a short-range ordered configuration appears to be favourable for the alloys under investigation: both disorder and long-range order are achieved with difficulty, if at all.

If a short-range ordered atomic configuration is generally energetically favourable, and a fully disordered structure is not normally present, then the presence of short-range order may contribute to many observed characteristics and measured properies in these alloys. Features such as low stacking-fault energy may, at least in part, be caused by the presence of short-range order. Since SFE affects the deformation mode of a crystal, short-range order may be seen to influence microstructure. Short-range order also contributes to the

high resistivity which makes these alloys attractive potentiometry materials.

5.6 OVERVIEW

The results of the present investigation show that the mechanisms affecting electrical and mechanical properties in palladium-tungsten and palladium-molybdenum alloys are neither simple nor completely independent. Changing degrees of order and changing defect densities both influence the properties of the alloys investigated: resistivity is in general more sensitive to changing degrees of order, whereas microhardness is more sensitive to microstructural changes. The degree to which each process influences properties depends not only on the annealing temperature, but also on the solute concentration of the alloys.

The introduction of dislocations into annealed alloys by cold deformation has the effect of reducing the structural order present; the simultaneous introduction of excess vacancies, however, serves to enhance the rearrangement of atoms to a short-range ordered configuration during subequent annealing. The presence of short-range order may in turn affect deformation processes by influencing the stacking-fault energy of the alloys.

In alloys containing more than 6 at.% solute, a significant increase in the degree of short-range order occurs after annealing in the temperature range 500°C - 700°C. In alloys containing less than 6 at.% solute, the degree of order does not show a significant increase until after annealing at higher temperatures, suggesting a higher activation energy for diffusion. The result of this is a dominance of dislocation density-related effects at low annealing temperatures, leading to a decrease in resistivity and microhardness; a more rapid increase at higher annealing temperatures in the degree of order leads to an increase resistivity and (in palladium 5.3 at.% molybdenum) microhardness. At no annealing temperature, however, is there evidence in any of the alloys investigated of a decrease in the degree of order as a result of annealing. A short-range ordered configuration thus appears to be stable in these alloys over a wide temperature range.

CHAPTER 6

SUMMARY AND CONCLUDING REMARKS

The recovery and recrystallisation of a formerly cold-worked metal or alloy results in a significant decrease in dislocation density; the consequent reduction in electron scattering from dislocations is expected to result in a reduced residual resistivity. Palladium-tungsten and palladium-molybdenum alloys, however, exhibit changes in electrical resistivity after annealing which are not consistent with a decrease in residual resistivity due to a decrease in defect concentration. The development of short-range order in an alloy at elevated temperatures may provide an additional contribution, either positive or negative, to both the residual and ideal resistivity. The presence of short-range order in annealed palladium-tungsten alloys has been reported; in addition, both palladium-tungsten and palladium-molybdenum alloys exhibit behaviour which is inconsistent with a random distribution of atoms, notably a contraction of the lattice when solute size considerations predict an expansion. The reported thermodynamic stability of the long-range ordered structures Pd_8W and Pd_8Mo, produced under proton irradiation, suggests that an atomic configuration containing unlike nearest neighbours is energetically favourable in these alloys. A quantitative analysis of the contribution to resistivity of structural order in palladium alloys on the basis of theoretical considerations presents some difficulty, since transition metals and alloys have complex electronic structures and do not lend themselves to simplifying approximations and models.

The results of the present work show that the electrical resistivity of palladium-tungsten and palladium-molybdenum alloys is sensitively dependent on annealing temperature; microhardness measurements and transmission electron microscopy of annealed alloys show that there is not a simple relationship between microhardness and

dislocation density. After consideration of other factors which may contribute to resistivity, it is concluded that an increase in the degree of short-range order during annealing is the only mechanism consistent with the experimental results.

The observed changes in electrical resistivity due to annealing arise from the relative contributions to resistivity of variations in the degree of short-range order and dislocation density; magnetic effects may also make a contribution in alloys of low solute concentration. The decrease in dislocation density as a result of annealing serves to decrease the residual resistivity; an increase in short-range order increases the residual resistivity, and also influences the ideal resistivity.

In alloys containing more than 6 at.% solute, there is a significant increase in the degree of short-range order as a result of annealing experiments which result in recovery and recrystallisation. The outcome of the simultaneous increase in structural order and decrease in dislocation density is an increase in resistivity (which is more sensitive to structural order) but a decrease in microhardness (which is more sensitive to dislocation density). Annealing above the recrystallisation temperature results in little further change in either resistivity or microhardness, suggesting that there is no further increase in the degree of order.

In alloys containing less than 6 at% solute, there is little increase in the degree of short-range order as a result of annealing experiments which result in recovery and recrystallisation. The effect of decreasing dislocation density, together with a decrease in magnetic susceptibility, is therefore predominant in the lower annealing temperature range: a decrease in both resistivity and microhardness is observed. As a result of annealing above the recrystallisation temperature, there is a significant increase in the degree of short-range order but little change in microstructure. The effect of structural order is predominant in this temperature range, leading to an increase in both resistivity and microhardness.

Under the enhanced diffusion conditions of proton irradiation, a long-range ordered structure is reported to be thermodynamically stable in a limited temperature range. The results of the present work show that under normal, thermally-activated diffusion conditions, a short-range ordered configuration is energetically favourable in palladium-tungsten and palladium-molybdenum over a wide temperature range.

6.1 FUTURE WORK

The present work has shown that the measured properties of palladium-tungsten and palladium-molybdenum alloys exhibit a sensitive dependence on prior heat treatment. This is a result of the enhancement, at elevated temperatures, of short-range order. The properties may therefore be expected to be sensitive to production and manufacturing processes; a knowledge of the influence of short-range order on properties of interest is thus a requirement for commercial application of these alloys.

Temperature dependence

The temperature dependence of properties such as resistivity and magnetic susceptibility, for a range of initial microstructural conditions, would provide an insight into the effect of short-range order on electronic structure in these alloys.

Thermo-emf

The thermo-emf of palladium alloys was not experimentally addressed in the present work. However, the reported variation in thermo-emf due to annealing and its sensitive dependence on solute concentration suggest that closer investigation of the effect of short-range order on this property, together with electrical resistivity, will provide information leading to an improved understanding of the effect of short-range order on electron transport properties in these alloys.

Neutron diffraction

The electron diffraction investigation in the present work was not successful in detecting scattering due to short-range order. An X-ray or neutron scattering investigation of these alloys in a range of microstructural conditions, correlated with measurement of properties of interest, wou structure/property relationhsips present.

Scanning Tunneling Microscopy

The recent development of scanning tunneling microscopy, with the associated technique of scanning tunneling potentiometry, offers a unique probe for the detailed examination of the influence of local microstructure on electrical properties. In the present work, the microstructure of alloys was investigated by examination of thin foil specimens by means of transmission electron microscopy; electrical resistivity was measured using macroscopic resistance specimens. Scanning tunneling microscopy and scanning tunneling potentiometry techniques allow the investigation of both microstructure and resistivity, by providing the means to determine the resistance of precisely the same specimen region which is microscopically imaged. These techniques can be applied to thin foil TEM specimens without damage; together with (prior or subsequent) TEM and electron diffraction investigations, detailed information regarding the microstructure and its effect on the electrical resistivity of alloys may be obtained.

APPENDIX

The only short-range order parameters α_i published for either palladium-tungsten or palladium-molybdenum alloys are those of Babanova et al[136], who investigated palladium-tungsten alloys using X-ray diffraction. These α_i (see Table 2.1) were calculated from diffuse X-ray scattering intensities, which may be used to obtain values for $|S^d(q)|^2$ and hence α_i. Conversely, $|S^d(q)|^2$ may be calculated from α_i[50]. The published α_i were used in the present work to calculate ρ_{SRO}, the resistivity due to short-range order, by the method of Rossiter and Wells[49] (see section 5.1.3).

The published α_i values suggest that a greater degree of short-range order is present in palladium 6.2 at.% tungsten than in palladium 7.7 at.% tungsten (see Table 2.1), which is counter to the observed trend of increasing short-range order with increasing concentration. This is also inconsistent with the published X-ray data of Babanova et al[136], shown in fig. A1 (a), in which the diffuse X-ray scattering intensity from palladium 6.2 at.% tungsten may be seen to be lower than that from palladium 7.7 at.% tungsten. Figure A1 (b) shows the results of a calculation of $|S^d(q)|^2$, using the α_i values of Babanova et al[136]. This calculation shows the published values of α_i for palladium 6.2 at.% tungsten and palladium 7.7 at.% tungsten to be consistent with a ***higher*** diffuse scattering intensity from palladium 6.2 at.% tungsten than from palladium 7.7 at.% tungsten.

There is thus an inconsistency between the published diffuse X-ray scattering intensities and α_i for palladium-tungsten alloys calculated by Babanova et al[136]. The α_i should therefore be treated with some caution. It may be seen from fig. 5.1, for example, that use of the published α_i to calculate resistivity leads to an unexpected decrease in resistivity at a composition of 7.7 at.%.

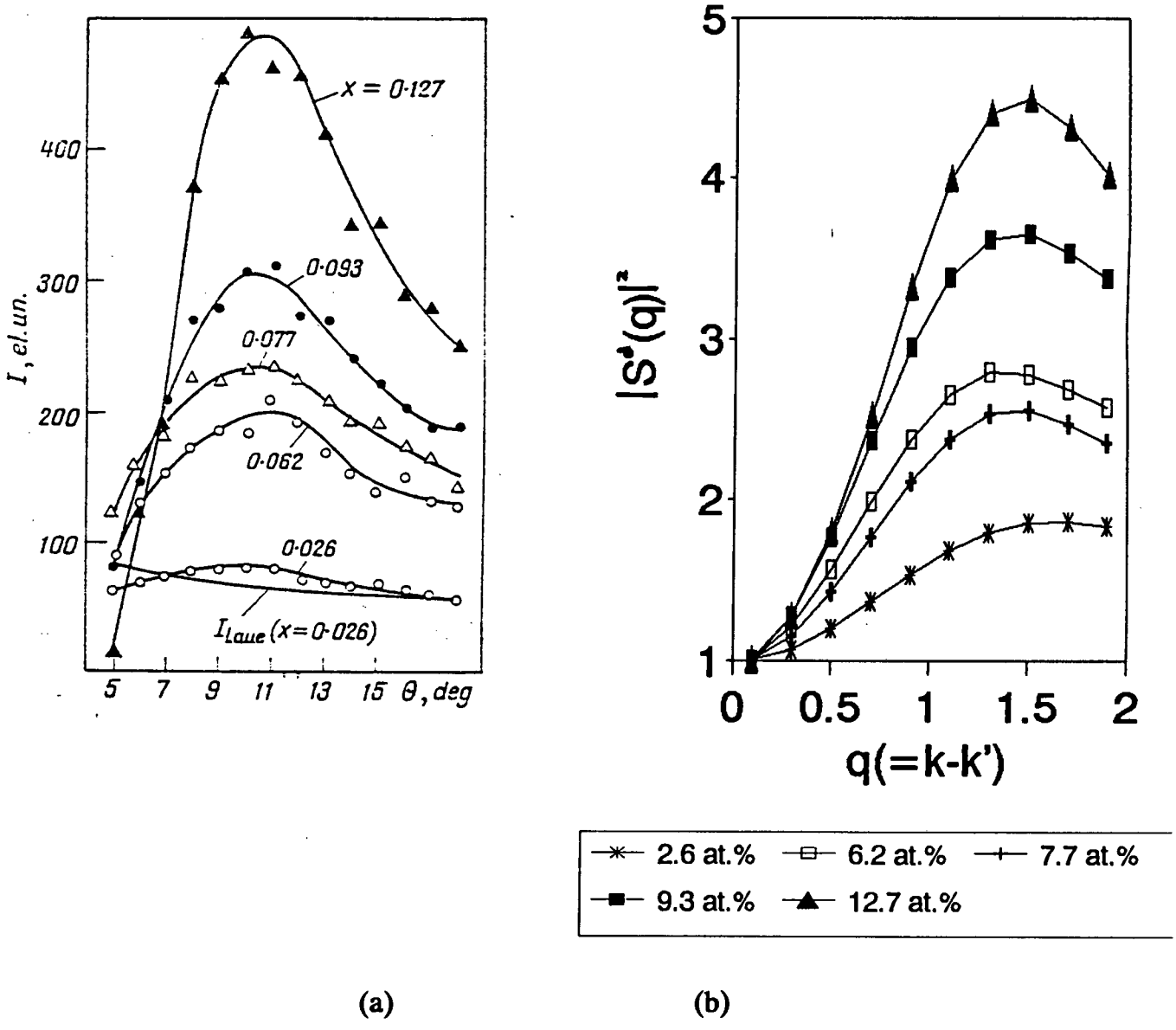

Figure A1: (a) Diffuse X-ray scattering intensity of palladium-tungsten alloys (from Babanova et al[136]); (b) $|S^d(q)|^2$ calculated from α^i of Babanova et al[136].

REFERENCES

1 J S Koehler, Phys. Rev. **75**, no.1, 106-117 (1949).

2 E A Kaner & E P Feld'man, Sov. Phys.-Sol. St. **10**, no.10, 2401-2405 (1969).

3 I Kovacs & E Nagy, Phys. Stat. Sol. **8**, 795-803 (1965).

4 J K Mackenzie and E H Sondheimer, Phys. Rev. **77**, no.2, 264-270 (1950).

5 R Landauer, Phys. Rev. **82**, no. 4, 520-521 (1951).

6 D L Dexter, Phys. Rev. **85**, 936-937 (1952).

7 D L Dexter, Phys. Rev. **86**, no. 5, 770-774 (1952).

8 S C Hunter & F R N Nabarro, Proc. Roy. Soc. (London) A **220**, 542-561 (1953).

9 W A Harrison, Phys. Rev. **110**, no.1, 14-25 (1958).

10 W A Harrison, J. Phys. Chem. Solids **5**, 44-46 (1958)

11 A B Bhatia & O P Gupta, Phys. Rev. B **1**, no.12, 4577-4583 (1970).

12 T Broom, Proc. Phys. Soc. (London) B **65**, 871-881 (1952).

13 A Howie, Phil. Mag. **5**, 251-271 (1960).

14 L M Clareborough, M E Hargreaves & M H Loretto, Phil. Mag. **7**, 115-120 (1962).

15 Z S Basinski, J S Dugdale & A Howie, Phil. Mag. **8**, 1989-1997 (1963).

16 A Sosin & J S Koehler, Phys. Rev. **101**, no.3, 972-977 (1956).

17 Z S Basinski & S Saimoto, Can. J. Phys. **45**, 1161-1176 (1967).

18 Z S Basinski & J S Dugdale, Phys. Rev. B **32**, no.4, 2149-2155 (1985).

19 J G Rider & C T B Foxon, Phil. Mag. **13**, 289-303 (1966).

20 J G Rider & C T B Foxon, Phil. Mag. **16**, 1133-1138 (1967).

21 J Schrank, M Zehetbauer, W Pfeiler & L Trieb, Scripta Metall. **14**, 1125-1128 (1980).

22 B R Watts, J. Phys. F **18**, 1183-1195 (1988).

23 J A Rowlands & S B Woods, J. Phys. F **8**, 1929-1939 (1978).

24 M Kaveh & N Wiser, J. Phys. F **11**, 1749-1763 (1981).

25 A Bergmann, M Kaveh & N Wiser, Phys. Rev. B **24**, no.12, 6807-6819 (1981).

26 M Kaveh & N Wiser, J. Phys. F **13**, 953-961 (1983).

27 Y K Chang & R J Higgins, Phys. Rev. B **12**, no. 10, 4261-4281 (1975).

28 Z S Basinski, P T Coleridge, A Howie, G G Lonzarich & T I Sigfusson, J. Phys. F **13**, L233-L238 (1983).

29 D Trattner, M Zehetbauer & V Groger, Phys. Rev. B **31**, no.2, 1172-1173 (1985).

30 B R Watts, J. Phys. F **18**, 1197-1209 (1988).

31 R A Brown, Phys. Rev. **156**, no.3, 692-700 (1967).

32 R A Brown, J. Phys. F **7**, no.7, 1269-1281 (1977).

33 R A Brown, J. Phys. F **7**, no.7, 1283-1295 (1977).

34 R A Brown, J. Phys. F **8**, no.7, 1467-1476 (1978).

35 B R Watts, J. Phys. F **17**, 1703-1716 (1987).

36 B R Watts, "Conduction electron scattering in dislocated metals", *Dislocations in Solids* **8**, Ed. F R N Nabarro, Elsevier (1989).

37 R A Brown, J. Phys. F **7**, no.8, 1477-1478 (1977).

38 Z Gierak, J W Moron & J Rasek, Acta Physica Polonica A **64**, no.6, 649-652 (1983).

39 L Nordheim, Ann. Phys. **9**, 607-640 (1931).

40 C S Barret, *The Structure of Metals*, 2nd ed., McGraw-Hill, New York (1952).

41 W L Bragg and E J Williams, Proc. Roy. Soc. A **145**, 699-730 (1934).

42 J M Cowley, Phys. Rev. **77**, no.5, 669-675 (1950).

43 P A Flinn, Phys. Rev. **104**, 350-356 (1956).

44 G L Hall, Phys. Rev. **116**, no.3, 604-605 (1959).

45 J B Gibson, J. Phys. Chem. Solids **1**, 27-34 (1956).

46 A E Asch & G L Hall, Phys. Rev. **132**, no.3, 1047-1057 (1963).

47 A A Katsnel'son & L M Shevchuk, Fiz. Metal. Metalloved. **24**, no.4, 97-100 (1967).

48 K P Wang and H Amar, Phys. Rev. B **1**, no.2, 582-587 (1970).

49 P L Rossiter & P Wells, J. Phys. C **4**, 354-363 (1971).

50 P L Rossiter, *The Electrical Resistivity of Metals and Alloys*, Cambridge University Press (1987).

51 P L Rossiter & P Wells, Phil. Mag. **28**, 505-512 (1973).

52 G Vigier & M Pelletier, Acta. Metall. **30**, 1851-1859 (1982).

53 A J Hillel, J T Edwards and P Wilkes, Phil. Mag. **32**, 189-209 (1975).

54 W Wagner, R Poerschke & H Wollenberger, Phil. Mag B **43**, no.2, 345-355 (1981).

55 W Kohl, R Scheffel, H Heidsiek & K Lucke, Acta Metall. **31**, no.11, 1895-1908 (1983).

56 W Pfeiler, P Meisterle & M Zehetbauer, Acta Metall. **32**, no.7, 1053-1060

(1984).

57 G J Stanisz, J Soltys & J M Holender, J. Phys.: Condens. Matter **1**, 6327-6333 (1989).

58 P L Rossiter & P Wells, Phil. Mag. **24**, 425 (1971).

59 P L Rossiter, Phil. Mag. **33**, no.6, 1015-1020 (1976).

60 A J Hillel, J T Edwards & P Wilkes, Phil. Mag. **35**, no.3, 829-830 (1977).

61 A J Hillel & P L Rossiter, Phil. Mag. B **44**, 383 (1981).

62 P L Rossiter, J. Phys. F **7**, no.3, 407-418 (1977).

63 A Cottrell, *Introduction to the Modern Theory of Metals*, Institute of Metals, London (1988).

64 N F Mott & H Jones, *The Theory of the Properties of Metals and Alloys*, Clarendon, Oxford (1936).

65 A N Voloshinskiy & L F Savitskaya, Fiz. Metal. Metalloved. **35**, no.3, 451-459 (1973).

66 P B Allen, T P Beaulac, F S Khan, W H Butler, F J Pinski and J C Swihart, Mat. Res. Symp. Proc. **63**, 259-271 (1985).

67 G K White & S B Woods, Phil. Trans. Roy. Soc. (London) A **251**, 273-302 (1959).

68 N V Grum-Grzhimailo, Fiz. Metal. Metalloved. **5**, no.1, 23-29 (1957).

69 B Velicky, Phys. Rev. **184**, no.3, 614-627 (1969).

70 W H Butler and G M Stocks, Phys. Rev. B **29**, no.8, 4217 (1984).

71 D D Johnson, F J Pinski & G M Stocks, Phys. Rev. B **30**, no.10, 5508-5515 (1984).

72 H Thomas, Z. Phys. **129**, 219-232 (1951)

73 H G Baer, Z. Metallk. **56**, 79-84 (1965).

74 A M Ammons & J E Spruiell, J. Appl. Phys. **39**, no.8 (1968).

75 F Adunka, M Zehetbauer & L Trieb, Phys. Stat. Sol. (a) **62**, 213-222 (1980).

76 M Plischke & D Mattis, Phys. Rev. Lett. **25**, 1748-1751 (1971).

77 M Plischke & D Mattis, Phys. Rev. B **7**, no.6, 2430-2434 (1973).

78 F Brouers, J Giner & J van der Rest, J. Phys. F **4**, 214-224 (1974).

79 L A Moraga & G Ramirez, J. Phys.: Condens. Matter **3**, 7709-7721 (1991).

80 F E Hoare and J B Yates, Proc. Roy. Soc. (London) A **240**, 42-53 (1957).

81 A J Manuel & J M P St Quinton, Proc. Roy. Soc. (London) A **273**, 412-426 (1963).

82 J Friedel, in *The Physics of Metals, I - Electrons* (ed. J M Ziman), 340-408, Cambridge University Press (1969).

83 J J Vuillemin, Phys. Rev. **144**, no.2, 396-405 (1966).

84 H Skriver, W Venema, E Walker & R Griessen, J. Phys. F **8**, no.11, 2313-2321 (1978).

85 C Cavalloni, W Joss, R Monnier & T Jarlborg, Phys. Rev. B **31**, no.4, 1744-1753 (1985).

86 S G Das, D D Koelling & F M Mueller, Solid St. Commun. **12**, 89-93 (1973).

87 O K Anderson & A R MacKintosh, Solid St. Commun. **6**, 285-290 (1968).

88 O K Anderson, Phys. Rev. B **2**, 883-906 (1970).

89 J G Gay, J R Smith, F J Arlinghaus & T W Capehart, Phys. Rev. B **23**, no. 4, 1559-1566 (1981).

90 F M Mueller, A J Freeman, J O Dimmock & A M Firdyna, Phys. Rev. B **1**, 9617-9635 (1970).

91 H Asonen, M Lindroos, M Pessa & N Dahlback, Solid St. Commun. **35**, 69-71 (1980).

92 J S Dugdale, "The Electrical Properties of Metals and Alloys", *The Structure and Properties of Solids* **5**, Ed. B R Coles, Edward Arnold, London (1977).

93 E Savitskii, V Polyakova, N Gorina & N Roshan, *Physical Metallurgy of Platinum Metals*, Pergamon Press, Oxford (1978).

94 R Evans, G D Gaspari & B L Gyorffy, J. Phys. F **3**, 39-54 (1973).

95 B Strizker, Phys, Rev. Lett. **42**, 1769-1773 (1979).

96 J D Meyer & B Stritzker, Phys. Rev. Lett. **48**, no.7, 502-505 (1982).

97 F J Pinski, P B Allen & W H Butler, Phys. Rev. Lett. **41**, no.6, 431-434 (1978).

98 F J Pinski, P B Allen & W H Butler, Phys. Rev. B **23**, no.10, 5080-5096 (1981).

99 J A Rowlands and S B Woods, J. Phys. F **8**, no.9, 1929-1939 (1978).

100 J W Zwart and P A Schroeder, J. Phys. F **15**, 639-649 (1985).

101 J T Schriempf, Phys. Rev. Lett. **20**, no.19, 1034-1036 (1968).

102 C Uher & P A Schroeder, J. Phys. F **8**, no.5, 865-871 (1978).

103 R W Powell, R P Tye & M J Woodman, J. Less-Common Metals **12**, no.1, 1-16 (1967).

104 E Kudielka-Artner & B B Argent, Proc. Phys. Soc. **80**, 1143-1148 (1962).

105 J C Fuggle, F U Hillebrecht, R Zeller, Z Zolnierek, P A Bennet & Ch Freiburg, Phys. Rev. B **27**, no.4, 2145-2178 (1982).

106 C Norris & H P Myers, J. Phys. F **1**, 62-77 (1971).

107 G M Stocks, R W Williams & J S Faulkner, J. Phys. F **3**, 1688-1703 (1973).

108 J Brooks, M H Loretto & I R Harris, Metal Science, MS 548, 397-400 (1976).

109 J C Huang, A J Ardell & O Ajaja, J. Mat. Sci. **23**, 1206-1218 (1988).

110 K Takao, K L Zhao & Y Sakamoto, J. Mat. Sci. **25**, 1225-1260 (1990).

111 M J Kim & W F Flanagan, Acta Metall. **15**, 753-764 (1967)

112 K Lucke, H Haas & H A Schulze, J. Phys. Chem. Solids **37**, 979-987 (1976).

113 R W Westerlund & M E Nicholson, Acta Metall **14**, 569-574 (1966).

114 A A Katsnel'son & Sh A Alimov, Fiz. Met. Metalloved **24**, no.6, 1117-1119 (1967).

115 A A Katsnel'son, Sh A Alimov, P Sh Dazhayev, V M Silonov & N N Stupina, Fiz. Met. Metalloved. **26**, no.6, 987-995 (1968).

116 D Gerstenberg, Annalen der Physik. **7**, no. 2, 236-261 (1958).

117 W Koster & D Hagmann, Z. Metallkde **52**, no.11, 721-734 (1961).

118 D Gerstenberg, Z. Metallkde **49**, no.9, 476-480 (1958).

119 G Zwingmann, Z. Metallkde **54**, no.5, 286-292 (1963).

120 A I Schindler, R J Smith & E I Salkovitz, J. Phys. Chem. Solids **1**, 39-41 (1956).

121 B R Coles & J C Taylor, Proc. Royal Soc. A **267**, 139-145 (1962?).

122 R Fletcher & D Greig, Phil. Mag. **17**, 1-35 (1968).

123 A T Aldred, J. Phys. Soc. Japan **22**, no.3, 762-766 (1967).

124 M J Kim & W F Flanagan, Acta Metall. **15**, 747-752 (1967).

125 M J Kim & W F Flanagan, Acta Metall. **15**, 735-745 (1967).

126 T Chen & J M Sivertson, Phys. Lett. **28A**, no.7, 520-521 (1969).

127 H Haas & K Lucke, Scripta Metall. **6**, 715-720 (1972).

128 M A Tylkina, V P Polyakova & E M Savitskii, Russian J. Inorganic Chem. **6**, no.6, 753-754 (1961).

129 W K Goetz & J H Brophy, J. Less-Common Metals **6**, 345-353 (1964).

130 H R Khan & Ch J Raub, J. Less-Common Metals **25**, 441-442 (1971).

131 L Weaver & A J Ardell, Scripta Metall. **14**, 765-768 (1980).

132 J Cheng & A J Ardell, Acta Metall. **37**, no. 7, 1891-1902 (1989).

133 I B Klyuyeva, A A Kuranov, L S Chemerinskaya, Ye N Babanova, A N Bashkatov, P N Syutkin, F A Sidorenko & P V Gel'd, Phys. Met. Metall. **47**, no.4, 46-49 (1980).

134 H L Luo, J. Less-Common Metals **15**, 299-302 (1968).

135 L S Darken and W Gurry, *Physical Chemistry of Metals*, McGraw-Hill, New York (1953).

136 Ye N Babanova, I B Klyuyeva, L S Chemerinskaya, F A Sidorenko, V Ya El'ner & P V Gel'd, Phys. Met. Metall, **49**, no.3, 184-186 (1980).

137 Sh A Alimov & A A Katsnel'son, Fiz. Metal. Metalloved. **22**, no.3, 151-153 (1966).

138 P Donze, Ph. D. Thesis, Archives des Sciences (Geneve) **22**, fasc. 3, 728-731 (1969).

139 H R Khan & Ch J Raub, Naturwissenschaften **58**, no. 11, 565 (1971).

140 V S Mes'kin, R I Sergi'enko & L A Popova, Fiz. Metal. Metalloved. **13**, no.1, 126-131 (1962).

141 E M Savitskii, M A Tylkina & O Kh Khamidov, Russian J. Inorganic Chem. **9**, no.12, 1475-1476 (1964).

142 E Anderson, J. Less-Common Metals **6**, 81-84 (1964).

143 C W Haworth & M A Hume-Rothery, J. Inst. Metals **87**, 265-269 (1958-1959).

144 M S Mostafa & A J Ardell, Mat. Lett. **6**, no.3, 67-70 (1987).

145 J Cheng, M S Mostafa & A J Ardell, J. Less-Common Metals **143**, 251-263 (1988).

146 E Raub, Z. Metallkde. **45**, no.1, 23-30 (1954).

147 M Huq & D E Moody, Physica **86-88B**, 485-486 (1977).

148 M J Witcombe, Metallography **22**, 117-120 (1989).

149 R J Willey, J. Mat. Sci. **13**, 871-875 (1978).

150 J H Mooij, Phys. Stat. Sol. A **17**, 521-530 (1973)

151 P R Okamoto & G Thomas, Acta Metall. **19**, 825-841 (1971).

152 D de Fontaine, Acta Metall. **23**, 553-571 (1975).

153 R de Ridder, G van Tendeloo, & S Amelinckx, Acta Crystallogr. A **32**, 216-224 (1976).

154 J Cowley, *Diffraction Physics*, (2 ed.), North-Holland (1984).

155 P M Fields & J M Cowley, Acta Crystallogr. A **34**, 103- (1978).

156 P Hirsch, A Howie, R B Nicholson, D W Pashley & M J Whelan, *Electron Microscopy of Thin Crystals*, Robert E Krieger, New York (1977).

157 S Crampin. K Hampel, D D Vvedensky & J M MacLaren, J. Mater. Res. **5**, no.10, 2107-2119 (1990).

158 R I Harris, I L Dillamore, R E Smallman & B E P Beeston, Phil. Mag. **14**, 325-333 (1966).

159 U Gahn & W Pitsch, Acta Metall. Mater. **38**, no.10, 1863-1870 (1990).

160 J Soltys, R Kozubski & E Roschel, Z. Metallkde **58**, 567-572 (1967).

161 J C Huang, A J Ardell & O Ajaja, J. Mat. Sci **23**, 1206-1218 (1988).

162 J B Cohen, J. Mat. Sci. **4**, 1012-1022 (1969).